COHERENT OPTICAL WIRELESS COMMUNICATIONS OVER ATMOSPHERIC TURBULENCE CHANNELS

by

MINGBO NIU

M.Sc., Northwestern Polytechnical University, China, 2006
B.Sc., Northwestern Polytechnical University, China, 2003

A THESIS SUBMITTED IN PARTIAL FULFILLMENT OF
THE REQUIREMENTS FOR THE DEGREE OF

DOCTOR OF PHILOSOPHY

in

The College of Graduate Studies

(Electrical Engineering)

THE UNIVERSITY OF BRITISH COLUMBIA
(OKANAGAN)

December 2012

Abstract

Recent advances in free-space optics have made outdoor optical wireless communication (OWC) an attractive solution to the "last-mile" problem of broadband access networks. Significant challenges can, however, arise for OWC links with increased levels of atmospheric turbulence from time-varying temperatures and pressures. As a promising alternative to the current generation of on-off keying (OOK) direct detection based OWC system, the coherent OWC system is studied in this thesis for a variety of turbulence conditions. Since coherent OWC system performance is found to be impaired severely under strong turbulence conditions, spatial diversity techniques, e.g., maximum ratio combining (MRC), equal gain combining (EGC), and selection combining (SC), are adopted to overcome turbulence impacts. The results are then generalized to Gamma-Gamma turbulence for MRC and EGC with perfect channel or phase estimation. The impacts of phase noise compensation error on coherent OWC system performance are investigated, and it is found that such impacts can be small when the standard deviation of the phase noise compensation error is kept below twenty degrees. A postdetection EGC scheme using differential phase-shift keying (PSK) is proposed and is shown to be a viable alternative to overcome phase noise impacts.

The subcarrier intensity modulation (SIM) based OWC system has been proposed as another alternative to the OOK system. With a unified average signal-to-noise ratio definition, system performance is compared for coherent and SIM links over the Gamma-Gamma turbulence channels. Closed-form error rate expressions are derived for coherent and SIM systems using MRC, EGC and SC schemes. It is found that the coherent systems outperform the SIM systems significantly. The benefits of coherent systems come chiefly from the large local oscillator power which eliminates the effects of the thermal and ambient noises that dominate in SIM systems.

To further enhance the system performance of coherent OWC links, an optical multiple-input multiple-output architecture is proposed and its performance is analyzed through turbulence channels. As expected, the system performance improves as the numbers of transmitters and/or receivers increase. Two space-time coded coherent M-ary PSK systems are also introduced. From the analytical results, the proposed systems are found to be useful in exploiting transmit diversity and mitigating turbulence effects.

Preface

This thesis is based on the research work conducted in the School of Engineering at The University of British Columbia's Okanagan campus under the supervision of Profs. Julian Cheng and Jonathan F. Holzman. Both published and submitted works are contained in this thesis.

With the exception of Chapter 5, I am the first author and principal contributor of all the thesis chapters under the supervision of Profs. Cheng and Holzman. The work in Chapter 5 has been partially published in *IEEE/OSA Journal of Optical Communications and Networking* with me being the first author along with two additional co-authors: Mr. Josh Schlenker and Prof. Robert Schober. Mr. Josh Schlenker, who was an undergraduate co-op student supervised by Profs. Schober and Cheng, assisted with the random number generation according to the Tikhonov distribution. Prof. Robert Schober suggested that we apply postdetection equal gain combining to the coherent free-space optical system in the Gamma-Gamma turbulence, and he was also involved in the editing and revision of the journal manuscript. I am the principal contributor of this work in terms of formulating the system model, performing analysis and numerical studies, as well as writing of the journal manuscript.

A list of my publications at The University of British Columbia is provided in the following.

Journal Papers Published

1. M. Niu, X. Song, J. Cheng, and J. F. Holzman, "Performance Analysis of Coherent Wireless Optical Communications with Atmospheric Turbulence," *Optics Express*, vol. 20, no. 6, pp. 6515-6520, Mar. 2012.

2. X. Song, M. Niu, and J. Cheng, "Error Rate of Subcarrier Intensity Modulations for Wireless Optical Communications," *IEEE Communications Letters*, vol. 16, pp. 540-543, Apr. 2012.

3. M. Niu, J. Schlenker, J. Cheng, J. F. Holzman, and R. Schober, "Coherent Wireless Optical Communications with Predetection and Postdetection EGC over Gamma-Gamma Atmospheric Turbulence Channels," *IEEE/OSA Journal of Optical Communications and Networking*, vol. 3, no. 11, pp. 860-869, Nov. 2011. (Part of Chapter 5)

4. M. Niu, J. Cheng, and J. F. Holzman, "Exact Error Rate Analysis of Equal Gain and Selection Diversity for Coherent Free-Space Optical Systems on Strong Turbulence Channels," *Optics Express*, vol. 18, no. 13, pp. 13915-13926, June 2010. (Part of Chapter 4)

5. M. Niu, J. Cheng, and J. F. Holzman, "Error Rate Analysis of M-ary Coherent Free-Space Optical Communication Systems with K-Distributed Turbulence" *IEEE Transactions on Communications*, vol. 59, no. 3, pp. 664-668, Mar. 2011. (Part of Chapter 3)

Journal Papers Submitted

1. M. Niu, J. Cheng, and J. F. Holzman, "Alamouti-Type STBC for Atmospheric Optical Communication Using Coherent Detection," Submitted, July 2012. (Part of Chapter 8)

2. M. Niu, J. Cheng, and J. F. Holzman, "A MIMO Architecture for Coherent Optical Wireless Communication: System Design and Performance Analysis," Submitted, Sept. 2012. (Part of Chapter 7)

3. M. Niu, J. Cheng, and J. F. Holzman, "Error Rate Performance Comparison of Coherent and Subcarrier Intensity Modulated Wireless Optical Communications," Submitted, Feb. 2012. (Part of Chapter 6)

Book Chapter

1. M. Niu, J. Cheng, and J. F. Holzman, "Terrestrial Coherent Free-Space Optical Communication Systems," in *Optical Communication*, N. K. Das, Ed. Publisher: In-Tech, Oct. 2012. (Invited)

Conference Papers Published

1. M. Niu, J. Cheng, and J. F. Holzman, "Space-Time Coded MPSK Coherent MIMO FSO Systems in Gamma-Gamma Turbulence," to appear in *Proceedings of IEEE Wireless Communications and Networking Conference*, Shanghai, China, Apr. 7-10, 2013.

2. M. Niu, J. Cheng, and J. F. Holzman, "A Novel Wireless Optical MIMO Architecture and Its Application," to appear in *Proceedings of IEEE International Conference on Computing, Networking and Communications*, San Diego, Jan. 28-31, 2013.

3. M. Niu, J. Cheng, and J. F. Holzman, "Optical MIMO Transmission Using A Heterodyne Receiver in K-Distributed Turbulence Channels," in *Proceedings of IEEE Photonics Society Summer Topical Meetings*, Seattle, WA, July 9-11, 2012.

4. M. Niu, J. Cheng, and J. F. Holzman, "Wireless Multiple-Input Single-Output Optical Links with Coherent Detection," in *Proceedings of the 26th Biennial Symposium on Communications*, Kingston, ON, Canada, May 28-29, 2012.

5. M. Niu, J. Cheng, and J. F. Holzman, "Asymptotic Analyses for Coherent and Subcarrier Modulated Wireless Optical Communications," in *Proceedings of IEEE International Conference on Computing, Networking and Communications*, Maui, Hawaii, USA, Jan. 30-Feb. 2, 2012.

6. M. Niu, J. Cheng, J. F. Holzman, and R. Schober, "Coherent Free-Space Optical Transmission with Diversity Combining for Gamma-Gamma Atmospheric Turbulence," in *Pro-*

ceedings of the 25th Biennial Symposium on Communications, Kingston, ON, Canada, May 12-14, 2010.

7. M. Niu, J. Cheng, and J. F. Holzman, "Diversity Reception for Coherent Free-Space Optical Communications over K-Distributed Atmospheric Turbulence Channels," in *Proceedings of IEEE Wireless Communications and Networking Conference*, Sydney, Australia, Apr. 18-21, 2010.

8. M. Niu, J. Cheng, J. F. Holzman, and L. McPhail, "Performance Analysis of Coherent Free Space Optical Communication Systems with K-Distributed Turbulence," in *Proceedings of IEEE International Conference on Communications*, Dresden, Germany, June 14-18, 2009.

Table of Contents

Appendices

List of Figures

List of Acronyms

Acronyms	Definitions
4G	Fourth-Generation
AC	Alternating Current
AWGN	Additive White Gaussian Noise
BER	Bit-Error Rate
BPSK	Binary Phase-Shift Keying
CDF	Cumulative Distribution Function
CHF	Characteristic Function
CSI	Channel State Information
DC	Direct Current
DPSK	Differential Phase-Shift Keying
DSP	Digital Signal Processing
EDFA	Erbium Doped Fiber Amplifier
EGC	Equal Gain Combining
FASCODE	The Fast Atmospheric Signature Code
FSO	Free-Space Optical
Gbit/s	Gigabit Per Second
HPF	High Pass Filter
i.i.d.	Independent and Identically Distributed
IM/DD	Intensity Modulation with Direct Detection
LO	Local Oscillator

LOS	Line-of-Sight
LPF	Low Pass Filter
MGF	Moment Generating Function
MRC	Maximum Ratio Combining
MIMO	Multiple-Input Multiple-Output
ML	Maximum Likelihood
MLSD	Maximum Likelihood Sequence Detection
MODTRAN	Moderate Resolution Atmospheric Transmission
MPSK	M-ary Phase-Shift Keying
NASA	The National Aeronautics and Space Administration
NCFSK	Noncoherent Frequency-Shift Keying
NEC	Nippon Electric Company
OOK	On-Off Keying
OWC	Optical Wireless Communications
PDF	Probability Density Function
PLL	Phase-Locked Loop
PPM	Pulse Position Modulation
RF	Radio Frequency
QPSK	Quadrature Phase-Shift Keying
RV	Random Variable
S+N	Signal-Plus-Noise
SC	Selection Combining
SIM	Subcarrier Intensity Modulation
SISO	Single-Input Single-Output
SIMO	Single-Input Multiple-Output
SNR	Signal-to-Noise Ratio

STBC	Space-Time Block Coding
STC	Space-Time Coding
STTC	Space-Time Trellis Coding

List of Symbols

Symbols	Definitions
$E[\cdot]$	Statistical expectation of a random variable
$Q(\cdot)$	Gaussian Q-function
$\Re\{\cdot\}$	The real part of a complex quantity
$\Im\{\cdot\}$	The imaginary part of a complex quantity
$n!$	The factorial of a positive integer n
$\mathrm{erfc}(\cdot)$	Complementary error function
$K_x(\cdot)$	Modified Bessel function of the second kind of the order x
$\Gamma(\cdot)$	Gamma function
$\Gamma(\cdot,\cdot)$	Upper incomplete Gamma function
${}_1F_1(\cdot,\cdot;\cdot)$	Confluent hypergeometric function
$M(\cdot,\cdot;\cdot)$	Kummer confluent hypergeometric function, same as ${}_1F_1(\cdot,\cdot;\cdot)$
${}_2F_1(\cdot,\cdot,\cdot;\cdot)$	Gaussian hypergeometric function
${}_1F_2(\cdot,\cdot,\cdot;\cdot)$	A generalized hypergeometric function
$M_{\cdot,\cdot}(\cdot)$	Whittaker function
$I_0(\cdot)$	Modified Bessel function of the first kind of the zeroth order
$o(x)$	A function $g(x)$ written as $o(x)$ if $\lim_{x\to 0} g(x)/x = 0$
Δf	Noise equivalent bandwidth of a photodetector
$B(\cdot,\cdot)$	Beta function
C_n^2	Index of refraction structure parameter
$D_\rho(\cdot)$	Parabolic cylinder function of the ρth order

σ_R^2	Rytov variance
σ_{si}^2	Scintillation index
$M_G(\cdot)$	Moment generating function of a random variable G
$\Phi_G(\cdot)$	Characteristic function of a random variable G
j	$j = \sqrt{-1}$
x^*	Complex conjugate of x
$x * y$	Convolution of x and y
R	Photodetector responsivity
$\Pr\{\cdot\}$	The probability of an event
$\mathbf{N}$	Collection of all nature numbers
$\mathcal{F}(\cdot)$	The Fourier transform of the complementary error function $\mathrm{erfc}(\cdot)$
$Ei(\cdot,\cdot)$	Exponential integration function
G_c	Coding gain of a wireless digital communication system
G_d	Diversity order of a wireless digital communication system

Acknowledgments

I would like thank my supervisors Prof. Julian Cheng and Prof. Jonathan F. Holzman for welcoming me to the group. I am so glad to have known them and work with them during my Ph.D. program. They granted me great flexibility and freedom in my research work. I am deeply grateful to my supervisors for their enthusiasm, guidance, advice, encouragement, support, and teaching me the academic and research skills. I will continue to be influenced by their rigorous scholarship, clarity in thinking, professional integrity, and their way in conducting research and teaching in my career. All I want to say is that I can hardly ask for more from supervisors, it is my honor to study and research under their supervision.

I would like to thank Prof. Robert Schober from the Department of Electrical and Computer Engineering for serving as the external examiner on my Ph.D. candidacy exam committee. I would like to express my thanks to Prof. John Q. Liu from Wayne State University, Detroit, MI for his willingness to serve as my Ph.D. defense external examiner. I would also like to thank Prof. Kenneth Chau, Prof. Heinz Bauschke from the Mathematics department, Prof. Stephen O'Leary and Prof. Thomas Johnson for serving on my doctoral examination committee. I really appreciate their valuable time and constructive comments on my thesis.

I owe many people for their generosity and support during my Ph.D. study at the University of British Columbia. I would like to thank my dear colleagues Chiun-Shen Liao, Junfeng Zhao, James Jianchen Sun, Xuegui Song, Xian Jin, Nick Kuan-Hsiang Huang, Chris Collier, Ning Wang, Nianxin (Nathan) Tang, Xianchang Li, and Yeyuan Xiao for sharing their academic experiences and constructive viewpoints generously with me during our discussions. I would also like to thank my dear friends Nan Wang, Kai Cai, Feng (Vicki) Wei, Luyan (Maggie) Mei, and Haibo Feng for

sharing in my excitement and encouraging me when I was frustrated during this journey. I would also like to thank all my friends in Vancouver, Edmonton, Santa Clara, Singapore, Hangchow, and Xi'an.

Special thanks go to my lovely family, for the endless and unconditional love, believing in me, and constant encouragement and support in my studies. This thesis is dedicated to the whole family as a token of my gratitude.

Finally, I would like to thank my parents for their patience, understanding and support over all these years. All my achievements would not have been possible without their constant encouragement and support.

Chapter 1

Introduction

1.1 Background and Motivation

In the past three decades, the demand for high-speed data communications has increased exponentially, and fiber optical communications has been applied as the backbone of the developed data transmission links. Optic fiber has numerous advantages over existing copper wire in long-distance and high-demand applications. However, optic fiber deployment in certain urban areas has proven to be difficult and time-consuming, and carry high infrastructure development costs [1]. Therefore, fiber optic communication systems have primarily been installed in ultra long-distance applications to make full use of their transmission capacity and offset the increased infrastructure cost [2].

In dense urban areas [3] or places where optical fiber infrastructure does not exist, outdoor optical wireless communication (OWC) systems, also known as free-space optical (FSO[1]) communication systems, have been considered. OWC uses light beams to transmit signals through free-space and typically requires line-of-sight (LOS) transmission links. The transmitter and receiver at both networking locations must "see" each other. An early light communications experiment was reported in a 1880 photophone patent in which Alexander G. Bell used a voice signal to modulate sunlight intensity and tested the link over hundreds of feets [4]. The discovery of new optical sources such as lasers in the 1960s started the development of practical OWC technology [5]. The original white paper on OWC, written by Dr. Erhard Kube, "Information transmission by light beams through the atmosphere," was published in German in *Nachrichtentechnik*, June 1968. In

[1] In this thesis, we will use the acronyms OWC and FSO interchangeably.

the same year, Honeywell built a frequency modulation based optical heterodyne communication system for the NASA Marshall Space Flight Center which demonstrated the receiver sensitivity improvement of coherent detection. Later, NEC Corporation developed the first wireless laser link for commercial use in 1970 [6]. From that time on, OWC has been continuously studied and used mainly in military and deep-space communications [7], [8]. Over the past decade, new advances in OWC techniques and devices have led to the rebirth of this optical broadband access technology. OWC is considered as an attractive technology for high-speed data transmission in future heterogeneous wireless communication networks [9]. Lower costs, larger license-free bandwidths, better information security, greater link flexibility, and a reduced time-to-market are all significant benefits of the OWC systems [1], [3], [10]. Whereas optical fiber is a predictable medium, OWC links can suffer from cloud coverage and harsh weather conditions, leading to atmospheric effects which degrade the system availability and performance. Rain, snow, sleet, fog are atmospheric properties that affect our viewing of distant objects [1], and these factors can affect the transmission of optical beams through the atmosphere. In these cases, radio frequency (RF) communication links could be used as back-ups. (More details on these RF/FSO hybrid communication systems can be found in [11], [12] and the references therein.)

There are three primary atmospheric factors that can affect optical beam propagation: absorbtion, scattering, and refractive index fluctuations (i.e., optical turbulence). Absorption and scattering are often grouped together under the topic of extinction, which is defined as the reduction or attenuation in the amount of radiation transmitted through the atmosphere. They are both deterministic effects and can be predicted by software packages such as FASCODE [13] or MODTRAN [14] as a function of the optical wavelength. Optical turbulence is considered as the most serious effect on propagating beams through atmospheric channels. To facilitate practical system design for OWC systems, this thesis will study the impacts from turbulence and/or phase noise on coherent OWC links as well as turbulence mitigation techniques for coherent OWC links.

1.2 Preliminaries

Coherent fiber optical communications attracted considerable attention in the late 1980s for its ability to approach the theoretical receiver sensitivity limit [15]. Since the invention of erbium doped fiber amplifier (EDFA), coherent fiber optical communication became less attractive because similar sensitivity can be achieved by EDFAs with reduced receiver complexity. However EDFAs can be expensive for certain OWC applications.

With recent advances in digital signal processing (DSP), coherent optical communication has received considerable recent attention [16]. OWC systems have great potential for improving channel usage when implemented with coherent detection [17]. It should be noted that the term "coherent" used in this thesis refers to a system where a local oscillator (LO) optical wave is added to the incoming optical signal at the receiver, and it is not necessary for the following electrical demodulation processes to have knowledge of the carrier phase and frequency information [18]. This definition is significantly different from that used in classical RF communications literature.

In general, a coherent OWC system uses a receiver which combines the received signal beam optically with a LO beam to produce an AC photocurrent signal. This AC photocurrent is proportional to the received optical signal electric field. In contrast, direct detection based OWC uses a photodetector to perform direct power detection in which the converted AC photocurrent is proportional to the optical signal power. One scheme of coherent optical detection is called homodyne detection, where the receiver demodulates the optical signal directly to the baseband because the LO laser frequency is synchronized to the optical signal carrier frequency. However, it can be unstable and costly to perform optical synchronization in practice. As a result, heterodyne detection is introduced to simplify the receiver design and make coherent OWC systems more applicable.

In heterodyne detection, the optical signal is first converted to an electrical signal with an intermediate frequency. Then a phase noise compensation scheme is used to track the phase noise of the signal. The received signals in coherent OWC systems can be made to be limited only by the shot noise given a sufficiently large LO beam power. The advantages of coherent OWC systems

with phase noise compensation over direct detection based OWC systems are excellent background noise rejection, higher sensitivity, and improved spectral efficiency [19].

An optical wave propagating through the atmosphere will experience irradiance fluctuations, also referred to as optical scintillation or turbulence-induced fading. Optical scintillation is caused by random fluctuations of refractive index due to temperature and pressure variations along the optical beam propagation path. Under a weak turbulence and plane wave assumption, the resulting irradiance fluctuations can be characterized by the Rytov variance defined as [1]

$$\sigma_R^2 = 1.23 C_n^2 k^{\frac{7}{6}} L_t^{\frac{11}{6}} \tag{1.1}$$

where C_n^2 stands for the index of refraction structure parameter in $m^{-2/3}$, $k = 2\pi/\lambda_w$ is the optical wave number (λ_w denotes the wavelength), and L_t is the transmission path length between the transmitter and receiver. C_n^2 is a measure of the strength of the fluctuations in the refractive index of the atmosphere and is an altitude-dependent variable. The most commonly used Hufnagel-Valley model for C_n^2 is [20]

$$C_n^2 = 0.00594 \left(\frac{v_w}{27}\right)^2 (h \times 10^{-5})^{10} e^{-\frac{h}{1000}} + 2.7 e^{-\frac{h}{1500}} \times 10^{-16} + A_c e^{-\frac{h}{100}} \tag{1.2}$$

where v_w is the root-mean-square wind speed in meters per second, h is the altitude in meters, and A_c is the nominal value of C_n^2 at the ground. The C_n^2 value can be related to changes in the refractive index δn over a distance R_i through [21]

$$\overline{(\delta n)^2} = C_n^2 R_i^{\frac{2}{3}} \tag{1.3}$$

where the overbar represents an ensemble average operator, and R_i lies within the inertial subrange [22] of atmospheric turbulence. The value of C_n^2 varies from approximately $10^{-17} m^{-2/3}$ for weak turbulence conditions to $10^{-13} m^{-2/3}$ for strong turbulence conditions [23]. Other models for the

vertical profile of C_n^2 can be found in [24]. For an average value of $C_n^2 = 10^{-15} m^{-2/3}$, δn is on the order of 10^{-6}.

The scintillation index is another important parameter related to the atmospheric turbulence level, and it is defined as the normalized variance of irradiance fluctuations

$$\sigma_{si}^2 = \frac{E[I^2] - (E[I])^2}{(E[I])^2} = \frac{E[I^2]}{(E[I])^2} - 1 \tag{1.4}$$

where I is the instantaneous optical irradiance, and $E[\cdot]$ denotes the expectation operation.

In weak turbulence regimes (when the scintillation index is less than unity), the scintillation index is found to be proportional to the Rytov variance [20]. When the optical turbulence strength extends to moderate-to-strong irradiance fluctuation regimes (when the scintillation index is greater than unity with increased C_n^2 and/or path length L_t), the scintillation index for a plane wave and that for a spherical wave with negligible inner-scale effects are, respectively, related to the Rytov variance through [25]

$$(\sigma_{si}^2)_{plane} = \exp\left(\frac{0.54\sigma_R^2}{(1+1.22\sigma_R^{\frac{12}{5}})^{\frac{7}{6}}} + \frac{0.509\sigma_R^2}{(1+0.69\sigma_R^{\frac{12}{5}})^{\frac{5}{6}}}\right) - 1 \tag{1.5}$$

and

$$(\sigma_{si}^2)_{sphere} = \exp\left(\frac{0.17\sigma_R^2}{(1+0.167\sigma_R^{\frac{12}{5}})^{\frac{7}{6}}} + \frac{0.225\sigma_R^2}{(1+0.259\sigma_R^{\frac{12}{5}})^{\frac{5}{6}}}\right) - 1. \tag{1.6}$$

The performance of OWC systems can be significantly degraded by the turbulence-induced fading as random fluctuations of the received beam may drive the signal to drop below a predetermined detection threshold.

To study and predict the effects of turbulence-induced fading on OWC system performance, the scientific community has introduced a variety of statistical models to describe the turbulence-induced fading in atmospheric channels. Of these turbulence-induced fading models, the most widely used models are the lognormal turbulence model (typically describing irradiance fluctua-

tions in weak turbulence conditions), K-distributed turbulence model (typically describing irradiance fluctuations in strong turbulence conditions), negative exponential turbulence model (suitable for describing the limiting case of optical scintillation in saturation regimes), and Gamma-Gamma turbulence model (providing a description of much wider irradiance fluctuation ranges across the weak-to-strong turbulence regimes).

1.3 Literature Review

OWC has great potential for applications in fourth-generation (4G) wireless systems [26] and can be a key building block for future wide-area wireless data networks [27], [28], [29]. Such networks will encompass a number of complementary access technologies with high channel capacities, multiple transceivers, and gigabit per second (Gbit/s) data rates.

In order to evaluate the FSO system performance, an accurate turbulence model is needed. In early studies, the lognormal distribution was used as the turbulence model in [17], [30], [31]. Although the lognormal distribution is one of the most widely used turbulence models, this probability density function (PDF) is only applicable for weak turbulence conditions. It was shown in [32], [33] that the K-distributed turbulence model provides good agreement with experimental data for radiation scattered by strong turbulence. The negative exponential model is well accepted for describing the saturated irradiance fluctuations [34], [35]. In a recent series of papers on scintillation theory [25], [36], Andrews *et al.* introduced the modified Rytov theory, and Al-Habash *et al.* proposed the Gamma-Gamma PDF as a tractable mathematical model for a wide range of atmospheric turbulence levels. The Gamma-Gamma turbulence model also has the K-distributed model and negative exponential model as its special cases. Other statistical models proposed in the FSO literature to describe atmospheric turbulence are the lognormal-Rician, Rayleigh, and $I-K$ models [37], [38], [39], [40].

The performance of IM/DD OWC systems for different turbulence models has been well stud-

ied in the literature. Zhu and Kahn studied the maximum likelihood sequence detection scheme for IM/DD FSO links [41]. They further studied the pairwise error probability of coded FSO links assuming the turbulence to be lognormal distributed [31]. In [42], Uysal *et al.* studied the pairwise error probability of on-off keying (OOK) FSO links with temporally correlated K-distributed turbulence. Riediger *et al.* investigated a multiple symbol detection decision metric for FSO systems in both lognormal and Gamma-Gamma turbulence [43]. Since FSO communication requires LOS links, pointing errors can affect the FSO system performance if the detector aperture size is small (non-negligible compared to the beam spot size). More details and recent research on pointing accuracy can be found in [44], [45], [46].

In the FSO literature, several techniques have been proposed to mitigate the turbulence fading effects. These techniques include error-control coding, aperture averaging, adaptive optics, and spatial diversity at both transmitter and receiver. Since turbulence channels are typically slowly changing, effective use of error-control coding requires large interleaver size in order to render the fading channel to be memoryless. This causes a large latency from a few milliseconds to hundreds of milliseconds. Aperture averaging generally requires large photodetector area, and it is effective when the lens diameter D_a is larger than $\sqrt{\lambda_w L_t}$. When the detector collection aperture reaches a certain size, further increases will not reduce the scintillation level [20]. Adaptive optics attempts to correct lightwave distortion by measuring the atmospheric induced distortion using a wavefront sensor. A deformable mirror and a receiver micro-computer are needed to correct the distortion. Such an implementation is complex and costly.

Spatial diversity reception is an effective technique to mitigate turbulence effects. Ibrahim and Ibrahim first proposed the use of spatial diversity for OWC systems [47]. Lee and Chan showed that equal gain combining (EGC) and optimal combining can enhance the link outage performance over independent lognormal turbulence channels [30]. Navidpour *et al.* studied BERs of multiple-input multiple-output (MIMO) OWC systems with both independent and correlated lognormal turbulence [48]. In [41], Zhu and Kahn studied a symbol-by-symbol maximum likelihood

detector with spatial diversity in correlated lognormal turbulence. In [49] and [50], Wilson *et al.* investigated MIMO OWC links employing pulse-position modulation (PPM) and Q-ary PPM with both Rayleigh and lognormal turbulence-induced fading. In a recent work, Tsiftsis *et al.* studied the K-distributed turbulence OWC link performance for an OOK IM/DD system using optimal combining, EGC, and selection combining [51]. BER solutions that require multi-dimensional integrations were presented, and approximate BER expressions were given using the Gaussian quadrature rule and an error function approximation. Bayaki *et al.* studied MIMO IM/DD OWC links over the Gamma-Gamma turbulence, and demonstrated a significant performance improvement by exploiting both transmitter and receiver diversity [52].

OOK is the most commonly used signal modulation format for IM/DD OWC systems owing to its simplicity and low cost. However, an OOK based system requires adaptive detection thresholds to achieve its optimal error rate performance. Such a system, if feasible, may be costly to implement and is subject to channel estimation errors. For simplicity, practical OOK based OWC systems are often implemented with a predetermined fixed detection threshold. This suboptimal scheme will lead to performance loss with undesirable irreducible error floors, which are more severe under strong turbulence conditions [53], [54]. In [53], Li *et al.* theoretically studied the effect of a fixed threshold for IM/DD systems with OOK modulation. The authors pointed out that the BER of OOK modulation is determined by both the turbulence level and the fixed detection threshold, and therefore it can not be made arbitrarily small in the presence of atmospheric turbulence by increasing SNR. PPM modulation has been proposed as an alternative to the OOK modulation, and its performance has been studied in atmospheric turbulence channels in [8], [49], [55]. However, PPM modulation needs a complex transceiver design because of the tight synchronization requirements, and it also suffers from poor bandwidth efficiency. Subcarrier intensity modulation (SIM) was first proposed by Huang *et al.* for OWC applications [54]. The authors studied the error rate performance for differential PSK (DPSK) and M-ary PSK (MPSK) modulations over the lognormal turbulence channels. Their theoretical analysis was also confirmed by experimental

results. The superiority of SIM to OOK modulation in the presence of atmospheric turbulence was also demonstrated. The error rate performance of SIM OWC systems employing various modulations over different atmospheric turbulence channels were then studied extensively in [53], [56], [57], [58]. However, these works did not provide accurate closed-form error rate expressions for the subcarrier modulations. Recently, Chatzidiamantis *et al*. proposed an adaptive subcarrier PSK system and studied the system performance over lognormal and Gamma-Gamma turbulence channels with approximate and exact error rate expressions in terms of the Meijer's G-function [59]. Using a direct integration approach, Song *et al.* studied the error rate of a subcarrier intensity modulated OWC system employing a variety of modulations over a single Gamma-Gamma turbulence link [60].

Unlike direct direction schemes, coherent optical signals are detected from the phase information carried on electric fields. Coherent OWC is an attractive alternative to OWC using direct detection. It offers improved frequency/spatial selectivity, higher spectral efficiency, better background noise rejection and increased detector sensitivity (compared to direct detection) while eliminating the need of the adaptive threshold in the IM/DD OOK systems. The main feature of coherent OWC systems is that the receiver of a coherent OWC system is limited only by LO induced shot noise when the power of the LO is sufficiently high. This is a significant difference from the intensity modulation based OWC systems, in which background and/or thermal noise are the dominant noise factors. Some early work on coherent OWC can be found in [17] and [61]. Recently, a comparison study was carried out by Lee and Chan [62] and showed performance improvement of coherent detection over IM/DD detection in a lognormal environment. The authors compared the IM/DD PPM and coherent BPSK OWC systems and demonstrated theoretically that coherent OWC systems can lead to lower error rates. It was also found that coherent detection can provide additional outage probability improvement over direct detection [62].

Kiasaleh developed an exact BER expression for DPSK OWC over K-distributed turbulence channels [63]. Tsiftsis evaluated the BER performance of coherent OWC with DPSK in Gamma-

Gamma distributed turbulence [64]. In both works, however, a detailed system model and receiver SNR analysis for coherent OWC links were not presented. Sandalidis *et al.* studied a heterodyne OWC system with pointing errors for Gamma-Gamma turbulence channels [45]. The authors derived closed-form fading statistics expressions that take into account both the turbulence and pointing error effects. In [65], Belmonte and Kahn developed a statistical model considering spatial phase noise with lognormal turbulence and performed a capacity evaluation [66], [67]. In [68] and [69], we studied the error rate performance of coherent OWC systems with MRC, EGC, and selection diversity reception in strong turbulence regions. Recently, Belmonte and Kahn studied the performance of a coherent OWC link with a large effective aperture [70]. Aghajanzadeh and Uysal adopted the receiver model in [66] and studied the diversity-multiplexing tradeoff and the finite-SNR diversity gain for a single-input multiple-output coherent OWC system [71]. In [72], Basak and Jalali experimentally demonstrated a linearized coherent optical receiver with high optical power dynamic range. A recent experiment carried out by Lange *et al.* has demonstrated that a coherent OWC system using a homodyne BPSK scheme can support a data rate of 5.625 Gbit/s over 142 km distance [73]. Cvijetic *et al.* studied a polarization-multiplexed coherent optical wireless transmission system where the phase information is modulated onto two orthogonal-polarization signal beams [74]. The authors experimentally showed that polarization-multiplexing QPSK can outperform IM/DD OOK by 14 dB in a 112 Gb/s coherent OWC link (within 2 km).

Space-time coded systems have demonstrated their usefulness in RF applications [75]. There are two types of space-time coding schemes: space-time trellis coding and space-time block coding (STBC). It is found that the complexity of the space-time trellis coding increases exponentially as a function of the diversity order and transmission rate [76]. To reduce the decoding complexity, Alamouti proposed a STBC scheme for RF wireless transmission with two transmitters [75]. The Alamouti space-time code can be readily adopted to OWC systems using direct detection with a positive bias added to the signal (as irradiance modulations are inherently positive). Recently, Simon and Vilnrotter proposed a modified Alamouti code [77] for OWC using direct detection by

employing OOK and PPM. In [78], Park *et al.* studied the BER performance of a subcarrier BPSK modulated OWC link using Alamouti-type STBC.

It is known that a simple scheme that sends the same information (i.e., repetition coding) at each transmitter will not achieve transmit diversity in coherent OWC turbulent links [79], [80]. In [80], Haas *et al.* presented a space-time codes design criterion for OWC links using heterodyne detection in lognormal turbulence. In [81], Bayaki and Schober presented simplified space-time codes design criteria for coherent and differential OWC links in Gamma-Gamma turbulence. However, a detailed system architecture was neither given nor described in both works. Ntogari *et al.* recently studied an indoor 2×2 STBC OWC system using coherent detection, and investigated its error rate performance numerically [82]. However, additional phase noises from different laser transmitters were not considered. Furthermore, the authors did not consider the turbulence-induced fading nor the turbulence-induced phase noise. In [83], we introduced an optical MIMO architecture using the concept of *wavelength diversity* [84] for coherent OWC links, and studied the error rates of such links employing quadrature phase-shift keying (QPSK) in [85].

1.4 Thesis Organization and Contributions

This thesis consists of nine chapters. Chapter 1 presents background knowledge of OWC history and development. This chapter also provides some FSO preliminaries and a comprehensive review of FSO literature pertaining to this thesis.

Chapter 2 describes essential technical background for the entire thesis. First, we introduce the basic concept and composition of a coherent OWC link as well as the instantaneous SNR statistics. Second, we present and classify several atmospheric turbulence models for different ranges of the scintillation level. Third, we describe three major spatial diversity schemes for fading mitigation. Finally, we present fundamentals of asymptotic analysis which will be used to study the error rate performance of FSO systems in large SNR regimes.

Chapter 3 derives closed-form moment generating function (MGF) expressions of the K-distributed turbulence. We use the derived MGF expressions to study the error rate performance for BPSK and DPSK of a SISO OWC link over strong turbulence. Furthermore, we introduce an asymptotic BER solution for BPSK based OWC links using the derived MGF expression. The results from our study allow precise BER performance evaluations for SISO coherent links under strong turbulence conditions, and suggest that we must adopt powerful turbulence mitigation techniques to overcome the performance impairment.

Chapter 4 uses the spatial diversity technique to mitigate the strong turbulence impacts on OWC links. We first derive a closed-form characteristic function (CHF) expression of the squareroot of the K-distributed random variable. Based on the MGF obtained in Chapter 3 and the CHF expressions of the K-distributed turbulence, we study the error rate performance of coherent OWC systems employing MRC, EGC and SC schemes. Based on our numerical results, we demonstrate the efficiency and usefulness of diversity reception techniques in enhancing the performance of coherent OWC links. We also find that the EGC scheme can offer comparable performance to that of the MRC scheme. Through the diversity order analysis, we further show that the MRC, EGC and SC schemes all achieve the same diversity order, which is equal to the number of diversity branches.

Chapter 5 first generalizes the analysis from strong turbulence channels to the Gamma-Gamma turbulence channels. We then investigate the system performance loss of coherent PSK EGC links caused by phase noise compensation error. We find that a small phase noise compensation error, when the standard deviation of the phase noise compensation error is kept below twenty degrees, will only suffer 1 dB or less SNR loss for two- and three-branch OWC links using the EGC scheme. When the standard deviation of the phase noise compensation error increases further, the coherent OWC link will be subject to large performance degradation. We propose an alternative technique employing DPSK with postdetecion EGC for coherent OWC links. Our analytical results show that the proposed technique is robust to phase noise within a coherent OWC link and thus can be a

viable choice in situations where large phase noise compensation errors are present.

Chapter 6 compares the BER performance of coherent and SIM BPSK systems. Since it is known that both coherent and SIM BPSK systems can achieve their optimal performance without the need of an adaptive detection threshold, it is of interest to compare the error rate performance of these two different types of OWC systems. The error rate performance comparison is carried out for MRC, EGC and SC schemes over the Gamma-Gamma turbulence channels. We also derive the diversity orders and coding gains for both systems through asymptotic analyses. With an assumption of the same path loss and average transmitted signal power, a performance comparison is carried out through BER versus average transmitted optical power. Our investigation shows that coherent OWC systems outperform SIM OWC systems under weak-to-strong turbulence conditions.

Chapter 7 proposes an optical MIMO architecture for coherent OWC links based on wavelength diversity. We study the BER and outage probability performance of the proposed architecture over the Gamma-Gamma turbulence channels. Our numerical results demonstrate the usefulness and the performance improvement of the proposed architecture with increased number of transmitters and/or receivers.

Chapter 8 introduces space-time coding to coherent OWC links by proposing two new Alamouti-type STBC coherent systems for atmospheric optical communications. Detailed signal processing flows are described. We develop an exact closed-form SER expression using a series expansion approach for coherent MPSK OWC systems employing STBC. Both truncation error and asymptotic error rate analyses are also presented. Our truncation error analysis shows that our series solutions are highly accurate and efficient. We also show that the proposed STBC systems can be extended to 2×2 systems to provide an enhanced diversity order in the Gamma-Gamma turbulence.

Chapter 9 summarizes the thesis. In addition, some further projects related to this thesis are suggested.

Chapter 2

Background on Coherent Atmospheric Optical Communication Systems

In this chapter, we first introduce some basic concepts and the composition of a coherent OWC system. We then present background knowledge on some widely used atmospheric turbulence channels. Finally, we review some important spatial diversity techniques as well as the asymptotic technique.

2.1 Coherent Optical Wireless System Model

The block diagram of a typical coherent FSO system is shown in Fig. 2.1 where the information data is modulated on the electric field of an optical signal beam. For a single link, the modulated electric field at the output of a laser transmitter is

$$e_{tx}(t) = E_0 \exp(j\omega_c t + j\phi + j\phi_t) \tag{2.1}$$

where E_0 denotes the amplitude of the transmitted electric field, $j = \sqrt{-1}$, ϕ denotes the encoded phase information, ω_c is the carrier frequency of the signal beam, and ϕ_t is the transmitter laser phase noise.

After the optical signal beam is transmitted through a free-space channel, the received optical signal is mixed with the LO beam. We can express the mixed beam incident on the photodetector

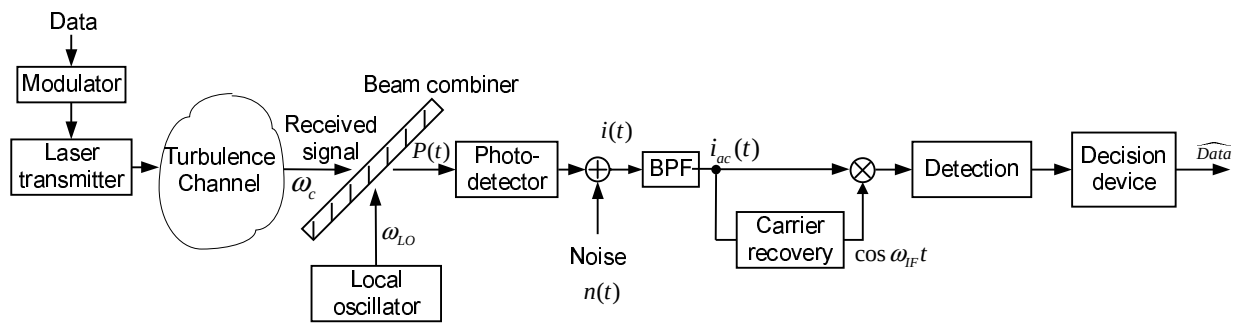

Figure 2.1: Block diagram of a typical coherent FSO system operating through an atmospheric turbulence channel.

in terms of electric fields as

$$e_{\text{combine}}(t) = E_s \exp(j\omega_c t + j\phi + j\phi_{tc}) + E_{LO} \exp(j\omega_{LO} t + j\phi_{LO}) \tag{2.2}$$

where E_s is the received electric field amplitude which is subject to optical scintillation, E_{LO} denotes the amplitude of the LO electric field, ω_{LO} is the frequency of the LO beam, $\phi_{tc} = \phi_t + \phi_c$ is the overall phase noise from the transmitter to the input of the coherent receiver with ϕ_c denoting the phase noise induced from a turbulent channel, and ϕ_{LO} denotes the LO phase noise arising within the coherent receiver. Using kilohertz linewidth lasers, transmitter/LO phase noises and the turbulence are varying on the order of milliseconds and have little change over the duration of hundreds of consecutive information bits. The overall phase noise therefore varies slowly compared to the high data rates in OWC systems.

Next we illustrate the photocurrent generated in the coherent receiver. From (2.2), we can write the incident mixing optical power as

$$\begin{aligned} P(t) &= e_{\text{combine}}(t) e^*_{\text{combine}}(t) \\ &= E_s^2 + E_{LO}^2 + E_s E_{LO} \exp(j(\omega_c - \omega_{LO})t + j\phi + j(\phi_{tc} - \phi_{LO})) \\ &\quad + E_{LO} E_s \exp(j(\omega_{LO} - \omega_c)t - j\phi + j(\phi_{LO} - \phi_{tc})) \\ &= \underbrace{E_s^2}_{P_s} + \underbrace{E_{LO}^2}_{P_{LO}} + 2\underbrace{E_s E_{LO}}_{\sqrt{P_s P_{LO}}} \cos((\omega_c - \omega_{LO})t + \phi + \phi_{tc} - \phi_{LO}) \end{aligned} \tag{2.3}$$

where the superscript * denotes the complex conjugate operation. Therefore, we find the total optical power incident on the photodetector[2] as

$$P(t) = P_s + P_{LO} + 2\sqrt{P_s P_{LO}}\cos(\omega_{IF}t + \phi + \phi_{tc} - \phi_{LO}) \tag{2.4}$$

where P_s is the received optical signal power, P_{LO} denotes the LO power, and $\omega_{IF} \triangleq \omega_c - \omega_{LO}$ denotes the intermediate frequency. Using the fact that the photocurrent from the photodetector is the product of the responsivity R and the incident optical power, the detected photocurrent can be expressed as $i(t) = i_{dc} + i_{ac}(t) + n(t)$ [68] where

$$i_{dc} = R(P_s + P_{LO}) \approx RP_{LO} \tag{2.5}$$

and

$$i_{ac}(t) = 2R\rho\sqrt{P_s P_{LO}}\cos(\omega_{IF}t + \phi + \phi_{tc} - \phi_{LO}) \tag{2.6}$$

represent the respective DC and AC terms in the received photocurrent, and $n(t)$ is a zero-mean additive white Gaussian noise (AWGN) process due to shot noise. In (2.6), ρ is a system constant and its value depends on the efficiency of optoelectronic conversion. Without losing generality, we assume that ρ is unity. Here we define $\phi_n = \phi_{tc} - \phi_{LO}$ as the total phase noise within an optical turbulence link. In practice, an OWC system can be employed with $P_{LO} \gg P_s$, and thus the DC term in (2.5) can be approximated by the dominant term RP_{LO}. For the same argument, the photocurrent due to thermal noise and dark current are negligible compared to RP_{LO}. The variance of the shot noise process $n(t)$ can be found as $\sigma^2_{n(t)} = 2q_e RP_{LO}\Delta f$ [86], where q_e is the electronic charge, and Δf denotes the noise equivalent bandwidth (NEB) of the photodetector.

The SNR of an optical receiver is defined as the ratio of the time-averaged AC photocurrent

[2] A sufficiently small photodetector area is assumed here, thus, we consider temporal phase noise from transmitter, LO as well as turbulence channel.

power to the total noise variance [87], and it can be expressed as

$$\gamma = \frac{\langle i_{ac}^2(t)\rangle}{\sigma_{tot}^2} \approx \frac{\langle i_{ac}^2(t)\rangle}{\sigma_{n(t)}^2} \tag{2.7}$$

where $\langle\cdot\rangle$ denotes the time average, and σ_{tot}^2 is the total noise variance.

For coherent detection with M-ary constant amplitude modulation, we define E_M to be the average symbol energy of the M-ary constellation. As a result, we can write the instantaneous SNR per symbol as

$$\gamma = \frac{RE_M A}{q\Delta f} I_s = \frac{\eta_e E_M A}{h\nu\Delta f} I_s \tag{2.8}$$

where η_e denotes the quantum efficiency of the photodetector, h is Planck's constant, and ν denotes the frequency of the received optical signal. Note that the instantaneous SNR is independent of the LO power P_{LO}.

2.2 Atmospheric Turbulence Channels

2.2.1 Lognormal Turbulence

When the optical channel is considered as a clear-sky atmospheric turbulence channel with several hundred meters propagation distance, the optical irradiance fluctuations can be modeled as a lognormal distribution. The corresponding scintillation index for the lognormal turbulence is less than unity. Although a lognormal model can be valid for longer propagation distances, the condition $\sigma_{si}^2 < 1$ limits the lognormal model valid only for a small index of refraction structure constant C_n^2 [63].

For weak turbulence conditions, Parry [88], Phillips and Andrews [89] independently suggested a lognormal PDF to model the irradiance, which is the power density of the optical beam. With a

log-scale parameter λ, the lognormal PDF of the irradiance I_s can be expressed as [20]

$$f_{I_s}(I_s) = \frac{1}{I_s\sqrt{2\pi\sigma_x^2}} \exp\left\{-\frac{(\ln I_s - \lambda)^2}{2\sigma_x^2}\right\}, \quad I_s \geq 0. \tag{2.9}$$

The nth moment of the lognormal PDF is

$$E[I_s^n] = \exp\left(n\lambda + \frac{n^2\sigma_x^2}{2}\right). \tag{2.10}$$

If we let $\lambda = -\frac{1}{2}\sigma_x^2$, the mean irradiance can be normalized to be $E[I_s] = 1$, and it can be shown from (1.4) that $\sigma_x^2 = \sigma_{si}^2$ represents the scintillation index.

2.2.2 K-distributed Turbulence

One of the widely accepted models under the strong turbulence regime is the K-distributed turbulence model. In the 1970s, Jakeman *et al.* introduced this turbulence model for a non-Rayleigh sea echo. They have shown that the K-distribution arises from the limiting form when the average number of multipath fluctuations becomes large in the random sinusoid model [90]. Then Phillips and Andrews proved the validity of this K-distribution by experiments in the strong turbulence regimes [88], [89]. The K-distribution is an accurate model of turbulence if moderate propagation distances are encountered ($\sim$1 km) or the scintillation index is confined to the range (2, 3) [63].

The PDF of the K-distributed turbulence is [63]

$$f_{I_s}(I_s) = \frac{2}{\Gamma(\alpha)\eta^{\alpha+1}} \alpha^{\frac{\alpha+1}{2}} I_s^{\frac{\alpha-1}{2}} K_{\alpha-1}\left(\frac{2}{\eta}\sqrt{\alpha I_s}\right), \quad I_s \geq 0 \tag{2.11}$$

where $\Gamma(\cdot)$ denotes the Gamma function, $K_x(\cdot)$ is the modified Bessel function of the second kind of order x, η^2 is the mean irradiance of the optical signal, α is a channel parameter related to the effective number of discrete time scatterers or scintillation index. The nth moment of the K

distribution can be shown to be

$$E[I_s^n] = \frac{\Gamma(\alpha+n)\eta^{2n}n!}{\alpha^n\Gamma(\alpha)}. \tag{2.12}$$

2.2.3 Gamma-Gamma Turbulence

In [25], Andrews *et al.* proposed the modified Rytov theory which defines the optical field as a function of perturbations due to large-scale and small-scale atmospheric effects. This leads to the Gamma-Gamma turbulence model. The PDF of the Gamma-Gamma distribution is

$$f_{I_s}(I_s) = \frac{2(\alpha\beta)^{(\alpha+\beta)/2}}{\Gamma(\alpha)\Gamma(\beta)I_0}\left(\frac{I_s}{I_0}\right)^{\frac{\alpha+\beta}{2}-1} K_{\alpha-\beta}\left(2\sqrt{\alpha\beta\frac{I_s}{I_0}}\right), \quad \alpha>0,\ \beta>0,\ I_s\geq 0 \tag{2.13}$$

where I_0 denotes the mean irradiance, α and β represent, respectively, the effective number of large-scale and small-scale cells of the scattering process. The Gamma-Gamma PDF of irradiance fluctuation in (2.13) is valid for all turbulence scenarios from weak-to-strong as it provides excellent fits with simulation data [20], [36]. Note that the Gamma-Gamma distribution will degenerate to the K-distribution when the channel parameter β is set to unity.

The nth moment of the Gamma-Gamma PDF is found as

$$E[I_s^n] = \frac{\Gamma(\alpha+n)\Gamma(\beta+n)}{\Gamma(\alpha)\Gamma(\beta)}\left(\frac{I_0}{\alpha\beta}\right)^n. \tag{2.14}$$

It can be shown that the channel parameters α and β are determined through the Rytov variance σ_R^2 [20], so they are not arbitrarily chosen. For the Gamma-Gamma turbulence model, we will show that the smaller channel parameter $\min\{\alpha,\beta\}$ has a major impact on system performance in large SNR regimes.

Assuming plane wave propagation through the optical turbulence channels, we have $\alpha>\beta$ in most scenarios. However, in the presence of a finite inner-scale l_0 [36], $\alpha>\beta$ may not hold as illustrated in Fig. 2.2. A crossing of the α and β curves occurs when the finite inner-scale

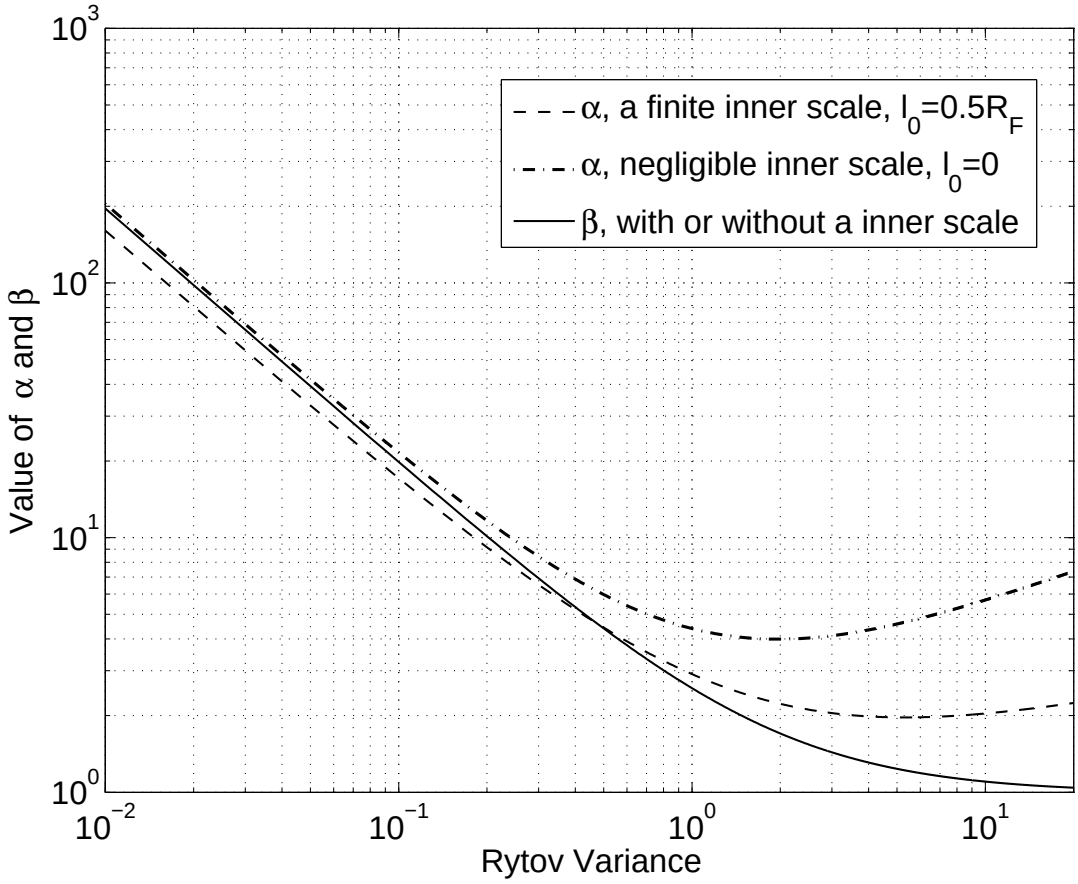

Figure 2.2: The relation of the Gamma-Gamma turbulence channel parameters α and β versus the Rytov variance σ_R^2 with a finite inner-scale ($l_0 = 0.5R_F$) or negligible inner-scale ($l_0 \to 0$).

is $l_0 = 0.5R_F$, where $R_F \triangleq \sqrt{D_a/k_w}$ denotes the first Fresnel zone [25]. When the inner-scale is negligible (i.e., $l_0 = 0$), the crossing of the α and β curves will disappear, and the relation $\alpha > \beta$ is preserved for weak-to-strong turbulence regimes. Note that the relationship $\alpha > \beta$ always holds in the special case of the K-distributed turbulence. Further details of the impact of inner-scale on atmospheric turbulence can be found in [25] and [91].

2.3 Diversity Combining Techniques

Among the techniques developed to combat atmospheric induced fading, diversity is a powerful and efficient technique. This technique can be readily combined with other fading mitigation techniques. Diversity provides the receiver with multiple replicas of the same information bearing signal through independent fading channels. Thus, the probability that all replicas are simultaneously in deep fading is small. Through appropriate combining at the receiver, one can reduce the depth of the fades and improve the performance of wireless communication systems.

Spatial diversity, time diversity and frequency diversity are the known methods in RF literature to obtain replicas of the signal. Here we briefly describe spatial diversity as it is suitable for coherent OWC links, and it is simpler to implement by separating multiple receiver apertures beyond the spatial coherent length [20]. The block diagram of a multi-channel diversity combining structure is shown in Fig. 2.3. In Fig. 2.3, r_l denotes the received signal at the lth channel, α_l denotes a weighting factor that is proportional to the electric field amplitude of the lth received optical signal, $\phi_{n,l}$ is the corresponding phase noise within the $l$the branch, and r denotes the combiner output. To explore the benefits of multi-channel transmission, different signal replicas combining schemes have been proposed based on the availability of channel state information (CSI). Three popular combining techniques are MRC, EGC and SC. The operating principles of these combining techniques are described in the ensuing subsections.

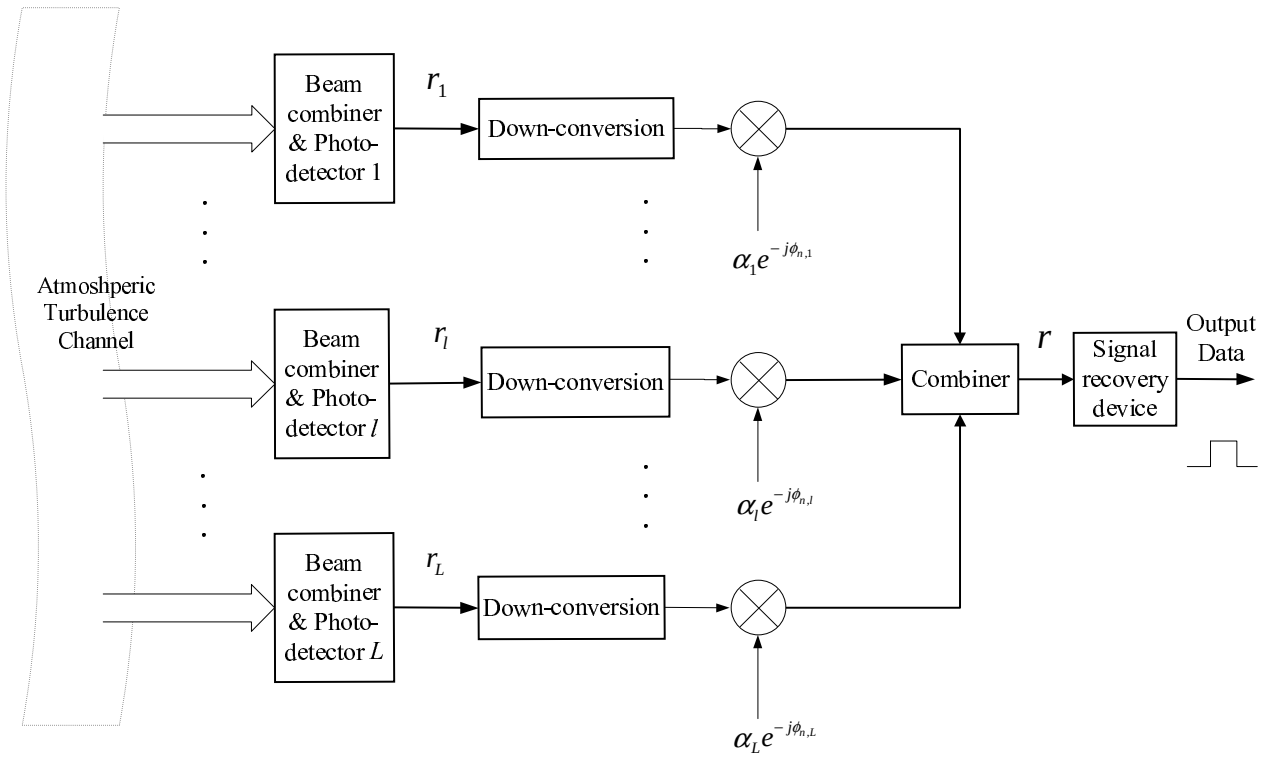

Figure 2.3: Structure of diversity combining in coherent OWC systems operating through atmospheric turbulence.

2.3.1 Maximum Ratio Combining Technique

In the MRC scheme, the received signal irradiance is estimated for each of the L received signals. The combiner eliminates the influence of random phase induced from multiple branches and lasers, i.e., co-phasing operation, and weighs the signals proportionally according to the amplitudes of the received signal electric fields. The MRC combiner output signal can be expressed as $r = \sum_{l=1}^{L} \alpha_l \exp(-j\phi_{n,l}) r_l$.

MRC is the optimal diversity combiner in terms of maximizing the combiner output SNR, in the absence of other interferences. However, MRC has the highest implementation complexity because the phase-tracking and signal amplitude estimation must be performed at the receiver. Therefore, suboptimal combining techniques have also been developed.

2.3.2 Equal Gain Combining Technique

For reduced implementation complexity, one can use EGC reception. In the EGC scheme, the weighting factors will be constant, and it is typically set to be unity. Therefore, the combiner only eliminates the influence of phase noise with equal weights (i.e., $\alpha_l = 1$ for $l = 1, 2, \cdots, L$) to the signals, which are summed and fed to the signal recovery circuit. Assuming equal noise power in all branches, one can write the instantaneous output signal of EGC combiner as $r = \sum_{l=1}^{L} \exp(-j\phi_{n,l}) r_l$. EGC becomes a practical combining scheme with lower implementation complexity than MRC when an accurate estimation of the received optical irradiance is difficult.

2.3.3 Selection Combining Technique

To reduce the system complexity further, one can choose the SC reception. The SC receiver monitors the received optical power level and selects the strongest signal for processing. The signal at the SC combiner output can be expressed as $r = r_{\text{index}(\max\{\alpha_l\}_{l=1}^{L})}$. Since SC processes the received signal in only one branch, it has lower complexity compared to MRC or EGC. However, as SC ignores information provided by other diversity branches, its performance is inferior to MRC and EGC. Because SC does not require the exact CSI, it is more suitable for optical links employing differential coherent modulations and noncoherent modulations.

2.4 Asymptotic Technique

The asymptotic technique has been shown to be a powerful tool in wireless digital communication system performance evaluation, as the resulting analytical solutions can often be used to reveal some important insights that can not be easily obtained otherwise.

Let $\gamma_l = \zeta_l \overline{\gamma}$ be the instantaneous SNR at the lth branch of an L-branch diversity combiner, where ζ_l's are assumed to be mutually independent RVs and are related to channel statistics, and $\overline{\gamma}$ is the average SNR per branch. One can write the average symbol-error rate (SER) in large SNR

regimes as

$$P_b = (G_c\overline{\gamma})^{-G_d} + o(\overline{\gamma}^{-G_d}) \tag{2.15}$$

where G_d and G_c, respectively, denote the diversity order and coding gain of a wireless communication system. We write a function $g(x)$ as $o(x)$ if $\lim_{x\to 0} g(x)/x = 0$. G_d determines the slope of the SER versus average SNR curve in large SNR regimes on a log-log scale, and G_c (in dB) determines the shift of the SER curve relative to the benchmark SER curve $\overline{\gamma}^{-G_d}$.

Alternatively, one can approximate the absolute value of the MGF of ζ_l by a single polynomial term as $\lim_{|s|\to\infty} |M_{\zeta_l}(s)| = b|s|^{-d} + o(|s|^{-d})$. As a result, considering a single branch coherent modulated system with conditional BER in the form of $P_{b|\zeta_l} = Q(\sqrt{k\zeta_l\overline{\gamma}})$ where $Q(\cdot)$ denotes the Gaussian Q-function defined as

$$Q(x) = \frac{1}{\sqrt{2\pi}} \int_x^\infty \exp\left(-\frac{t^2}{2}\right) dt \tag{2.16}$$

one can express the diversity order and coding gain offered by the lth branch respectively as [92] $G_{dl} = d$ and

$$G_{cl} = k\left(\frac{2^{d-1} b\Gamma\left(d+\frac{1}{2}\right)}{\sqrt{\pi}\Gamma(d+1)}\right)^{-\frac{1}{d}}. \tag{2.17}$$

Here k is a constant related to specific modulation formats with $k = 1$ for BPSK. Considering single branch DPSK or noncoherent frequency-shift keying (NCFSK) modulated systems with conditional BER in the form of $P_{b|\zeta_l} = 0.5\exp(-\rho\zeta_l\overline{\gamma})$ where $\rho = 1$ for DPSK and $\rho = 1/2$ for NCFSK, one can find the diversity order and coding gain offered by the lth branch respectively as $G_{dl} = d$ and

$$G_{cl} = \rho\left(\frac{b\Gamma(d+1)}{\Gamma(d+1)}\right)^{-\frac{1}{d}}. \tag{2.18}$$

When MRC or EGC schemes are used, the aggregate coding gains are given by [92]

$$G_c^M = \left[\frac{2^{L-1}\pi^{\frac{L-1}{2}}\Gamma\left(\frac{1}{2}+\sum_{l=1}^{L} G_{dl}\right)\left[\prod_{l=1}^{L} G_{dl}\Gamma(G_{dl})\right]}{\Gamma\left(1+\sum_{l=1}^{L} G_{dl}\right)\left[\prod_{l=1}^{L} G_{cl}^{G_{dl}}\Gamma\left(G_{dl}+\frac{1}{2}\right)\right]} \right]^{-\frac{1}{\sum_{l=1}^{L} G_{dl}}} \tag{2.19}$$

and

$$G_c^E = \left[\frac{2^{2(L-\sum_{l=1}^{L} G_{dl})}\pi^{\frac{L}{2}} L^{\sum_{l=1}^{L} G_{dl}}\Gamma\left(\frac{1}{2}+\sum_{l=1}^{L} G_{dl}\right)\left[\prod_{l=1}^{L} G_{dl}\Gamma(2G_{dl})\right]}{\Gamma\left(1+\sum_{l=1}^{L} G_{dl}\right)\left[\prod_{l=1}^{L} G_{cl}^{G_{dl}}\Gamma\left(G_{dl}+\frac{1}{2}\right)\right]} \right]^{-\frac{1}{\sum_{l=1}^{L} G_{dl}}}. \tag{2.20}$$

Both MRC and EGC achieve the same diversity order as $G_d^M = G_d^E = \sum_{l=1}^{L} G_{dl}$.

When the SC scheme is used, one can express the aggregate diversity order and coding gain, respectively, as $G_d^S = \sum_{l=1}^{L} G_{dl}$ and

$$G_c^S = \left[\frac{2^{L-1}\Gamma\left(\sum_{l=1}^{L} G_{dl}\right)\left(\sum_{l=1}^{L} G_{dl}\right)}{\sum_{l=1}^{L} G_{cl}^{G_{dl}}\Gamma(G_{dl})G_{dl}} \right]^{-\frac{1}{\sum_{l=1}^{L} G_{dl}}}. \tag{2.21}$$

Substituting the diversity orders and coding gains into (2.15), one can readily obtain the asymptotic error rate of a given digital communication system operating in fading channels.

Chapter 3

Performance Analysis of Coherent Detection Over Strong Turbulence

In this chapter, we derive closed-form expressions of the MGF for the K-distributed turbulence model. By employing the MGF technique, we obtain exact BER expressions for BPSK and DPSK signalings over K-distributed turbulence. Furthermore, we introduce an asymptotic solution, which can be used to obtain rapid error rate estimation when SNR values are sufficiently large.

3.1 MGF of K-Distributed Turbulence

The PDF of K-distributed irradiance I_s is given in (2.11). To obtain the MGF of I_s, a direct calculation using the definition of the MGF can be difficult. Therefore, we consider the mathematical properties of the K-distribution and express I_s as the product $I_s = I_x I_y$ [42], where I_x and I_y are two independent RVs having the exponential and Gamma PDFs, respectively, as

$$f(I_x) = \frac{1}{\eta^2} e^{-\frac{I_x}{\eta^2}}, \;\; I_x > 0 \tag{3.1}$$

and

$$f(I_y) = \frac{\alpha(\alpha I_y)^{\alpha-1} e^{-\alpha I_y}}{\Gamma(\alpha)}, \;\; I_y > 0. \tag{3.2}$$

Using [93, Eq.381(4)], one can show the MGF of I_s conditioned on I_x is

$$M_{I_s|I_x}(s) = \left(\frac{\alpha}{\alpha - sI_x}\right)^{\alpha}. \tag{3.3}$$

Averaging (3.3) over I_x, we obtain

$$M_{I_s}(s) = E_{I_x}[M_{I_s|I_x}(s)] = \frac{1}{\eta^2}\int_0^{\infty}\left(\frac{\alpha}{\alpha - sI_x}\right)^{\alpha} e^{-\frac{I_x}{\eta^2}} dI_x. \tag{3.4}$$

With a change of variable (assuming $\Re\{s\} < 0$), Eqn. (3.4) becomes

$$M_{I_s}(s) = -\frac{\alpha}{s\eta^2}\int_0^{\infty}(1+y)^{-\alpha} e^{\frac{\alpha y}{s\eta^2}} dy. \tag{3.5}$$

Finally, from [93, Eq.3.382(4)], we obtain the MGF of I_s as

$$M_{I_s}(s) = \left(-\frac{\alpha}{s\eta^2}\right)^{\alpha} e^{-\frac{\alpha}{s\eta^2}} \Gamma\left(-\alpha+1, -\frac{\alpha}{s\eta^2}\right), \ \ \Re\{s\} < 0 \tag{3.6}$$

where $\Gamma(\cdot,\cdot)$ denotes the upper incomplete Gamma function defined as $\Gamma(\alpha,x) = \int_x^{\infty} e^{-t} t^{\alpha-1} dt$ [93]. To facilitate our asymptotic error analysis, we express the upper incomplete Gamma function in terms of the two-parameter exponential integration function using $Ei(\alpha,z) = z^{(-1+\alpha)}\Gamma(-\alpha+1,z)$ where the two-parameter exponential integration function is defined as $Ei(\alpha,z) = \int_1^{\infty} \frac{e^{-zt}}{t^{\alpha}} dt$ [93]. Using this relationship and (3.6), we obtain an alternative expression for the MGF of I_s as

$$M_{I_s}(s) = -\frac{\alpha}{s\eta^2} e^{-\frac{\alpha}{s\eta^2}} Ei\left(\alpha, -\frac{\alpha}{s\eta^2}\right), \ \ \Re\{s\} < 0. \tag{3.7}$$

Section 3.2.2 will show that the MGF form in (3.7) is particularly suitable for asymptotic analysis.

3.2 Link Performance Studies Using MGF

In this section, we employ the MGF derived in Section 3.1 to study coherent OWC error rate performance in K-distributed turbulence with different modulation formats. Since the mean signal irradiance is given by $E[I_s] = \eta^2$, we define the average SNR as $\overline{\gamma} = E[\gamma] = C\eta^2$ where $C = \frac{\eta_e E_s A}{h\nu\Delta f}$.

3.2.1 BER for BPSK

The average BER of BPSK over a turbulence channel can be expressed as $P_e = \int_0^\infty P_e(I_s) f(I_s) dI_s$, where $P_e(I_s)$ denotes the conditional bit-error probability of BPSK signaling and it is given by

$$P_e(I_s) = Q\left(\sqrt{\gamma}\right) = Q\left(\sqrt{I_s\overline{\gamma}}\right) \tag{3.8}$$

where $Q(\cdot)$ is the Gaussian Q-function in (2.16). Using the alternative form of the Gaussian Q-function

$$Q(x) = \frac{1}{\pi}\int_0^{\frac{\pi}{2}} \exp\left(-\frac{x^2}{2\sin^2\theta}\right) d\theta, \;\; x > 0 \tag{3.9}$$

we express the average BER with BPSK as

$$\begin{aligned} P_{e,\,BPSK} &= \frac{1}{\pi}\int_0^{\frac{\pi}{2}}\int_0^\infty \exp\left(-\frac{I_s\overline{\gamma}}{2\sin^2\theta}\right) f(I_s) dI_s d\theta \\ &= \frac{1}{\pi}\int_0^{\frac{\pi}{2}} M_{I_s}\left(-\frac{\overline{\gamma}}{2\sin^2\theta}\right) d\theta. \end{aligned} \tag{3.10}$$

The BER expression in (3.10) only involves a definite integration, and simple numerical integration methods such as Simpson's rule can be applied to calculate the BER accurately.

3.2.2 Asymptotic BER Analysis for BPSK

For system design purposes, we are interested in finding the diversity order of a communication link. In this section, we analyze the asymptotic BER performance using the derived alternative

form of the MGF of the K-distribution. This result does not require any integration and can be used for a fast BER estimation in large SNR regimes.

The K-distribution has been found to be a reliable turbulence model when the scintillation index σ_{si}^2 is confined to the range (2, 3) [63]. Thus, we assume the channel parameter α lies within the range (1,2) when performing this asymptotic analysis. With the closed-form MGF expression derived in (3.7), when $|s| \to \infty$, we can show the MGF of I_s can be approximated by

$$M_{I_s}(s) = -\frac{\alpha}{s\eta^2} Ei(\alpha, 0) + o(s^{-1}). \tag{3.11}$$

The two-parameter exponential function in (3.11) for α in (1,2) can be simplified to

$$Ei(\alpha, 0) = \lim_{b\to\infty} \int_1^b \frac{1}{t^\alpha} dt = \frac{1}{\alpha - 1}. \tag{3.12}$$

Applying (3.12) to (3.11) gives

$$M_{I_s}(s) = \left[\frac{\alpha}{\eta^2(\alpha-1)}\right] s^{-1} + o(s^{-1}), \;\; 1 < \alpha < 2. \tag{3.13}$$

It can be shown from Section 2.4, for $|s| \to \infty$, if the MGF of I_s can be expressed through

$$|M(s)| = b|s|^{-d} + o(|s|^{-d}) \tag{3.14}$$

the asymptotic BER can be expressed as [92]

$$P_e^{asym} = \frac{2^{d-1}\Gamma(d+\frac{1}{2})b}{\sqrt{\pi}\Gamma(d+1)} \left(\frac{1}{k\overline{\gamma}}\right)^d. \tag{3.15}$$

Now comparing (4.13) with (3.14), we have $b = \frac{\alpha}{\eta^2(\alpha-1)}$ and $d = 1$. With $k = 1$ (for BPSK), we obtain the asymptotic BER as

$$P_e^{asym} = \frac{\alpha}{2\eta^2(\alpha-1)} \overline{\gamma}^{-1}. \tag{3.16}$$

The diversity order and coding gain for a SISO link are respectively

$$G_d = 1 \tag{3.17}$$

and

$$G_c = \frac{2\eta^2(\alpha-1)}{\alpha}. \tag{3.18}$$

3.2.3 BER for DPSK

In [63], Kiasaleh derived a closed-form BER for DPSK of a coherent OWC system with K-distributed turbulence. We now use the MGF of K-distributed turbulence to obtain an alternative closed-form error rate expression. For DPSK, it is well known that the conditional BER is $P_e(I_s) = \frac{1}{2}\exp(-\overline{\gamma}I_s)$, hence the unconditional BER is obtained as

$$P_{e,\,DPSK} = \frac{1}{2}\int_0^\infty \exp(\overline{\gamma}I_s) f(I_s) dI_s = \frac{1}{2}M_{I_s}(-\overline{\gamma}) \tag{3.19}$$

which is an alternative closed-form DPSK error rate expression to the one obtained by Kiasaleh [63, Eq.(14)][3].

3.3 Outage Probability

Outage probability is another important performance criterion to evaluate digital wireless communication systems. The outage probability is defined as the probability that the instantaneous SNR falls below a specified threshold. For a given OWC system, the outage probability can be found by

$$P_{outage}(\Lambda) = \Pr\{\gamma < \Lambda\} = \int_0^\Lambda f_\gamma(\gamma) d\gamma \tag{3.20}$$

[3] A factor of two is missing in the derivation of the uncoded BER in [63]. The correct DPSK error rate is $P_e = \frac{\Gamma(1-\alpha)\zeta^\alpha}{2\Gamma(1)}M(\alpha,\alpha;\zeta) + \frac{\Gamma(\alpha-1)\zeta}{2\Gamma(\alpha)}M(1,2-\alpha;\zeta)$, where $M(\cdot,\cdot;\cdot)$ is the Kummer confluent hypergeometric function.

where $\Pr\{\cdot\}$ denotes the probability of an event, Λ is a predefined outage probability threshold, and $f_\gamma(\gamma)$ is the PDF of the instantaneous SNR. To facilitate the outage probability analysis, making use of a change of variables and [93, Eq. 6.561(8)], we can obtain the cumulative distribution function (CDF) of the K-distributed RV as

$$F_{I_s}(I_s) = 1 - \frac{2(\alpha I_s)^{\frac{\alpha}{2}}}{\Gamma(\alpha)\eta^\alpha} K_\alpha\left(\frac{2}{\eta}\sqrt{\alpha I_s}\right), \quad I_s \geq 0. \tag{3.21}$$

Substituting the relationship $\gamma = \overline{\gamma} I_s$ into (3.20), we obtain the outage probability for coherent OWC systems as

$$P_{outage}(\Lambda) = 1 - \frac{2(\alpha)^{\frac{\alpha}{2}}}{\Gamma(\alpha)\eta^\alpha}\left(\frac{\Lambda}{\overline{\gamma}}\right)^{\frac{\alpha}{2}} K_\alpha\left(\frac{2}{\eta}\sqrt{\frac{\alpha\Lambda}{\overline{\gamma}}}\right). \tag{3.22}$$

3.4 Numerical Results

In this section we present the error performance of coherent OWC systems over K-distributed turbulence assuming $\eta^2 = 1$. The BER curves for BPSK, obtained from (3.6), are presented in Fig. 3.1 for average SNR values ranging from 5 dB to 50 dB. Because the parameter α is inversely proportional to the scintillation index, an improved BER is achieved as α increases or when the scintillation index decreases. Not shown in Fig. 3.1, we have also verified the accuracy of our MGF based solution using Monte Carlo simulation. Our simulated BERs have excellent agreement with the ones obtained analytically. Figure 3.1 also shows that the asymptotic error rate curves are valid for large SNR values. It is readily apparent that these asymptotic solutions become increasingly accurate as the SNRs become sufficiently large.

Figure 3.2 plots the outage probabilities for the K-distributed turbulence channels with $\alpha = 1.1, 1.3, 1.6$ where the outage threshold is set as 10 dB. As expected, the outage probability also decreases when scintillation index increases.

From the numerical results, we comment that, unlike OWC links with small scintillation index (e.g., lognormal turbulence channels) [48], OWC links suffer from substantial performance impair-

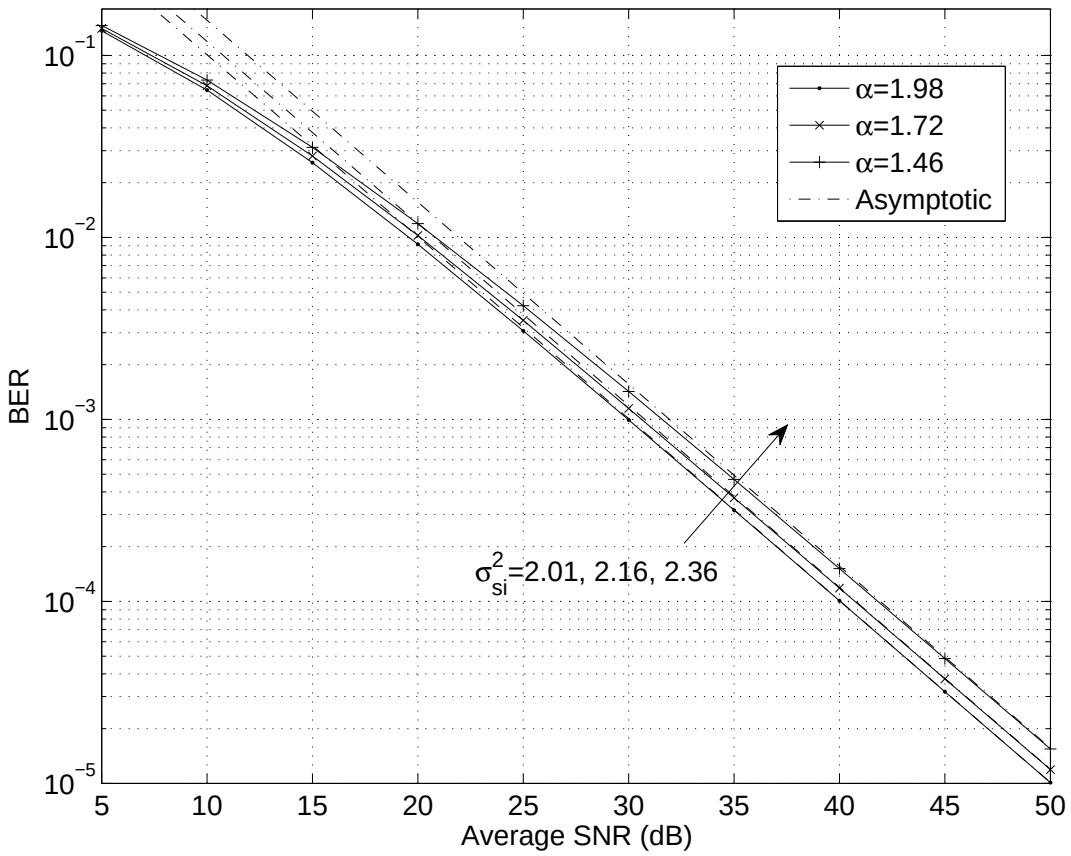

Figure 3.1: BERs of BPSK SISO links over K-distributed turbulence channels.

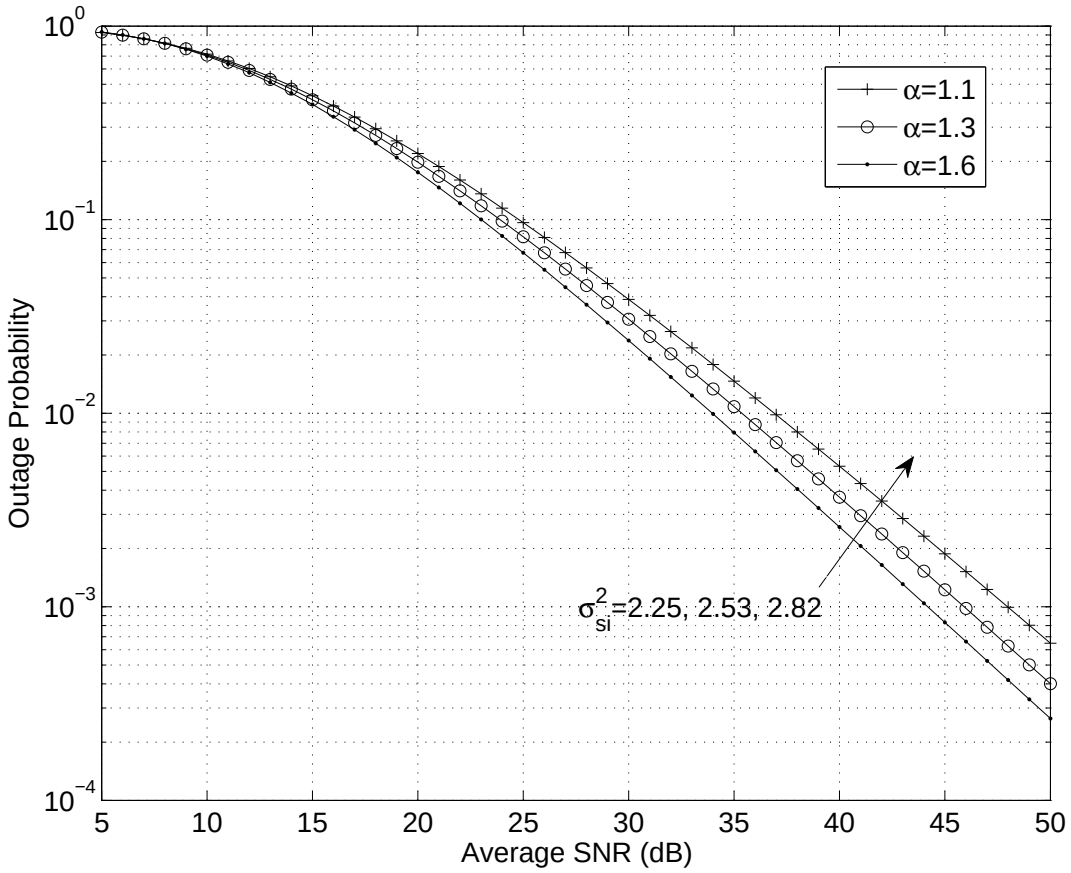

Figure 3.2: Outage probabilities of coherent OWC systems over K-distributed turbulence channels.

ments with strong turbulence cases (as discussed here for large values of scintillation index). A SISO OWC link operating through strong turbulence may not achieve an acceptable level of BER performance. Thus, we need to employ powerful techniques to mitigate the turbulence effects, especially for OWC links over strong turbulence channels.

3.5 Summary

In this chapter, a closed-form expression of the MGF for K-distributed turbulence has been derived. By employing this MGF, the exact BER expressions for BPSK and DPSK have been obtained. Furthermore, an asymptotic solution has been introduced, and it can be used to obtain rapid error rate estimation for large values of SNR.

Chapter 4

Performance of Coherent Systems Using Spatial Diversity Over Strong Turbulence Channels

As we have concluded from Chapter 3, the BER performance for coherent OWC links suffers from severe performance degradation under strong turbulence conditions. We must therefore apply a fading mitigation technique in such cases. In this chapter, we perform case studies on coherent OWC systems employing multiple receivers operating over strong turbulence channels. We will demonstrate the effectiveness of spatial diversity techniques in mitigating the atmospheric turbulence effects. We carry out studies for three important diversity reception techniques: maximal ratio combining, equal gain combining and selection combining. We show that EGC systems can provide practical implementations along with comparable error performance to the optimal MRC OWC systems.

4.1 Coherent Link Using Maximum Ratio Combining

Considering an OWC link with L receivers, we denote the instantaneous SNR in the lth diversity subchannel by γ_l for $l \in \{1,2,...,L\}$. Since the noise in these subchannels is independent of each other, the MRC combiner output SNR is $\sum_{l=1}^{L} \gamma_l = \overline{\gamma}\left(\sum_{l=1}^{L} I_{s,l}\right)$ where $I_{s,l}$ denotes the optical signal irradiance at the lth branch having a K-distributed PDF. If the turbulence is i.i.d., and the average

SNR per diversity branch is equal for all L subchannels, then the MGF of the combiner output SNR can be expressed as $M(s) = [M_{I_s}(s)]^L$. Making use of (3.9), we obtain the BER for BPSK with MRC reception as

$$P_{e,\,MRC} = \frac{1}{\pi}\int_0^{\frac{\pi}{2}} \left[M_{I_s}\left(-\frac{\overline{\gamma}}{2\sin\theta^2}\right)\right]^L d\theta \tag{4.1}$$

where the MGF $M_{I_s}(\cdot)$ was derived in (3.6).

4.2 Coherent Link Using Equal Gain Combining

For EGC with L diversity branches, the received signals at different branches are co-phased and added with equal weight. In such a case, as shown in Appendix A, the instantaneous SNR at the output of the combiner becomes

$$\gamma_{EGC} = \frac{R\left(\sum\limits_{l=1}^{L}\sqrt{P_{s,l}}\right)^2}{Lq\Delta f} \tag{4.2}$$

where q denotes the electronic charge and Δf is the noise equivalent bandwidth of the photodetector. Given A as the photodetector area and using the relationship $P_{s,l} = AI_{s,l}$, where $I_{s,l}$ is the instantaneous received optical irradiance of the lth branch, we rewrite the instantaneous SNR as

$$\gamma_{EGC} = \frac{RA\left(\sum\limits_{l=1}^{L}\sqrt{I_{s,l}}\right)^2}{Lq\Delta f} = g^2\left(\sum_{l=1}^{L}\sqrt{I_{s,l}}\right)^2 \tag{4.3}$$

where $g \triangleq \sqrt{RA/(Lq\Delta f)}$ is a positive scalar factor. For $L = 1$, the instantaneous SNR in (4.3) specializes to $\gamma_{EGC} = RAI_{s,1}/(q\Delta f)$, which agrees with the single-branch SNR obtained in (2.8). Note that the SNR expression shown in (4.3) is fundamentally different from the SNR of EGC in the direct detection based OWC applications, which is simply related to the sum of the irradiance

[30], [50]-[51], [94]. The instantaneous SNR at the output of the equal gain combiner for coherent OWC systems is instead related to the sum of the squareroot of the irradiance in each branch. This distinction can greatly impact the system performance.

The average BER of BPSK over a turbulence channel can be derived by averaging the conditional bit-error probability as

$$P_e = \int_0^\infty P_e(z_s) f(z_s) dz_s \tag{4.4}$$

where z_s is the sum of L squareroots of the irradiance with K-distribution, i.e., $z_s = \sum_{l=1}^{L} \sqrt{I_{s,l}}$. In (4.4), $f(z_s)$ is the PDF of z_s and $P_e(z_s)$ denotes the conditional bit-error probability given by

$$P_e(z_s) = \frac{1}{2}\,\mathrm{erfc}\left(\sqrt{\frac{\gamma_{EGC}}{2}}\right) = \frac{1}{2}\,\mathrm{erfc}\left(\frac{g z_s}{\sqrt{2}}\right) \tag{4.5}$$

where $\mathrm{erfc}(\cdot)$ is the complementary error function defined as $\mathrm{erfc}(x) = 2\int_x^\infty \exp(-t^2)dt/\sqrt{\pi}$. One can obtain the PDF of z_s by

$$f(z_s) = \frac{1}{2\pi}\int_{-\infty}^{\infty} \Phi_{z_s}(\omega) e^{-j\omega z_s} d\omega = \frac{1}{2\pi}\int_{-\infty}^{\infty} \prod_{l=1}^{L} \Phi_{z_l}(\omega) e^{-j\omega z_s} d\omega \tag{4.6}$$

where $\Phi_{z_s}(\omega)$ is the CHF of z_s, $j = \sqrt{-1}$, and $\Phi_{z_l}(\omega)$ is the CHF of z_l with $z_l = \sqrt{I_{s,l}}$, which is easily obtained from (B.9)-(B.11) in Appendix B. Substituting (4.6) into (4.4), we obtain the average BER as

$$P_e = \frac{1}{2\pi}\int_{-\infty}^{\infty} \Phi_{z_s}^*(\omega) \int_0^\infty P_e(z_s) e^{j\omega z_s} dz_s d\omega \tag{4.7}$$

where $\Phi_{z_s}^*(\cdot)$ denotes the conjugate of $\Phi_{z_s}(\cdot)$. Equation (5.24) can be rewritten as

$$P_e = \frac{1}{2\pi}\int_{-\infty}^{\infty} \prod_{l=1}^{L} \Phi_{z_l}^*\left(\frac{g\omega}{\sqrt{2}}\right) \frac{F(\omega)}{2} d\omega \tag{4.8}$$

where we have defined

$$\digamma(\omega) = \int_0^\infty \mathrm{erfc}(z_s) e^{j\omega z_s} dz_s = \frac{1}{\sqrt{\pi}} {}_1F_1\left(1, \frac{3}{2}; -\frac{\omega^2}{4}\right) + \frac{j}{\omega}\left(1 - e^{-\frac{\omega^2}{4}}\right) \tag{4.9}$$

where ${}_1F_1(\cdot,\cdot;\cdot)$ denotes the confluent hypergeometric function. With a change of variable, $\omega = \tan\theta$, it is possible to rewrite (4.8) in terms of a definite integration for a convenient numerical evaluation

$$P_e = \frac{1}{2\pi} \int_{-\frac{\pi}{2}}^{\frac{\pi}{2}} \sec^2\theta \prod_{l=1}^{L} \Phi_{z_l}^*\left(\frac{g\tan\theta}{\sqrt{2}}\right) \frac{\digamma(\tan\theta)}{2} d\theta. \tag{4.10}$$

Though only the BPSK-modulated optical signal is considered here, error rates of other coherent modulations can be similarly obtained.

4.3 Coherent Link Using Selection Combining

SC has the least complexity when compared to MRC and EGC, as it simply selects the branch with the strongest instantaneous received SNR. In the following, we present precise error rate expressions for coherent OWC systems with SC reception. Given the lth branch instantaneous SNR as γ_l, the instantaneous SNR for SC is

$$\gamma_{SC} = \max\{\gamma_1, \gamma_2, \cdots, \gamma_L\} = \frac{R}{q\Delta f} \max\{P_{s,l}; l = 1, \cdots, L\}. \tag{4.11}$$

We can observe from (4.3) and (4.11) that the instantaneous SNRs are independent of the LO power.

The desired error rate derivation requires the PDF of $I_{s,SC} \triangleq \max\{I_{s,l}, l = 1, \cdots, L\}$. For identically distributed turbulence, we can show the PDF of $I_{s,SC}$ to be $f_{I_{s,SC}}(I_s) = L[F_{I_{s,l}}(I_s)]^{L-1} f(I_s)$ where $F_{I_{s,l}}(\cdot)$ denotes the CDF of $I_{s,l}$, which has been derived in (3.21).

Differential detection and noncoherent detection are two practical alternatives for synchronous detection to minimize the impact of phase noise, and the conditional BER (with an average SNR of $\overline{\gamma}$) is known to be $P_e(I_s) = \frac{1}{2}\exp(-\rho\overline{\gamma}I_s)$ [86] where $\rho = 1$ for DPSK and $\rho = 1/2$ for NCFSK. Hence, the average BER for DPSK or NCFSK with SC is

$$P_e = \frac{1}{2}\int_0^{\infty} \exp(-\rho\overline{\gamma}I_s) f_{I_{s,SC}}(I_s) dI_s = \frac{1}{2}\int_0^{\frac{\pi}{2}} \sec^2\theta \exp(-\rho\overline{\gamma}\tan\theta) f_{I_{s,SC}}(\tan\theta) d\theta. \tag{4.12}$$

4.4 Diversity Order and Coding Gain

Using the alternative form of the MGF of the K-distribution derived in Chapter 3, we have

$$\lim_{|s|\to\infty} M_{I_s}(s) = \left[\frac{\alpha}{\eta^2(\alpha-1)}\right] s^{-1} + o(s^{-1}), \;\; 1 < \alpha < 2. \tag{4.13}$$

Thus, for $|s| \to \infty$, the MGF of the combiner output SNR becomes

$$\lim_{|s|\to\infty} |M(s)| = \left[\frac{\alpha}{\eta^2(\alpha-1)}\right]^L |s|^{-L} + o(|s|^{-L}), \;\; 1 < \alpha < 2. \tag{4.14}$$

Consequently, making use of (3.15), one can find the diversity order and coding gain offered by BPSK MRC coherent systems with K-distributed turbulence as

$$G_{d,MRC} = \sum_{l=1}^{L} G_{d,l} = L \tag{4.15}$$

and

$$G_{c,MRC} = \frac{2\eta^2(\alpha-1)}{\alpha}\left[\frac{2(L!)^2}{(2L)!}\right]^{\frac{1}{L}} \tag{4.16}$$

respectively, where $G_{d,l}$ denotes the diversity order of the lth branch. ($G_{d,l}$ has been shown to be unity for K-distributed turbulence in Chapter 3.)

For EGC reception, we can obtain the diversity order and coding gain as

$$G_{d,EGC} = \sum_{l=1}^{L} G_{dl} = L \tag{4.17}$$

and

$$G_{c,EGC} = \frac{\sqrt{\pi}\eta^2(\alpha-1)}{2L\alpha}\left[\frac{L!}{\Gamma\left(L+\frac{1}{2}\right)}\right]^{\frac{1}{L}} \tag{4.18}$$

respectively. Since the instantaneous SNR of each diversity branch is independent of each other, as expected, both EGC and MRC achieve the same diversity order, which is the sum of the diversity order $G_{dl} = 1$ offered by each branch.

For SC reception, one can show that the diversity order and coding gain are

$$G_{d,SC} = \sum_{l=1}^{L} G_{dl} = L \tag{4.19}$$

and

$$G_{c,SC} = \frac{\rho\eta^2(\alpha-1)}{\alpha}\left(\frac{2}{L!}\right)^{\frac{1}{L}} \tag{4.20}$$

respectively. Based on (4.20) and (4.18), one can readily obtain the asymptotic average BERs for large SNR regimes. We comment that the diversity order for MRC and EGC with BPSK is the same as that of SC with DPSK and FSK.

4.5 Numerical Results

In this section we present several numerical case studies for coherent OWC systems with diversity reception. The average SNR (per branch) is given as $\overline{\gamma} = RA\eta^2/(q\Delta f)$.

As shown in Fig. 4.1, coherent MRC systems outperform EGC systems. As the average SNR increases, the benefits from diversity reception of coherent systems are increasingly clear. When the number of diversity branches increases, the BER performance improves. It is notable that EGC

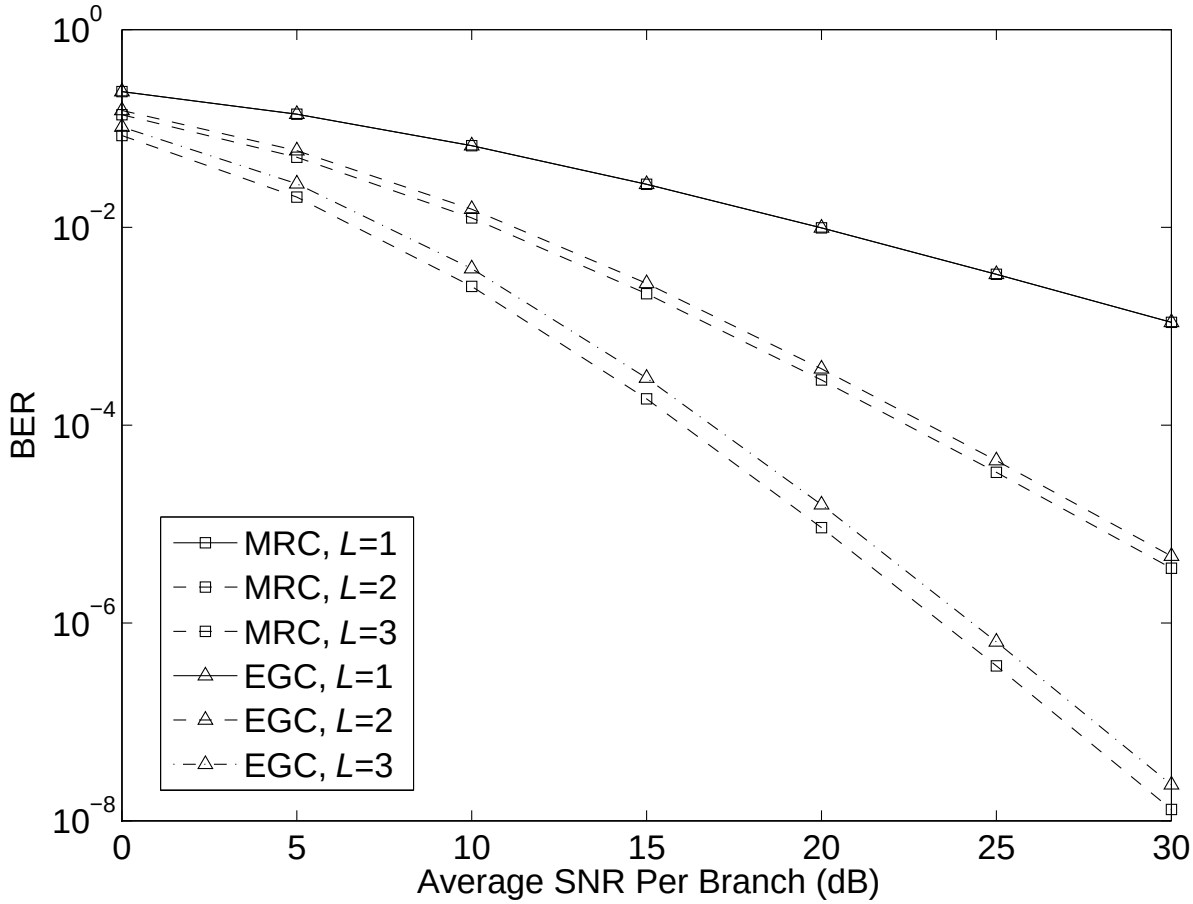

Figure 4.1: Comparison of the exact BERs with BPSK between coherent MRC and EGC operating on L-branch K-distributed turbulence channels for $\alpha = 1.8$.

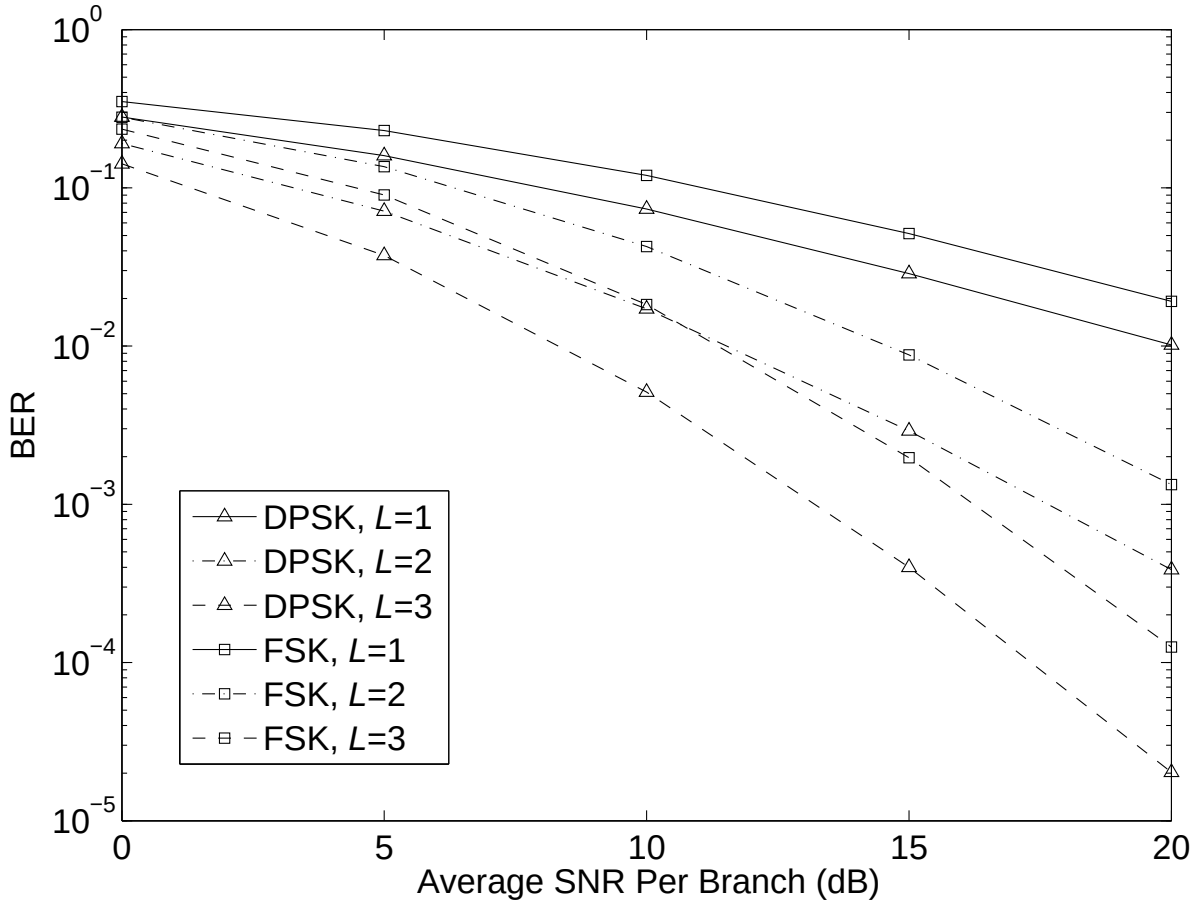

Figure 4.2: The exact BERs with DPSK and NCFSK for SC operating on L-branch K-distributed turbulence channels for $\alpha = 1.8$.

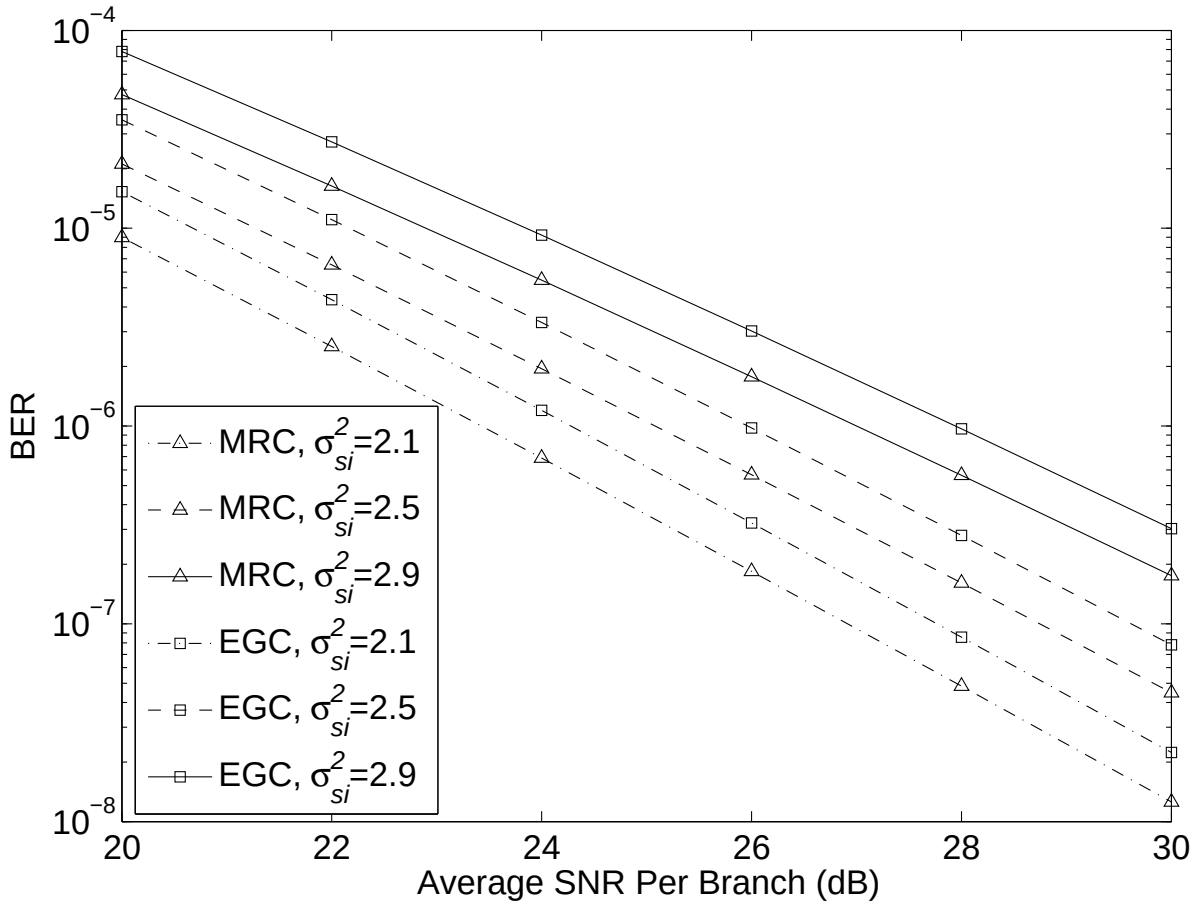

Figure 4.3: The impact of scintillation index σ_{si}^2 on BERs with BPSK for MRC and EGC operating on three diversity branches on K-distributed turbulence channels.

has a close error performance to that of the optimal MRC scheme. For instance, at a BER of 10^{-7}, only an additional 1 dB average SNR or less is required for EGC to achieve the same performance as MRC; at an average SNR of 30 dB, a three-branch EGC reception achieves a practical error rate of 2.5×10^{-8}. Therefore, EGC can be a preferable choice in designing a coherent OWC system as it provides comparable performance to MRC and can be implemented with reduced complexity, as EGC does not require the estimation of instantaneous irradiance fluctuation.

To further reduce the complexity of a coherent OWC system, SC would become a viable alternative since it does not require knowledge of the phase noise. For communication scenarios with little knowledge of the turbulence phase noise characteristics, DPSK and NCFSK with SC become the preferred choices. BER curves for these two modulation schemes are presented in Fig. 4.2. It is readily apparent that SC reception can also mitigate the turbulence effects for coherent OWC systems with differential and noncoherent modulations.

In addition to the impact of modulation schemes on system performance, it is known that the scintillation index σ_{si}^2 for a given OWC environment will impact the system performance. These turbulence effects are introduced to the OWC channel model through the channel parameter α, whose effects are shown in Fig. 4.3 for scintillation index σ_{si}^2 values ranging from 2.1 to 2.9. The results are displayed for both MRC and EGC cases. As expected, the BER performance improves for a coherent OWC communication system as the value of σ_{si}^2 decreases.

4.6 Summary

In this chapter, we have studied the performance of diversity reception for coherent OWC communication systems in strong atmospheric turbulence. New analytical exact BER expressions with MRC, EGC and SC schemes have been obtained. Our numerical results have shown that coherent OWC transmission with EGC outperforms that with SC and gives comparable performance to that of MRC with reduced implementation complexity. The numerical results have also demonstrated

that diversity techniques are useful in providing substantial performance improvement of coherent OWC systems. In addition, we have studied the diversity order and coding gain for coherent OWC diversity combining schemes which show the performance impact of optical systems and channel parameters.

Chapter 5

Coherent Optical Wireless Communications in the Presence of Gamma-Gamma Turbulence and Phase Noise Impacts

In this chapter, we first generalize our analysis from strong turbulence channels to the Gamma-Gamma turbulence channels, and then we investigate the performance degradation of coherent PSK using EGC when phase noise compensation error is present. As an alternative to coherent PSK, DPSK using postdetection EGC is proposed for coherent OWC links since the scheme is robust to phase noise.

5.1 A Revised Coherent Optical Wireless Receiver Model

Here we present a revised coherent receiver model to facilitate the analysis with phase noise impacts. We consider a coherent FSO system where a phase-locked loop (PLL) phase noise compensation mechanism is implemented at the receiver for the Gamma-Gamma turbulence channels. The optical power incident on the lth photodetector can be rewritten as [68]

$$P_l(t) = P_{s,l} + P_{LO} + 2\sqrt{P_{s,l}P_{LO}}g(t)\cos(\omega_{IF}t + \phi_s + \phi_{n,l}), \quad l = 1,2,...,L \tag{5.1}$$

where $P_{s,l}$ is the instantaneous incident optical signal power on the beamsplitter at the lth branch, P_{LO} denotes the LO power which is assumed to be the same for all branches, ϕ_s is the encoded phase

information, $\phi_{n,l}$ denotes the phase noise for the lth branch, and $\omega_{IF} = \omega_0 - \omega_{LO}$ is the intermediate frequency, where ω_0 and ω_{LO} denote the carrier frequency and LO frequency, respectively. In (5.1), $g(t)$ represents a signal pulse, which is defined as

$$g(t) = \begin{cases} \sqrt{\frac{1}{T}}, & 0 \leq t \leq T \\ 0, & \text{elsewhere} \end{cases} \tag{5.2}$$

where T denotes the symbol duration. In obtaining (5.1), we have assumed that the received optical beam and the LO beam are mixed in perfect spatial coherence over a sufficiently small photodetector area. This allows us to focus on the temporal phase noise from the turbulence channel as well as the lasers. The incident optical power results in the photocurrent

$$i_l(t) = RP_l(t) = i_{dc,l} + i_{ac,l}(t) + n_l(t), \quad l = 1,2,...,L \tag{5.3}$$

where we have

$$i_{dc,l} = R(P_{s,l} + P_{LO}), \quad l = 1,2,...,L \tag{5.4}$$

and

$$i_{ac,l}(t) = 2R\sqrt{P_{s,l}P_{LO}}g(t)\cos(\omega_{IF}t + \phi_s + \phi_{n,l}), \quad l = 1,2,...,L \tag{5.5}$$

representing, respectively, the DC and AC terms at the receiver, and $n_l(t)$ is an AWGN process with equal variance σ^2 for all branches. In practice, a coherent OWC system is operated in the regime $P_{LO} \gg P_{s,l}$, and the DC term in (6.3) can be approximated by the dominant term RP_{LO}. The variance of the shot noise process $n_l(t)$ can then be expressed by [87]

$$\sigma^2 = 2qRP_{LO}\Delta f. \tag{5.6}$$

Note that the DC term can be removed easily using an appropriate bandpass filter.

5.2 Statistics of the Gamma-Gamma Model

To facilitate the performance analysis of coherent OWC systems with diversity reception in Gamma-Gamma turbulence, we study the statistical properties of the optical irradiance I_s following a Gamma-Gamma distribution, i.e., the MGF of I_s and the CHF of the squareroot of I_s. Both will be shown to be effective tools for the error rate performance analysis of coherent OWC transmission in Gamma-Gamma turbulence channels.

First, with [93, Eq. 6.643(3), Eq. 9.220(4)], the MGF[4] of the Gamma-Gamma RV I_s can be directly obtained from its definition

$$\begin{aligned} M_{I_s}(s) &= \int_0^\infty e^{sI_s} f_{I_s}(I_s) dI_s \\ &= \frac{(\alpha\beta)^{\frac{\alpha+\beta-1}{2}} e^{-\frac{\alpha\beta}{2s}}}{(-s)^{\frac{\alpha+\beta-1}{2}}} \left[\frac{\Gamma(\beta-\alpha)}{\Gamma(\beta)} M_{k_1,k_2}\left(-\frac{\alpha\beta}{s}\right) + \frac{\Gamma(\alpha-\beta)}{\Gamma(\alpha)} M_{k_1,-k_2}\left(-\frac{\alpha\beta}{s}\right) \right] \end{aligned} \tag{5.7}$$

where $M_{\cdot,\cdot}(\cdot)$ denotes the Whittaker function [93], $k_1 = 1-\alpha-\beta/2$ and $k_2 = \alpha-\beta/2$. Equation (5.7) can be further expressed in terms of the confluent hypergeometric function ${}_1F_1(\cdot,\cdot;\cdot)$ through [93, Eq. 9.220(2), Eq. 9.220(3)]

$$M_{k_1,k_2}\left(-\frac{\alpha\beta}{s}\right) = \left(-\frac{\alpha\beta}{s}\right)^{\frac{\alpha-\beta+1}{2}} e^{-\frac{\alpha\beta}{2s}} {}_1F_1\left(\alpha, \alpha-\beta+1; -\frac{\alpha\beta}{s}\right) \tag{5.8}$$

and

$$M_{k_1,-k_2}\left(-\frac{\alpha\beta}{s}\right) = \left(-\frac{\alpha\beta}{s}\right)^{\frac{\beta-\alpha+1}{2}} e^{-\frac{\alpha\beta}{2s}} {}_1F_1\left(\beta, \beta-\alpha+1; -\frac{\alpha\beta}{s}\right). \tag{5.9}$$

Next, we seek the CHF for the squareroot of the irradiance I_s. We denote the squareroot of the

[4] A different form of the MGF of Gamma-Gamma distributed RVs has been documented in a technical report [55].

irradiance by $z \triangleq \sqrt{I_s}$, and we can show the PDF of z to be

$$f_z(z) = \frac{4}{\Gamma(\alpha)\Gamma(\beta)}(\alpha\beta)^{\frac{\alpha+\beta}{2}} z^{\alpha+\beta-1} K_{\alpha-\beta}\left(2\sqrt{\alpha\beta}z\right), \quad z > 0. \tag{5.10}$$

To obtain the CHF of z, a direct calculation using the definition of the CHF can be difficult. Alternatively, we consider the property of $I_s = I_x I_y$ [36], where I_x and I_y are two independent RVs with Gamma PDFs, respectively, defined as

$$f_{I_x}(I_x) = \frac{\alpha(\alpha I_x)^{\alpha-1} e^{-\alpha I_x}}{\Gamma(\alpha)}, \;\; I_x > 0 \tag{5.11}$$

and

$$f_{I_y}(I_y) = \frac{\beta(\beta I_y)^{\beta-1} e^{-\beta I_y}}{\Gamma(\beta)}, \;\; I_y > 0. \tag{5.12}$$

We let $z = xy$ with $x \triangleq \sqrt{I_x}$ and $y \triangleq \sqrt{I_y}$, and x and y can be shown to be two independent RVs with their PDFs given by

$$f_x(x) = \frac{2\alpha^{\alpha} x^{2\alpha-1} e^{-\alpha x^2}}{\Gamma(\alpha)}, \;\; x > 0 \tag{5.13}$$

and

$$f_y(y) = \frac{2\beta^{\beta} y^{2\beta-1} e^{-\beta y^2}}{\Gamma(\beta)}, \;\; y > 0 \tag{5.14}$$

respectively. The PDFs in (5.13) and (5.14) are Nakagami-m PDFs if $\alpha \geqslant 1/2$ and $\beta \geqslant 1/2$.

The CHF of z is defined as

$$\Phi_z(\omega) = \int_0^{\infty} e^{j\omega z} f_z(z) dz = E[e^{j\omega z}], \;\; \omega \in \mathbf{R}. \tag{5.15}$$

By [93, Eq. 3.462(1)], the CHF of z conditioned on x can be obtained as

$$\Phi_{z|x}(\omega) = E_{z|x}[e^{j\omega z}] = \frac{2^{1-\beta}\Gamma(2\beta)}{\Gamma(\beta)} \exp\left(\frac{-\omega^2 x^2}{8\beta}\right) D_{-2\beta}\left(\frac{-j\omega x}{\sqrt{2\beta}}\right) \tag{5.16}$$

where $D_\rho(\cdot)$ is the parabolic cylinder function of the ρth order. The parabolic cylinder function in (5.16) can be further expanded into the confluent hypergeometric function [93, Eq. 9.240]. As a result, we can rewrite (5.16) as

$$\Phi_{z|x}(\omega) = {}_1F_1\left(\beta, \frac{1}{2}; -\frac{\omega^2 x^2}{4\beta}\right) + j\frac{\Gamma\left(\beta+\frac{1}{2}\right)}{\Gamma(\beta)}\left(\frac{\omega x}{\sqrt{\beta}}\right){}_1F_1\left(\beta+\frac{1}{2}, \frac{3}{2}; -\frac{\omega^2 x^2}{\beta}\right). \tag{5.17}$$

Averaging the CHF of z conditioned on x gives the desired CHF as[5]

$$\Phi_z(\omega) = \Re\{\Phi_z(\omega)\} + j\Im\{\Phi_z(\omega)\} \tag{5.18}$$

where

$$\Re\{\Phi_z(\omega)\} = {}_2F_1\left(\beta, \alpha, \frac{1}{2}; -\frac{\omega^2}{4\alpha\beta}\right) \tag{5.19}$$

and

$$\Im\{\Phi_z(\omega)\} = \frac{\Gamma\left(\alpha+\frac{1}{2}\right)\Gamma\left(\beta+\frac{1}{2}\right)\omega}{\Gamma(\alpha)\Gamma(\beta)}(\alpha\beta)^{-\frac{1}{2}}{}_2F_1\left(\beta+\frac{1}{2}, \alpha+\frac{1}{2}, \frac{3}{2}; -\frac{\omega^2}{4\alpha\beta}\right). \tag{5.20}$$

Here, $\Re\{\cdot\}$ and $\Im\{\cdot\}$ denote the real and imaginary operations, respectively, and ${}_2F_1(\cdot,\cdot,\cdot;\cdot)$ is the Gaussian hypergeometric function defined in [93, Eq. 9.100].

5.3 Error Rate Performance of Coherent Systems in Gamma-Gamma Turbulence

In this section, we employ the MGF of I_s and the CHF of z derived in Section 5.2 to study the error rate performance of coherent OWC systems in Gamma-Gamma turbulence.

[5]The MGF of the product of two independent Nakagami RVs was derived independently in [95] in terms of the Meijer's G-function.

5.3.1 MRC with Perfect Channel Estimation

Assuming perfect channel estimation, the instantaneous SNR at the MRC combiner output is

$$\gamma_{MRC} = \frac{RA\left(\sum_{l=1}^{L} I_{s,l}\right)}{q\Delta f} = \overline{\gamma}\sum_{l=1}^{L} I_{s,l} \tag{5.21}$$

where $\overline{\gamma} = RA/(q\Delta f)$ denotes the average SNR per branch for a given coherent OWC system. Note that the SNR expression in (6.5) is proportional to the sum of the instantaneous signal irradiances. Since $I_{s,l}, l = 1, \cdots, L$, are i.i.d. Gamma-Gamma RVs, the MGF of $\sum_{l=1}^{L} I_{s,l}$ can be expressed as $M(s) = [M_{I_s}(s)]^L$. Hence, it is straightforward to show that the BER of MRC OWC systems with Gamma-Gamma turbulence is

$$P_e = \frac{1}{\pi}\int_0^{\frac{\pi}{2}} \left[M_{I_s}\left(-\frac{\overline{\gamma}}{2\sin\theta^2}\right)\right]^L d\theta \tag{5.22}$$

where the closed-form expression of $M_{I_s}(\cdot)$ is given in (5.7).

5.3.2 EGC with Perfect Phase Noise Compensation

In this section, we assume the phase noise has been fully compensated at the EGC receiver. The instantaneous SNR at the output of the combiner is

$$\gamma_{EGC} = \frac{RA\left(\sum_{l=1}^{L}\sqrt{I_{s,l}}\right)^2}{Lq\Delta f} = g^2\left(\sum_{l=1}^{L}\sqrt{I_{s,l}}\right)^2 \tag{5.23}$$

where $g \triangleq \sqrt{RA/(Lq\Delta f)}$ is a positive scalar factor. We can express the average BER of BPSK over Gamma-Gamma atmospheric turbulence as

$$P_e = \int_0^{\infty} \frac{1}{2}\mathrm{erfc}\left(\frac{gz_s}{\sqrt{2}}\right) f_{z_s}(z_s)dz_s \tag{5.24}$$

where $z_s = \sum_{l=1}^{L} \sqrt{I_{s,l}}$.

The CHF $\Phi_{z_s}(\omega)$ of z_s can be obtained in closed-form as $\Phi_{z_s}(\omega) = [\Phi_z(\omega)]^L$, where $\Phi_z(\omega)$ is given in (5.18)-(5.20). We make use of a Fourier inverse transform and express the PDF of z_s as

$$f_{z_s}(z_s) = \frac{1}{2\pi}\int_{-\infty}^{\infty} \Phi_{z_s}(\omega) e^{-j\omega z_s} d\omega = \frac{1}{2\pi}\int_{-\infty}^{\infty} [\Phi_z(\omega)]^L e^{-j\omega z_s} d\omega. \tag{5.25}$$

Using the Fourier transform of the complementary error function

$$F(\omega) = \frac{1}{\sqrt{\pi}} {}_1F_1\left(1, \frac{3}{2}; -\frac{\omega^2}{4}\right) + \frac{j}{\omega}\left(1 - e^{-\frac{\omega^2}{4}}\right) \tag{5.26}$$

and substituting (5.25) into (5.24) with a substitution of variables $\omega = \tan\theta$, we can obtain the desired average BER expression as

$$\begin{aligned} P_e &= \frac{1}{2\pi}\int_{-\infty}^{\infty} \Re\left\{\left[\Phi_z^*\left(\frac{g\omega}{\sqrt{2}}\right)\right]^L \frac{F(\omega)}{2}\right\} d\omega \\ &= \frac{1}{2\pi}\int_{-\frac{\pi}{2}}^{\frac{\pi}{2}} \Re\left\{\sec^2\theta \left[\Phi_z^*\left(\frac{\sqrt{\bar{\gamma}}\tan\theta}{\sqrt{2L}}\right)\right]^L \frac{F(\tan\theta)}{2}\right\} d\theta. \end{aligned} \tag{5.27}$$

Equation (5.27) can be easily evaluated numerically as it involves only a single definite integration.

The average BER of Gamma-Gamma turbulence-induced fading in L independent atmospheric channels with MRC and EGC is plotted in Fig. 5.1 for BPSK when $\sigma_R^2 = 2$ (with the corresponding channel parameters $\alpha = 2.23, \beta = 1.70$), for strong turbulence conditions. In Fig. 5.1, the channel states are assumed to be known at the MRC/EGC receiver. As expected, the BER performance improves as the number of diversity branches increases. It is readily seen that even a small diversity order increase can significantly mitigate the effects of atmospheric turbulence. Furthermore, the error rate performance of a coherent OWC system employing EGC is close to the MRC case. For example, it is apparent from Fig. 5.1 that there is less than 1 dB SNR difference between four-branch MRC and EGC reception at a BER of 2×10^{-6}. Though it is not shown in Fig. 5.1, and the

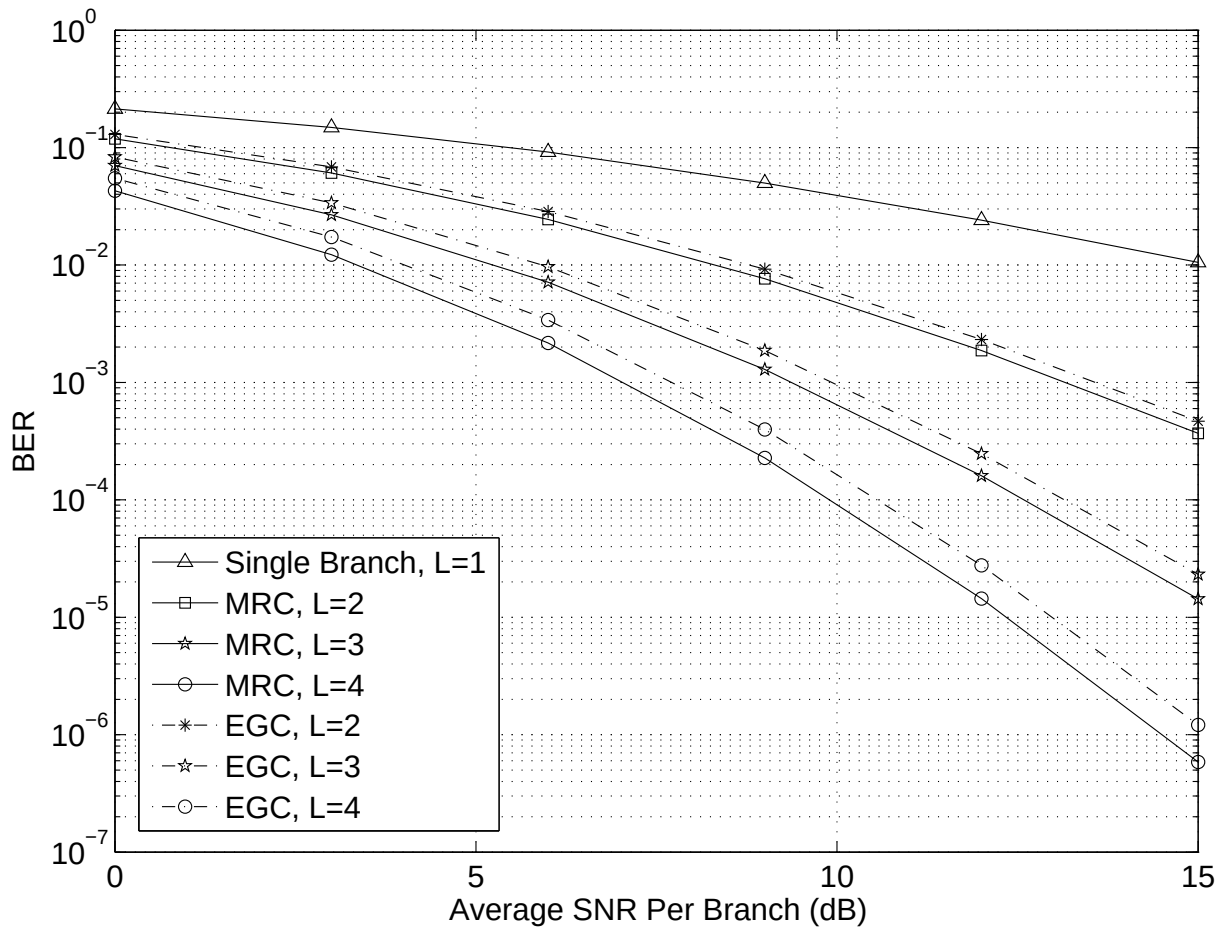

Figure 5.1: BER of BPSK for MRC and EGC reception (assuming perfect channel state information) operating over L strongly turbulent Gamma-Gamma channels with channel parameters $\alpha = 2.23, \beta = 1.70$.

following figures, all the numerical results have been verified by computer simulations.

5.4 Impacts of Imperfect Phase Noise Compensation

In this section, we investigate the impact of phase estimation error on system performance. We first derive the demodulator output decision statistics in the presence of phase noise compensation error. Following the signal flow in Section 5.1, we let $\xi_l \triangleq 2R\sqrt{P_{s,l}P_{LO}}$ and express the AC current

as

$$i_{ac,l}(t) = \xi_l g(t) \left[\cos\phi_s \cos(\omega_{IF} t + \phi_{n,l}) - \sin\phi_s \sin(\omega_{IF} t + \phi_{n,l})\right]. \tag{5.28}$$

Two filters are then used to implement the complex filtering in the down-conversion process. The real and imaginary parts of the baseband signal are, respectively, obtained as

$$y_{c,l}(t) = \sqrt{2}\left\{\xi_l g(t)[\cos\phi_s \cos(\omega_{IF} t + \phi_{n,l}) - \sin\phi_s \sin(\omega_{IF} t + \phi_{n,l})]\right\} \cos(\omega_{IF} t) \tag{5.29}$$

and

$$y_{s,l}(t) = -\sqrt{2}\left\{\xi_l g(t)[\cos\phi_s \cos(\omega_{IF} t + \phi_{n,l}) - \sin\phi_s \sin(\omega_{IF} t + \phi_{n,l})]\right\} \sin(\omega_{IF} t). \tag{5.30}$$

After passing through a lowpass filter, we obtain the equivalent baseband signal $\tilde{i}_{ac,l}(t)$. Thus, the equivalent baseband signal of $i_l(t)$ can be found as

$$\tilde{i}_l(t) = \tilde{i}_{ac,l}(t) + \tilde{n}_l(t) = \sqrt{2} R \sqrt{A P_{LO}} g(t) \sqrt{I_{s,l}} e^{j\phi_s} e^{j\phi_{n,l}} + \tilde{n}_l(t), \quad l = 1, 2, ..., L \tag{5.31}$$

where $\tilde{n}_l(t)$ is the complex-envelope of the real white Gaussian noise process.

After correlation and sampling, assuming perfect bit synchronization, we obtain

$$\begin{aligned} \tilde{i}_l &= \int_0^T \sqrt{2A} R \sqrt{I_{s,l} P_{LO}} g(t) e^{j\phi_{n,l}} e^{j\phi_s} g(t) dt + \int_0^T \tilde{n}_l(t) g(t) dt \\ &= \sqrt{2A} R \sqrt{I_{s,l} P_{LO}} e^{j\phi_{n,l}} e^{j\phi_s} + \tilde{n}_l, \quad l = 1, 2, ..., L \end{aligned} \tag{5.32}$$

where $\tilde{n}_l$ is a zero-mean complex Gaussian RV, and its real and imaginary parts are Gaussian RVs with equal variance σ^2. The receiver removes the random phase noise in the optical links on all diversity branches by multiplying the received signals with the complex conjugate of the phase

noise estimates from the respective channels. The output of the combiner can then be found as

$$\begin{aligned}\tilde{i} &= \sum_{l=1}^{L} e^{-j\hat{\phi}_{n,l}}\sqrt{2}R\sqrt{P_{s,l}P_{LO}}e^{j\phi_{n,l}}e^{j\phi_s} + \sum_{l=1}^{L} e^{-j\hat{\phi}_{n,l}}\tilde{n}_l \\ &= \sum_{l=1}^{L} e^{j\Delta\phi_l}\sqrt{2}R\sqrt{I_{s,l}AP_{LO}}e^{j\phi_s} + \nu \end{aligned} \tag{5.33}$$

where $\hat{\phi}_{n,l}$ is the estimation of $\phi_{n,l}$ at the lth branch, $\Delta\phi_l = \phi_{n,l} - \hat{\phi}_{n,l}$ denotes the phase noise compensation error, $\nu = \sum_{l=1}^{L} e^{-j\hat{\phi}_{n,l}}\tilde{n}_l$ is the complex noise term at the output of the combiner. The real and imaginary parts of the noise term ν are Gaussian RVs with equal variance $L\sigma^2$. We assume that the phase noise estimations are derived from an unmodulated carrier using a first-order PLL and only Gaussian noise is present in the PLL circuit. In this case, the PDF of the phase noise compensation error $\Delta\phi$ is given by [96]

$$f_{\Delta\phi}(\Delta\phi_l) = \frac{\exp\left(\frac{\cos(\Delta\phi_l)}{\sigma^2_{\Delta\phi}}\right)}{2\pi I_0\left(\frac{1}{\sigma^2_{\Delta\phi}}\right)}, \quad |\Delta\phi| \leq \pi \tag{5.34}$$

where $I_0(\cdot)$ is the modified Bessel function of the first kind of the zeroth order, and $\sigma_{\Delta\phi}$ denotes the standard deviation of the phase noise compensation error $\Delta\phi_l$ for $l = 1, \cdots, L$. We note that $\sigma_{\Delta\phi}$ is the standard deviation of $\Delta\phi_l$ as long as the loop SNR is large [96], which is true for practical links. We assume that $\Delta\phi_1, \Delta\phi_2, \cdots, \Delta\phi_L$ are i.i.d. RVs and the irradiance $I_{s,l}$ is independent of $\Delta\phi_l$. In a typical OWC link, the turbulence has little change over the duration of hundreds or thousands of consecutive information bits, and the phase noise varies slowly compared to the high data rates in OWC applications.

Since BPSK is assumed here, one finally obtains the demodulator decision variable by taking the real part of (5.33) as

$$D = \sum_{l=1}^{L} \sqrt{2}R\sqrt{AP_{LO}}\cos\phi_s\sqrt{I_{s,l}}\cos\Delta\phi_l + \Re\{\nu\} = \cos\phi_s\sum_{l=1}^{L} S_l + \nu_R$$

where $S_l = \sqrt{2}R\sqrt{AP_{LO}}\sqrt{I_{s,l}}\cos\Delta\phi_l$, and $\nu_R = \Re\{\nu\}$ is a real valued zero-mean Gaussian noise RV with variance $\sigma^2_{\nu_R} = L\sigma^2$. Based on the decision variable at the output of the combiner, we can find the SNR for EGC reception with phase noise compensation error as

$$\tilde{\gamma}_{EGC} = \frac{2R^2AP_{LO}}{L\sigma^2}\left(\sum_{n=1}^{L}\sqrt{I_{s,l}}\cos\Delta\phi_l\right)^2 = \frac{\overline{\gamma}}{L}\left(\sum_{n=1}^{L}\sqrt{I_{s,l}}\cos\Delta\phi_l\right)^2. \tag{5.35}$$

Of importance to the on-going investigation is the fact that the SNR in (5.35) is related to $\sqrt{I_{s,l}}$ and $\cos\Delta\phi_l$, but it is independent of the LO power.

Without loss of generality, we assume $\phi_s = 0$. From the expression of the decision variable in (5.35), we now derive the average BER for EGC with phase noise compensation error through a CHF approach. We define the cumulative distribution function (CDF) of the decision variable as

$$F_D(\xi|\phi_s = 0) = \Pr\{D < \xi|\phi_s = 0\}. \tag{5.36}$$

The average BER can, thus, be written as $P_e = F_D(0|\phi_s = 0)$ when (5.36) is evaluated at $\xi = 0$.

To find $F_D(\cdot|\phi_s = 0)$, we write the conditional CHF of D as

$$\Phi_D(\omega|\phi_s = 0) = \Phi_{\nu_R}(\omega)\prod_{l=1}^{L}\Phi_{S_l}(\omega) = \Phi_{\nu_R}(\omega)[\Phi_{S_1}(\omega)]^L \tag{5.37}$$

for i.i.d. RVs S_l's ($l = 1,\cdots,L$), where $\Phi_{S_l}(\omega)$ is the CHF of S_l for $l = 1,2,\cdots,L$, and $\Phi_{\nu_R}(\omega) = \exp(-L\sigma^2\omega^2/2)$ is the CHF of the Gaussian RV ν_R. The CHF of S_1 conditioned on $\Delta\phi_1$ can be found to be

$$\Phi_{S_1|\Delta\phi_1}(\omega) = \Phi_z\left(\omega\sqrt{2AP_{LO}}R\cos\Delta\phi_1\right). \tag{5.38}$$

Averaging (5.38) over $\Delta\phi_1$ gives the CHF of S_1 as $\Phi_{S_1}(\omega) = E_{\Delta\phi_1}[\Phi_z(\omega\sqrt{2AP_{LO}}R\cos\Delta\phi_1)]$. Then,

the CHF of D can be found as

$$\begin{aligned}\Phi_D(\omega|\phi_s=0) &= [\Phi_{S_1}(\omega)]^L \Phi_{\nu_R}(\omega) \\ &= (E_{\Delta\phi_1}[\Phi_z(\omega\sqrt{2AP_{LO}}R\cos\Delta\phi_1)])^L \Phi_{\nu_R}(\omega). \end{aligned} \tag{5.39}$$

The CDF $F_D(\xi|\phi_s=0)$ can be calculated through the Gil-Pelaez formula [97]

$$F_D(\xi|\phi_s=0) = \frac{1}{2} - \frac{1}{\pi}\int_0^\infty \frac{\Im\{\Phi_D(\omega|\phi_s=0)e^{-j\omega\xi}\}}{\omega} d\omega. \tag{5.40}$$

Finally, we find the BER with phase noise compensation errors to be

$$P_e = \frac{1}{2} - \frac{1}{\pi}\int_0^\infty \frac{\Im\{\Phi_D(\omega|\phi_s=0)\}}{\omega} d\omega. \tag{5.41}$$

Substituting (5.39) into (5.40) gives the BER expression for EGC reception with phase noise compensation error. Two integrations are required to evaluate the BER performance of an L-branch EGC system using (5.39)-(5.41).

In Fig. 5.2 and Fig. 5.3, the impact of phase noise is presented for L-branch EGC OWC systems for strong and weak turbulence conditions, respectively. One can see that there is a performance loss due to the phase noise compensation error. The performance degradation, as expected, worsens when the standard deviation of the phase noise compensation error increases. A notable point in Fig. 5.2 is that there is relatively little difference in the error performance between the system with perfect phase noise compensation and ones with phase noise compensation errors of $\sigma_{\Delta\phi} = 10^\circ$ or $\sigma_{\Delta\phi} = 20^\circ$. In particular, only small performance losses (less than 1 dB SNR loss) are observed with a phase noise compensation error of $\sigma_{\Delta\phi} = 20^\circ$ for both two- and three-branch reception. As the standard deviation of the phase noise compensation error increases, however, the optical wireless systems suffer from larger performance degradation. For instance, for an SNR per branch of 15 dB, the BER is 2.8×10^{-5} for $\sigma_{\Delta\phi} = 20^\circ$, but it degrades to 1.6×10^{-3} for $\sigma_{\Delta\phi} = 30^\circ$.

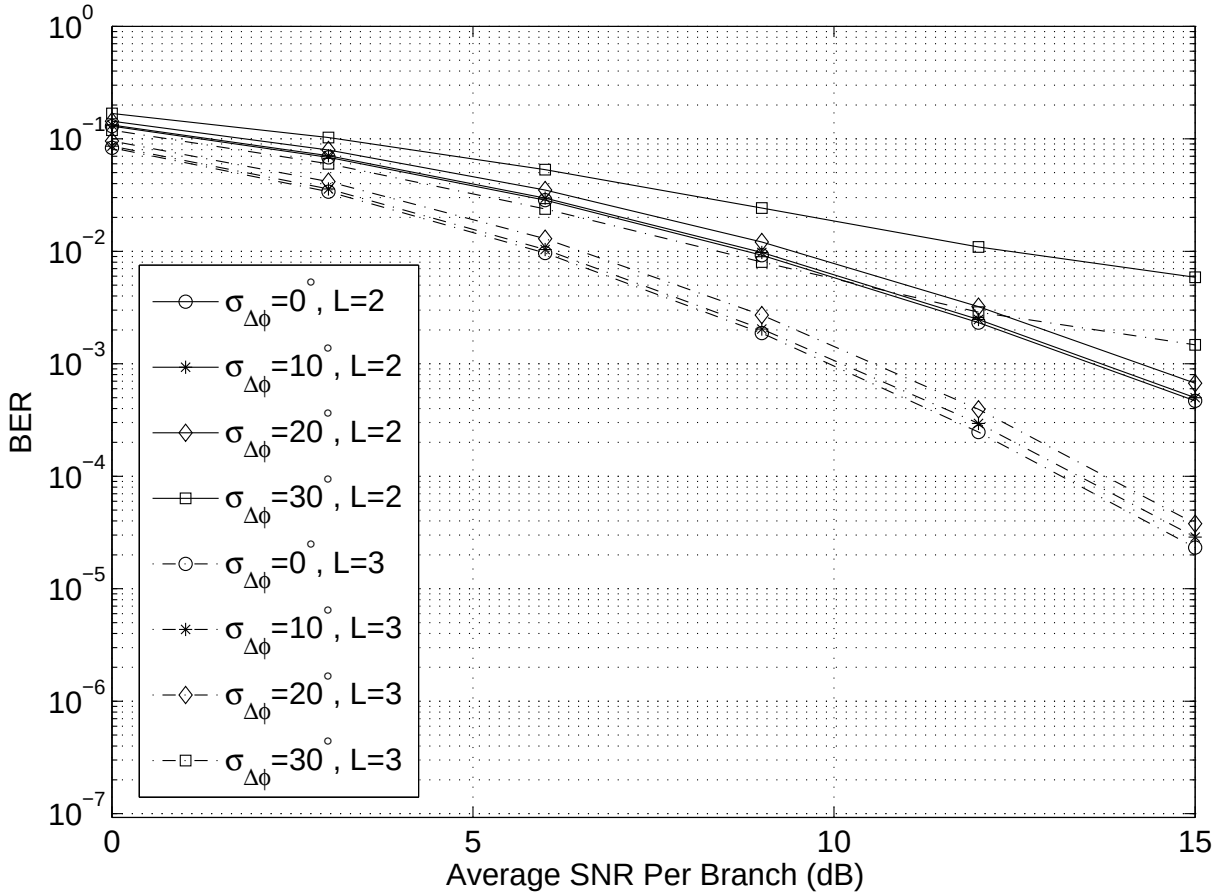

Figure 5.2: BER of BPSK for EGC reception with phase noise compensation error operating over L strongly turbulent Gamma-Gamma channels with channel parameters $\alpha = 2.23, \beta = 1.70$.

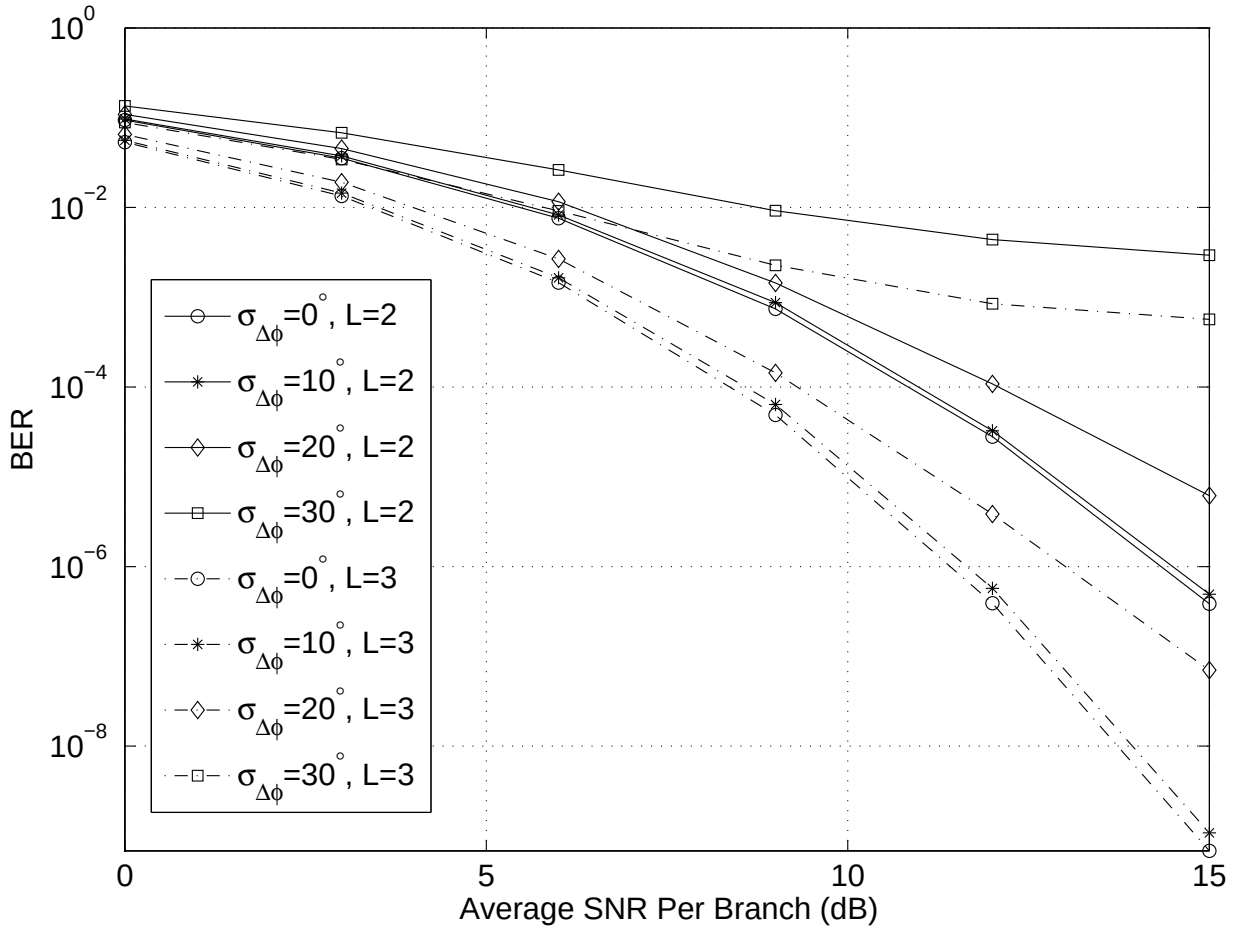

Figure 5.3: BER of BPSK for EGC reception with phase noise compensation error operating over L weakly turbulent Gamma-Gamma channels with channel parameters $\alpha = 6.52, \beta = 6.92$.

As a point of comparison to Fig. 5.2 in strong turbulence conditions, Fig. 5.3 presents two- and three-branch EGC reception in weak optical wireless turbulence links when $\sigma_R^2 = 0.3$ (with the corresponding channel parameters $\alpha = 6.52, \beta = 6.92$). Again, we observe that the performance degradation becomes larger when the standard deviation of the phase noise compensation error increases. We also find that, comparing Figs. 5.2 and 5.3, the error rate performance in weak turbulence is much better than that in strong turbulence, as expected. For example, at an average SNR per branch of 10 dB, the BER with three-branch EGC reception is on the order of 10^{-3} in strong turbulence but the BER is on the order of 10^{-5} in weak turbulence.

From Figs. 5.2 and 5.3, we also conclude that the standard deviation of the phase noise compensation error is a crucial parameter in performance estimation of an OWC system with EGC reception. We find that EGC is a viable choice with a relatively simple implementation when $\sigma_{\Delta\phi}$ is less than 20°. When $\sigma_{\Delta\phi}$ is larger, EGC suffers from great performance losses. Thus, we need to either employ a proper phase tracking technique or an alternative scheme.

5.5 Differential Phase-Shift Keying for Coherent Optical Wireless Systems

Since phase noise levels from laser sources and from atmospheric turbulence channels are time variant, the phase tracking device may be subject to carrier phase estimation error. This can lead to system performance losses as discussed at the end of the last section. Motivated by postdetection EGC applications in RF communications [98], in this section we present a postdetection scheme for coherent OWC communications over the Gamma-Gamma turbulence channels. DPSK modulation is used instead of coherent PSK for diversity reception, as there is no need to estimate the phase noise.

Here, we propose a coherent OWC system employing postdetection EGC to mitigate amplitude fading, as it is well suited to differential coherent detection. Its receiver block diagram is shown

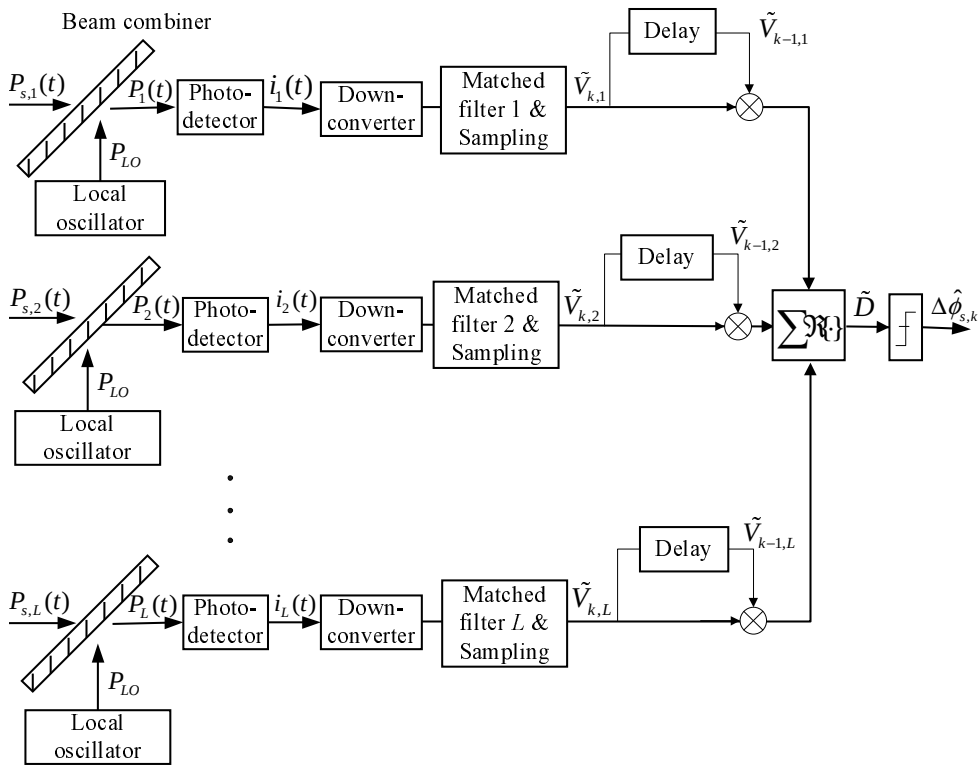

Figure 5.4: Block diagram of a postdetetion EGC coherent OWC system through an atmospheric turbulence channel.

in Fig. 5.4. The proposed OWC system is set up with L-branch optical wireless links operating through Gamma-Gamma turbulence. From (5.31) the received complex envelope at the lth branch in the kth bit interval can be written as

$$\tilde{i}_{k,l}(t) = \tilde{i}_{ac,k,l}(t) + \tilde{n}_{k,l}(t) = \sqrt{2}R\sqrt{AP_{LO}}g(t)\sqrt{I_{s,l}}e^{j\phi_{s,k}}e^{j\phi_{n,l}} + \tilde{n}_{k,l}(t) \tag{5.42}$$

where $\phi_{s,k} = \phi_{s,k-1} + \Delta\phi_{s,k}$ is the differentially coded phase. Here, $\Delta\phi_{s,k} \in \{0, \pi\}$ denotes the differential carrier phase, and the encoded phase differences are assumed to be equally likely transmitted. Due to the high data rate (Gbit/s), one can assume a "frozen atmosphere" model [63], where the atmospheric turbulence characteristics remain constant over at least two successive symbol intervals. At the same branch, the signal in the $(k-1)$th bit interval can, therefore, be obtained as

$$\tilde{i}_{k-1,l}(t) = \tilde{i}_{ac,k-1,l}(t) + \tilde{n}_{k-1,l}(t) = \sqrt{2}R\sqrt{AP_{LO}}g(t)\sqrt{I_{s,l}}e^{j\phi_{s,k-1}}e^{j\phi_{n,l}} + \tilde{n}_{k-1,l}(t).$$

The shot noise processes $\tilde{n}_{k,l}(t)$ and $\tilde{n}_{k-1,l}(t)$ are i.i.d. complex Gaussian random processes with power spectral density $4qRP_{LO}u(\omega + \omega_{IF})$. In postdetection EGC reception, we can obtain the outputs of the correlator at the lth branch as

$$V_{k,l} = \int_0^T \tilde{i}_{k,l}(t)g(t)dt = \sqrt{2}R\sqrt{AP_{LO}}\sqrt{I_{s,l}}e^{j\phi_{s,k}}e^{j\phi_{n,l}} + \mu_{k,l} \tag{5.43}$$

and

$$V_{k-1,l} = \int_0^T \tilde{i}_{k-1,l}(t)g(t)dt = \sqrt{2}R\sqrt{AP_{LO}}\sqrt{I_{s,l}}e^{j\phi_{s,k-1}}e^{j\phi_{n,l}} + \mu_{k-1,l} \tag{5.44}$$

respectively. Here, $\mu_{k,l}$ and $\mu_{k-1,l}$ are filtered complex-valued zero-mean Gaussian RVs with equal variance for both the real and imaginary parts. For simplicity, we drop the subscript l for the noise terms. Without loss of generality, we normalize the variance of μ_k and μ_{k-1} to be unity for

convenience of later applications. After normalization, we obtain

$$\tilde{V}_{k,l} = \frac{R\sqrt{A}}{\sqrt{qR\Delta f}}\sqrt{I_{s,l}}e^{j\phi_{s,k}}e^{j\phi_{n,l}} + \tilde{\mu}_k = \sqrt{\bar{\gamma}}\sqrt{I_{s,l}}e^{j\phi_{s,k}}e^{j\phi_{n,l}} + \tilde{\mu}_k \tag{5.45}$$

and

$$\tilde{V}_{k-1,l} = \frac{R\sqrt{A}}{\sqrt{qR\Delta f}}\sqrt{I_{s,l}}e^{j\phi_{s,k-1}}e^{j\phi_{n,l}} + \tilde{\mu}_{k-1} = \sqrt{\bar{\gamma}}\sqrt{I_{s,l}}e^{j\phi_{s,k-1}}e^{j\phi_{n,l}} + \tilde{\mu}_{k-1} \tag{5.46}$$

where $\tilde{\mu}_k$ and $\tilde{\mu}_{k-1}$ are i.i.d. Gaussian RVs with unity variance. Therefore, the decision variable $\tilde{D}$ at the output of the postdetection combiner is obtained as

$$\tilde{D} = \sum_{l=1}^{L}\tilde{U}_l = \sum_{l=1}^{L}\Re\{\tilde{V}^*_{k-1,l}\tilde{V}_{k,l}\} \tag{5.47}$$

where $\tilde{U}_l = \Re\{\tilde{V}^*_{k-1,l}\tilde{V}_{k,l}\}$. With [96, Eq. (B.5)], the CHF of $\tilde{U}_l$ conditioned on $I_{s,l}$ can be found as

$$\Phi_{\tilde{U}|I_{s,l}}(\omega|\Delta\phi_{s,k}=0) = \frac{1}{\omega^2+1}\exp\left(-\bar{\gamma}\frac{\omega^2-j\omega}{\omega^2+1}I_{s,l}\right). \tag{5.48}$$

With the help of [93, Eq. 6.643(3)], averaging (5.48) over $I_{s,l}$ gives the CHF of $\tilde{U}_l$ as

$$\Phi_{\tilde{U}}(\omega|\Delta\phi_{s,k}=0) = \frac{1}{\omega^2+1}M_I\left(-\bar{\gamma}\frac{\omega^2-j\omega}{\omega^2+1}\right) \tag{5.49}$$

where $M_I(\cdot)$ is given by (5.7). For i.i.d. Gamma-Gamma turbulence branches, we can express the CHF of $\tilde{D}$ as

$$\Phi_{\tilde{D}}(\omega|\Delta\phi_{s,k}=0) = \Phi^L_{\tilde{U}}(\omega|\Delta\phi_{s,k}=0) = \frac{1}{(\omega^2+1)^L}\left[M_I\left(-\bar{\gamma}\frac{\omega^2-j\omega}{\omega^2+1}\right)\right]^L. \tag{5.50}$$

With the Gil-Pelaez formula, we can obtain the average BER for DPSK with postdetection EGC

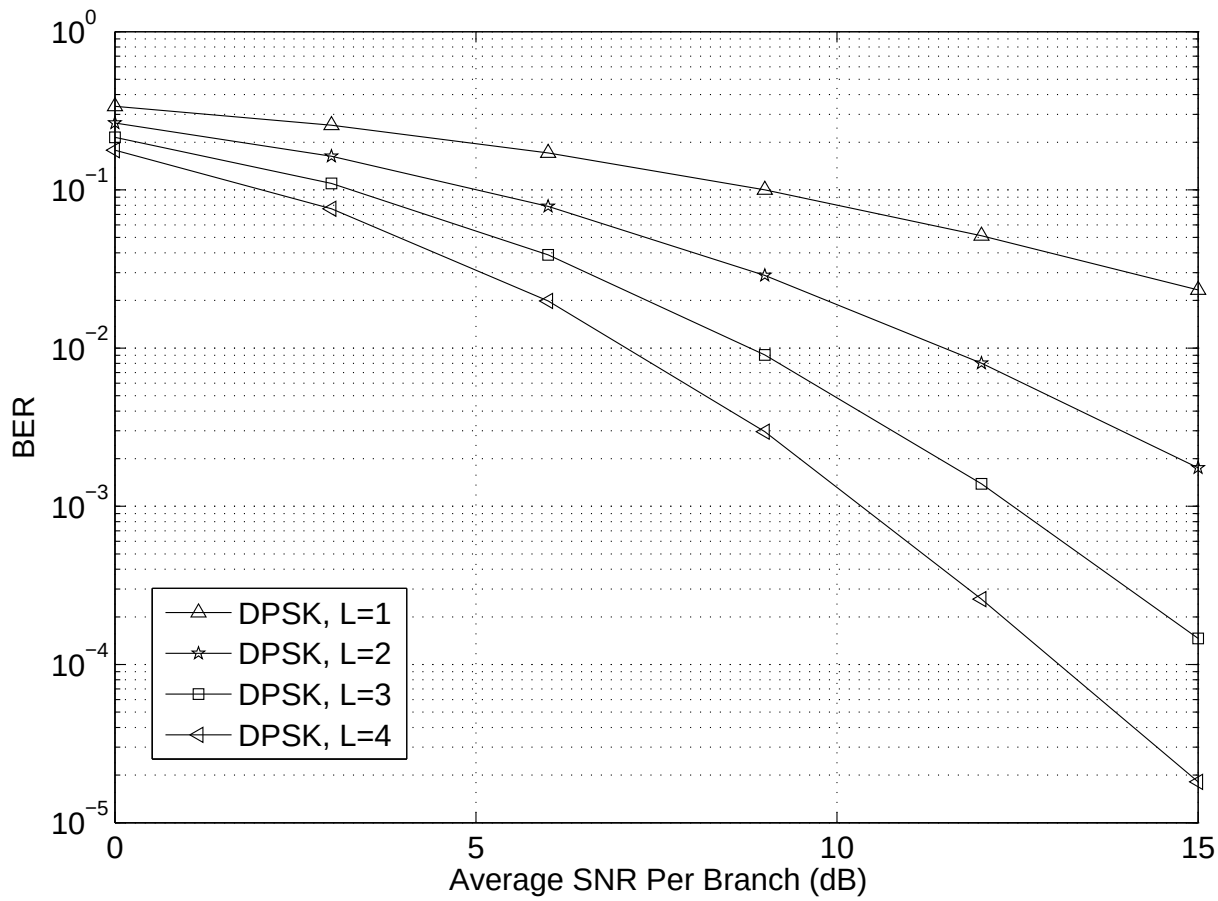

Figure 5.5: BER of DPSK for postdetection EGC reception operating over L strongly turbulent Gamma-Gamma channels with channel parameters $\alpha = 2.23, \beta = 1.70$.

as

$$P_e = \Pr\{\tilde{D} < 0 | \Delta\phi_{s,k} = 0\} = \frac{1}{2} - \frac{1}{\pi}\int_0^\infty \frac{\Im\left\{\left[M_I\left(-\bar{\gamma}\cdot\frac{\omega^2 - j\omega}{\omega^2+1}\right)\right]^L\right\}}{\omega(\omega^2+1)^L} d\omega \tag{5.51}$$

which can be used in the BER calculation for coherent DPSK systems with the MGF with (5.7).

Figure 5.5 demonstrates DPSK operation for L-branch postdetection EGC under strong turbulence conditions ($\sigma_R^2 = 2$ with the corresponding channel parameters $\alpha = 2.23, \beta = 1.70$). We find that postdetection EGC enjoys the full benefits of the diversity order. For instance, at an average SNR per branch of 15 dB, a BER of 1.8×10^{-5} is achieved. This point is further evident from Fig.

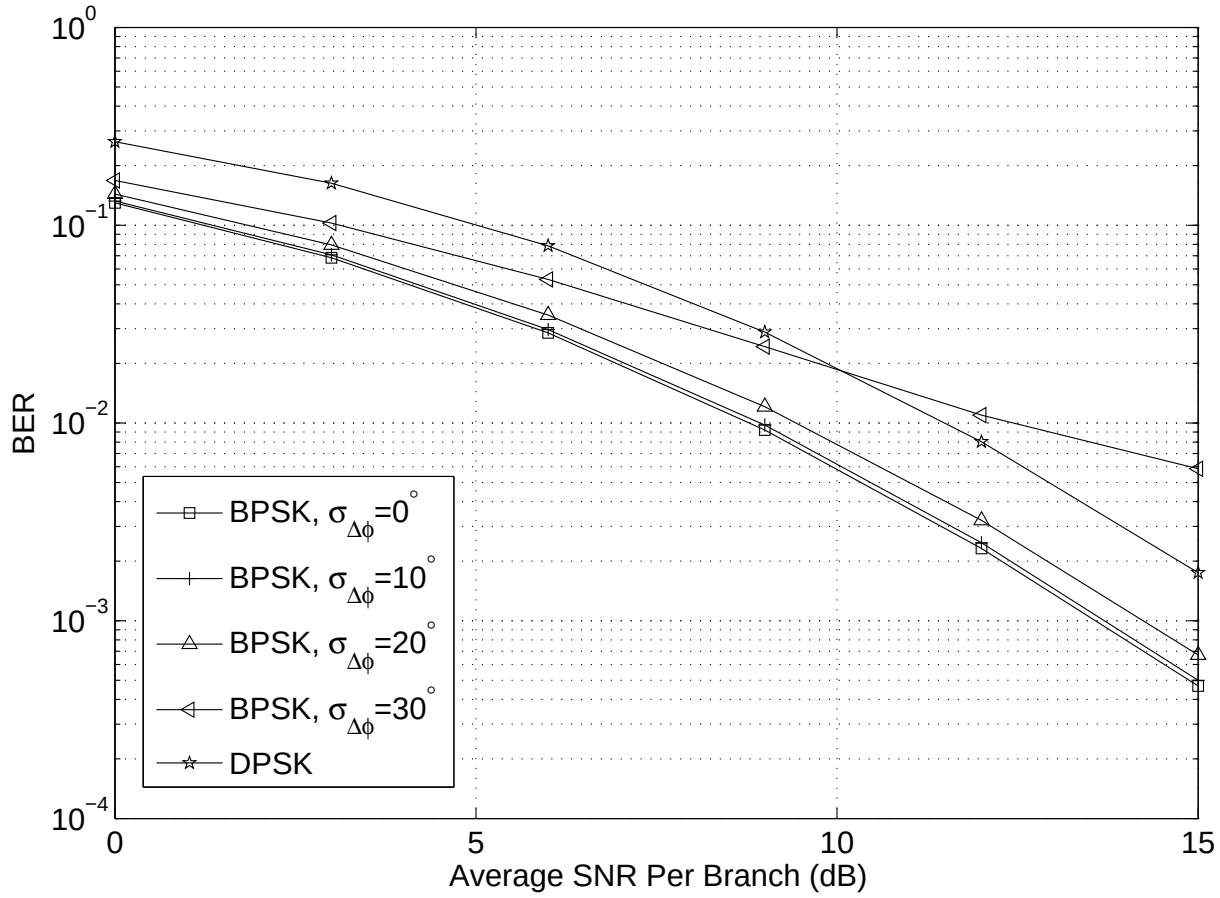

Figure 5.6: BER of BPSK with EGC and DPSK with postdetection EGC reception operating over dual-branch strongly turbulent Gamma-Gamma channels with channel parameters $\alpha = 2.23, \beta = 1.70$.

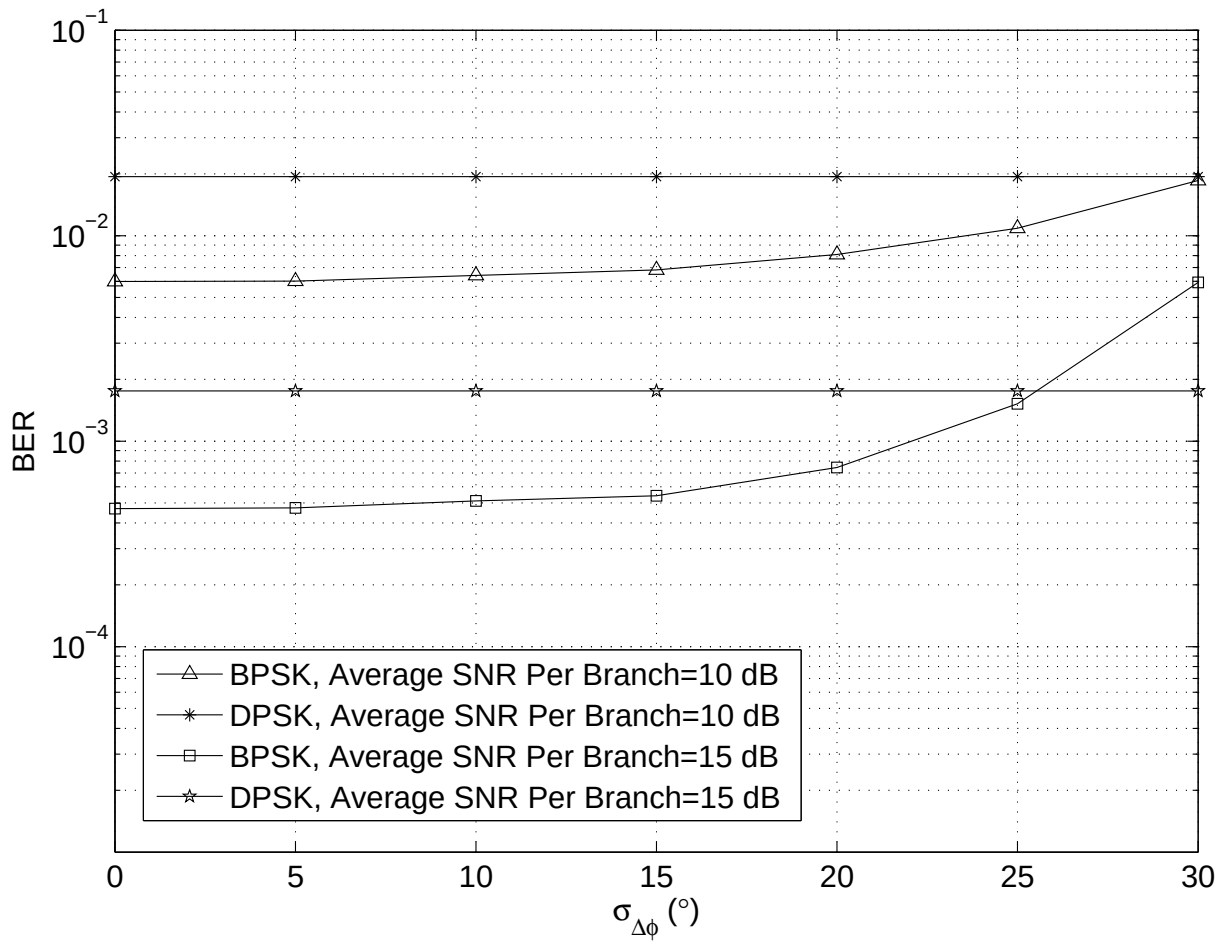

Figure 5.7: BER versus standard deviation of phase noise compensation error for BPSK with EGC and DPSK with postdetection EGC reception operating over dual-branch strongly turbulent Gamma-Gamma channels with channel parameters $\alpha = 2.23, \beta = 1.70$.

5.6, which gives a performance comparison between BPSK with EGC and DPSK with postdetection EGC for dual-branch reception. BPSK with EGC outperforms DPSK with postdetection EGC when the phase noise is compensated perfectly or the standard deviation of the phase noise compensation error is relatively small. However, DPSK with postdetection EGC outperforms BPSK with EGC when $\sigma_{\Delta\phi} = 30^\circ$ and the SNR per branch is greater than approximately 10 dB.

A complete comparison between the performance of BPSK with EGC and DPSK with postdetection EGC can be seen in Fig. 5.7, which shows the BER versus standard deviation of phase noise compensation error $\sigma_{\Delta\phi}$ from 0° to 30°. For low levels of phase noise, the displayed curves

are largely independent of $\sigma_{\Delta\phi}$. When $\sigma_{\Delta\phi}$ reaches 20°, however, the performance of BPSK worsens. At approximately 25°, the BPSK performance degrades below that of postdetection DPSK at an average SNR per branch of 15 dB. These observations agree with those in Fig. 5.6. We conclude that DPSK with postdetection EGC is an excellent alternative to BPSK with EGC in coherent OWC communication systems with large phase noise compensation errors. The presented results can be useful in coherent OWC system design and performance evaluation.

5.6 Summary

In this chapter, we have analyzed the error rate performance of coherent OWC systems and computed the BER of BPSK with the EGC diversity scheme in the Gamma-Gamma turbulence channels. Error rates for EGC OWC links with perfect phase noise compensation have been obtained, and EGC is shown to greatly improve system performance (compared to a single branch OWC link). Furthermore, it has been found that an OWC system with a small phase noise compensation error (with standard deviations of 20° for strong turbulence and 10° for weak turbulence) offers comparable error rate performance to that of the perfect phase compensation case. As a solution for coherent OWC systems operating with large phase compensation errors, DPSK with postdetection EGC scheme was proposed and shown as a viable alternative to BPSK with EGC.

Chapter 6

Comparison of Optical Communication Using Coherent Detection and Subcarrier Intensity Modulation

Given the advantages of adaptive-threshold-free OWC operation, attention from the scientific research community has been drawn to subcarrier intensity modulation (SIM) [53], [60] and coherent optical systems [63], [99]. In this chapter, we carry out a detailed error rate performance comparison of the adaptive-threshold-free coherent and SIM types of OWC systems operating over the Gamma-Gamma turbulence channels. Closed-form error rate expressions are derived and compared for MRC, EGC, and SC schemes. Diversity order and coding gain expressions are both obtained in closed-form for coherent and SIM OWC systems. The error rates of both coherent and subcarrier intensity modulated OWC systems are then compared for binary phase-shift keying, differential phase-shift keying, and frequency-shift keying when both systems are subject to the same average transmitted optical power constraints. To emphasize the differences of coherent and subcarrier systems, we start with a comparison of the coherent and subcarrier receivers and their SNRs in Section 6.1.

6.1 Receivers and SNR Comparison

6.1.1 Coherent OWC Receiver

For single branch coherent OWC systems using BPSK, the received signal and LO beams are mixed in perfect spatial coherence over a sufficiently small photodetector area[6], and the optical power incident on the photodetector can be written as

$$P(t) = P_s + P_{LO} + 2\sqrt{P_s P_{LO}}\cos(\omega_{IF} t + \phi) \tag{6.1}$$

where P_s is the received optical signal power incident on the beamsplitter, P_{LO} is the LO power[7], the phase information is $\phi \in \{0, \pi\}$ and $\omega_{IF} = \omega_c - \omega_{LO}$ is the intermediate frequency, where ω_c and ω_{LO} denote the carrier frequency and LO frequency, respectively. The incident optical power then generates the photodetector current

$$i_c(t) = i_{dc} + i_{ac}(t) + n_c(t) \tag{6.2}$$

where $i_{dc} = R(P_s + P_{LO})$ and $i_{ac}(t) = 2R\sqrt{P_s P_{LO}}\cos(\omega_{IF} t + \phi)$ are the respective DC and AC terms, and $n_c(t)$ is a shot-noise-limited AWGN process.

As the SNR of an optical receiver is defined as the ratio of the time-averaged AC photocurrent power to the total noise variance [87], we can write the instantaneous SNR at the input of a BPSK demodulator as

$$\gamma_c = \frac{2R^2 P_s P_{LO}}{2qR\Delta f P_{LO} + 2\Delta f(qRAI_b + 2k_b T_k F_n / R_L)} \approx \frac{RA}{q\Delta f} I = \frac{\eta_e A}{h\nu\Delta f} I_s = C_c I_s \tag{6.3}$$

where I_b is the background light irradiance, k_b is Boltzmann's constant, T_k is the temperature in Kelvin, F_n represents a thermal noise enhancement factor due to amplifier noise, R_L is the load

[6] A p-i-n photodiode is assumed for both the coherent and SIM receivers.

[7] The LO power is assumed to be the same for all branches in the case of diversity receptions.

resistance, and $C_c = \eta_e A/(h\nu\Delta f)$ denotes a multiplicative constant for a given coherent system. Here, a sufficiently large LO power P_{LO} is used, thus the thermal noise and background noise are negligible.

6.1.2 Subcarrier OWC Receiver

In a SIM system, a premodulated RF signal $m(t)$ is used to modulate the irradiance of a continuous wave optical beam at the laser transmitter. Considering a BPSK modulated subcarrier signal, one adds a DC bias to the message signal $m(t)$ and uses it to drive the transmit laser directly. For a turbulence-free channel, the incident optical power and resulting photocurrent at the receiver will be proportional to $m(t)$. For a single branch channel with turbulence, the photocurrent at the receiver is given by

$$i_r(t) = RP_{in}[1+\xi m(t)] + n_s(t) = RI_sA[1+\xi\cos(\omega_{sc}t+\phi)] + n_s(t) \tag{6.4}$$

where ξ is the modulation index and the condition $-1 < \xi m(t) < 1$ must be satisfied to avoid overmodulation. In (6.4), P_{in} denotes the incident optical power on the photodetector, ω_{sc} denotes the frequency of the RF subcarrier, the phase $\phi \in \{0,\pi\}$ represents the bit information (as defined in the coherent receiver model), and $n_s(t)$ is the AWGN process due to thermal and/or background noise. If we normalize the power of $m(t)$ to be unity, we can express the instantaneous SNR for SIM OWC systems at the input of the BPSK demodulator as

$$\gamma_s = \frac{(RA\xi)^2}{2\Delta f(qRAI_b + 2k_bT_kF_n/R_L)} I_s^2 = C_s I_s^2 \tag{6.5}$$

where Δf is assumed to be the same as that for the coherent receiver, and $C_s = (RA\xi)^2/(2\Delta f(qRAI_b + 2k_bT_kF_n/R_L))$ is a multiplicative constant for a given SIM system.

6.1.3 Electrical SNR and Average SNR

Within the OWC literature, there exist two common SNR definitions: electrical SNR and average SNR. We clarify these two averaged SNRs and discuss their relationship in this subsection. For simplicity, we normalize the first moment of the irradiance I to unity for both coherent and SIM links.

The average SNR for coherent OWC systems is defined as the statistical average of the instantaneous SNR γ_c according to

$$\overline{\gamma}_c = E\left[\gamma_c\right] = C_c E\left[I\right] = C_c. \tag{6.6}$$

Similarly, we define the average SNR for subcarrier OWC systems to be

$$\overline{\gamma}_s = E\left[\gamma_s\right] = C_s E\left[I^2\right] = C_s \frac{(\alpha+1)(\beta+1)}{\alpha\beta} \tag{6.7}$$

and relate $\overline{\gamma}_s$ to the instantaneous SNR γ_s by

$$\gamma_s = C_s I^2 = \frac{\alpha\beta\overline{\gamma}_s}{(\alpha+1)(\beta+1)} I^2. \tag{6.8}$$

An alternative definition of SNR, called electrical SNR for direct detection systems, is defined as [77]

$$\overline{\gamma}_e = (E[I])^2 \gamma_e = \gamma_e \tag{6.9}$$

where γ_e is the total bit energy-to-noise spectral density ratio in the absence of turbulence. We observe from (6.9) that the electrical SNR is independent of the channel parameters for the normalized turbulence models (i.e., $E[I] = 1$). The electrical SNR definition is popular in direct detection based OWC systems, as only the first moment of the irradiance is required. However, the electrical SNR definition is not applicable to coherent OWC systems. This is because the received signal power for coherent optical systems is not equal to the optical power incident on the photodetector (in the absence of turbulence). By virtue of mixing the received signal with a strong local oscillator

field at the beamsplitter, the received signal power will be amplified by the local oscillator creating a large composite optical power on the photodetector. The resulting bit energy at the photodetector is not the same as the bit energy at the beamsplitter. Consequently, the electrical SNR is not applicable for coherent OWC links. For this reason, average SNR is widely used for coherent systems in the literature [63], [65], [68].

In the following, we first derive the error rates of coherent and SIM systems in terms of the respective average SNR ($\overline{\gamma}_c$ and $\overline{\gamma}_s$), then we express these error rates as a function of average transmitted optical power to facilitate the comparison of coherent and SIM systems when both systems are subject to the same average transmitted power constraints.

6.2 SNR Comparison

Without loss of generality, we assume BPSK is employed for both coherent and SIM systems with MRC and EGC receptions, and DPSK and NCFSK are employed for both systems with SC reception. For a fair comparison, we also assume that the coherent and SIM systems have the same channel parameters.

6.2.1 MRC Combiner Output SNR

For coherent MRC systems using MRC, the instantaneous SNR at the output of the combiner is

$$\gamma_{c,MRC} = \frac{RA\left(\sum_{l=1}^{L} I_{s,l}\right)}{q\Delta f} = \overline{\gamma}_c \left(\sum_{l=1}^{L} I_{s,l}\right) \tag{6.10}$$

where $I_{s,l}$ denotes the optical signal irradiance at the lth branch. For subcarrier systems using MRC, the instantaneous SNR at the output of the combiner is

$$\gamma_{s,MRC} = \frac{\alpha\beta\overline{\gamma}_s}{(\alpha+1)(\beta+1)} \left(\sum_{l=1}^{L} I_{s,l}^2\right). \tag{6.11}$$

6.2.2 EGC Combiner Output SNR

For coherent systems using EGC, the instantaneous SNR at the output of the combiner is [99]

$$\gamma_{c,EGC} = \frac{RA\left(\sum_{l=1}^{L}\sqrt{I_{s,l}}\right)^2}{Lq\Delta f} = \frac{\overline{\gamma}_c}{L}\left(\sum_{l=1}^{L}\sqrt{I_{s,l}}\right)^2. \tag{6.12}$$

For subcarrier systems using EGC, the instantaneous SNR at the output of the combiner is

$$\gamma_{s,EGC} = \frac{\alpha\beta\overline{\gamma}_s}{L(\alpha+1)(\beta+1)}\left(\sum_{l=1}^{L} I_{s,l}\right)^2. \tag{6.13}$$

6.2.3 SC Combiner Output SNR

For coherent systems using SC, the instantaneous SNR at the output of the combiner is

$$\gamma_{c,SC} = \frac{RA\max\{I_{s,l}; l=1,\cdots,L\}}{q\Delta f} = \overline{\gamma}_c \max\{I_{s,l}; l=1,\cdots,L\}. \tag{6.14}$$

For subcarrier systems using SC, the instantaneous SNR at the output of the combiner is

$$\gamma_{s,SC} = C_s \max\{I_{s,l}^2; l=1,\cdots,L\} = \frac{\alpha\beta\overline{\gamma}_s}{(\alpha+1)(\beta+1)}\max\{I_{s,l}^2; l=1,\cdots,L\}. \tag{6.15}$$

6.3 BER Analyses with Diversity Reception

6.3.1 BER with MRC Reception

Coherent Systems With MRC: We use the MGF method to evaluate the BER according to (4.1)

$$P_{c,MRC} = \frac{1}{\pi}\int_0^{\frac{\pi}{2}}\left[M_{I_s}\left(-\frac{\overline{\gamma}_c}{2\sin^2\theta}\right)\right]^L d\theta \tag{6.16}$$

where $M_{I_s}(\cdot)$ denotes the MGF of I_s which is given in Eqs. (5.7)-(5.9). From (6.10), we define $V = \sum_{l=1}^{L} I_{s,l}$ and rewrite (6.16) as

$$P_{c,MRC} = \frac{1}{\pi}\int_0^{\frac{\pi}{2}} M_V\left(-\frac{\overline{\gamma}_c}{2\sin^2\theta}\right) d\theta \tag{6.17}$$

where $M_V(s)$ is the MGF of V. Using a series expansion of the modified Bessel function of the second kind [52, Eq. (6)]

$$K_\nu(x) = \frac{\pi}{2\sin(\pi\nu)}\sum_{p=0}^{\infty}\left(\frac{(x/2)^{2p-\nu}}{\Gamma(p-\nu+1)p!} - \frac{(x/2)^{2p+\nu}}{\Gamma(p+\nu+1)p!}\right),\ \nu \notin \mathbf{Z},\ |x| < \infty \tag{6.18}$$

we can find the MGF of V as [52]

$$M_V(r) = \sum_{q=0}^{L}\binom{L}{q}\left(\sum_{p=0}^{\infty} a_p(\alpha,\beta)\Gamma(p+\beta)(-s)^{-(p+\beta)}\right)^{L-q}\left(\sum_{p=0}^{\infty} a_p(\beta,\alpha)\Gamma(p+\alpha)(-s)^{-(p+\alpha)}\right)^{q} \tag{6.19}$$

where

$$a_p(x,y) \triangleq \frac{(xy)^{p+y}\Gamma(x-y)\Gamma(y-x+1)}{\Gamma(x)\Gamma(y)\Gamma(p-x+y+1)p!}. \tag{6.20}$$

Thus, we obtain a closed-form expression of the BER for coherent MRC systems as

$$\begin{aligned}
P_{c,MRC} =& \frac{1}{\pi}\sum_{q=0}^{L}\binom{L}{q}\sum_{p=0}^{\infty}[\Gamma(p+\beta)a_p(\alpha,\beta)]^{[L-q]} * [\Gamma(p+\alpha)a_p(\beta,\alpha)]^{[q]}\left(\frac{\overline{\gamma}_c}{2}\right)^{-p-L\beta-q(\alpha-\beta)} \\
&\times \int_0^{\frac{\pi}{2}}(\sin\theta)^{2[p+L\beta+q(\alpha-\beta)]}d\theta \\
=& \frac{1}{2\pi}\sum_{q=0}^{L}\binom{L}{q}\sum_{p=0}^{\infty} B\left(\frac{1}{2}, p+L\beta+q(\alpha-\beta)+\frac{1}{2}\right)[\Gamma(p+\beta)a_p(\alpha,\beta)]^{[L-q]} \\
&* [\Gamma(p+\alpha)a_p(\beta,\alpha)]^{[q]}\left(\frac{\overline{\gamma}_c}{2}\right)^{-p-L\beta-q(\alpha-\beta)}
\end{aligned} \tag{6.21}$$

where $*$ denotes the convolution operator and $[a_p(\alpha,\beta)\Gamma(p+\beta)]^{[n]}$ denotes $a_p(\alpha,\beta)\Gamma(p+\beta)$ convolved $n-1$ times with itself. Specifically, we have $[a_p(\alpha,\beta)\Gamma(p+\beta)]^{[0]}=1$ and $[a_p(\alpha,\beta)\Gamma(p+\beta)]^{[1]}=a_p(\alpha,\beta)\Gamma(p+\beta)$. In deriving (6.21), we have also used an integral property [93, Eq. 3.621(1), Eq. 8.384(4)]

$$\int_0^{\frac{\pi}{2}}(\sin\theta)^{p+\alpha}d\theta = B\left(\frac{1}{2},\frac{p+\alpha+1}{2}\right)\Big/2 \tag{6.22}$$

where $B(x,y)=\frac{\Gamma(x)\Gamma(y)}{\Gamma(x+y)}$ denotes the Beta function [93, Eq. 8.384(1)] which is defined as

$$B(x,y)\triangleq\int_0^1 t^{x-1}(1-t)^{y-1}dt,\quad \Re\{x\}>0,\ \Re\{y\}>0. \tag{6.23}$$

SIM Systems With MRC: Letting $G=\sum_{l=1}^{L}I_{s,l}^2$, we can similarly find the average BER for SIM MRC systems as

$$P_{s,MRC}=\frac{1}{\pi}\int_0^{\frac{\pi}{2}}M_G\left(-\frac{\alpha\beta\overline{\gamma_s}}{2(\alpha+1)(\beta+1)\sin^2\theta}\right)d\theta \tag{6.24}$$

where $M_G(\cdot)$ denotes the MGF of G and it is obtained in the following way. Let $X={I_s}^2$ be a channel-dependent RV. Using (6.18) and an integral identity [93, Eq. 3.478(1)], we obtain the MGF of X as [78, Eq. (7)]

$$M_X(s)=\frac{1}{2}\sum_{p=0}^{\infty}\left[a_p(\alpha,\beta)\Gamma\left(\frac{p+\beta}{2}\right)(-s)^{-\frac{p+\beta}{2}}-a_p(\beta,\alpha)\Gamma\left(\frac{p+\alpha}{2}\right)(-s)^{-\frac{p+\alpha}{2}}\right]. \tag{6.25}$$

Since $\{I_{s,l}^2, l=1,\cdots,L\}$ are independent RVs, the MGF of G can be found as

$$M_G(s)=\frac{1}{2^L}\sum_{q=0}^{L}\binom{L}{q}\sum_{p=0}^{\infty}c_p(\alpha,\beta,L-q,q)(-s)^{\frac{-p-L\beta-q(\alpha-\beta)}{2}} \tag{6.26}$$

where $c_p(x,y,m,n)=[a_p(x,y)\Gamma(p/2+y/2)]^{[m]}*a_p(y,x)\Gamma(p/2+x/2)]^{[n]}$. Substituting (6.26) into

(6.24), we obtain the BER for SIM MRC systems as

$$P_{s,MRC} = \frac{1}{2^{L+1}\pi}\sum_{q=0}^{L}\binom{L}{q}\sum_{p=0}^{\infty}c_p(\alpha,\beta,L-q,q)B\left(\frac{1}{2},\frac{p+L\beta+q(\alpha-\beta)+1}{2}\right) \times\left[\frac{\alpha\beta\overline{\gamma_s}}{2(\alpha+1)(\beta+1)}\right]^{\frac{-p-L\beta-q(\alpha-\beta)}{2}}. \tag{6.27}$$

6.3.2 BER with EGC Reception

Coherent Systems With EGC: The average BER of coherent EGC over Gamma-Gamma turbulence channels was obtained in terms of an integral of the CHF $\Phi_{\sqrt{I_s}}(\omega)$ of $\sqrt{I_s}$ in (5.27). Alternatively, we can obtain a series solution by expressing the average BER in terms of the MGF of $U = (\sum_{l=1}^{L}\sqrt{I_{s,l}})^2$ as

$$P_{c,EGC} = \frac{1}{\pi}\int_0^{\frac{\pi}{2}} M_U\left(-\frac{\overline{\gamma_c}}{2\sin^2\theta}\right)d\theta. \tag{6.28}$$

As shown in Appendix C, the MGF of U is

$$M_U(s) = 2^{L-1}\sum_{q=0}^{L}\binom{L}{q}\sum_{p=0}^{\infty}\frac{\Gamma((p+(L-q)\beta+q\alpha))}{\Gamma(2(p+(L-q)\beta+q\alpha))}\eta_p(\alpha,\beta,L-q,q)(-s)^{-[p+(L-q)\beta+q\alpha]} \tag{6.29}$$

where

$$\eta_p(x,y,m,n) \triangleq b_p^{[m]}(x,y) * b_p^{[n]}(y,x) \tag{6.30}$$

with $b_p(x,y) \triangleq a_p(x,y)\Gamma(2p+2y)$. Substituting (6.29) into (6.28), we obtain the closed-form BER for coherent OWC with EGC as

$$P_{c,EGC} = \frac{2^{L-2}}{\pi}\sum_{q=0}^{L}\binom{L}{q}\sum_{p=0}^{\infty}B\left(\frac{1}{2},p+(L-q)\beta+q\alpha+\frac{1}{2}\right) \times\frac{\eta_p(\alpha,\beta,L-q,q)\Gamma((p+(L-q)\beta+q\alpha))}{\Gamma(2(p+(L-q)\beta+q\alpha))}\left(\frac{\overline{\gamma}}{2L}\right)^{-(p+(L-q)\beta+q\alpha)}. \tag{6.31}$$

SIM Systems With EGC: We obtain the CHF of the lth branch received irradiance, $\Phi_{I_s}(\omega)$, by replacing s with $j\omega$ in $M_{I_s}(s)$. The average BER for SIM EGC is then

$$P_{s,EGC} = \int_{-\infty}^{\infty} \left[\Phi_{I_s}^{*} \left(\frac{\sqrt{\alpha\beta\overline{\gamma_s}}\omega}{\sqrt{2L(\alpha+1)(\beta+1)}} \right) \right]^{L} \frac{\Lambda(\omega)}{4\pi} d\omega \tag{6.32}$$

where $\Phi_{I_s}(\cdot)$ and $F(\cdot)$ are given in (5.7) and (5.26), respectively.

To facilitate the comparison, an alternative expression can be obtained in terms of the MGF of $M = (\sum_{l=1}^{L} I_{s,l})^2$ as

$$P_{s,EGC} = \frac{1}{\pi} \int_{0}^{\frac{\pi}{2}} M_M \left(-\frac{\overline{\gamma_c}}{2\sin^2\theta} \right) d\theta \tag{6.33}$$

where one can show $M_M(s)$ to be

$$\begin{aligned} M_M(s) = &\sum_{q=0}^{L} \binom{L}{q} \sum_{p=0}^{\infty} \frac{\vartheta_p(\alpha,\beta,L-q,q)\Gamma(\frac{p+(L-q)\beta+q\alpha}{2})}{2\Gamma(p+(L-q)\beta+q\alpha)} \\ &\times (-s)^{-\frac{p+(L-q)\beta+q\alpha}{2}} \end{aligned} \tag{6.34}$$

where $\vartheta_p(x,y,m,n) \triangleq (d_p(x,y))^{[m]} * (d_p(y,x))^{[n]}$ with $d_p(x,y) \triangleq a_p(x,y)\Gamma(p+y)$. Using the series approach, we then find the average BER of SIM EGC in a closed-form as

$$\begin{aligned} P_{s,EGC} = &\frac{1}{2\pi} \sum_{q=0}^{L} \binom{L}{q} \sum_{p=0}^{\infty} \frac{\vartheta_p(\alpha,\beta,L-q,q)\Gamma(\frac{p+(L-q)\beta+q\alpha}{2})}{2\Gamma(p+(L-q)\beta+q\alpha)} B\left(\frac{1}{2}, \frac{p+(L-q)\beta+q\alpha+1}{2}\right) \\ &\times \left[\frac{\alpha\beta\overline{\gamma_s}}{2L(\alpha+1)(\beta+1)} \right]^{-\frac{p+(L-q)\beta+q\alpha}{2}}. \end{aligned} \tag{6.35}$$

Here, we have only presented closed-form error rate results for BPSK due to space limitations. Similar analyses can be performed for coherent and SIM MPSK.

6.4 Diversity Order and Coding Gain for MRC and EGC Receptions

In this section, asymptotic error performance is studied and compared for both coherent and SIM OWC systems with MRC and EGC receptions. Closed-form expressions are derived for diversity order G_d and coding gain G_c, which can be obtained through

$$P_e^{asym} \approx (G_c \overline{\gamma})^{-G_d} \tag{6.36}$$

where $\overline{\gamma}$ represents $\overline{\gamma}_c$ or $\overline{\gamma}_s$ for the coherent system or SIM system, respectively.

As we discussed in Section 2.2.3, for the Gamma-Gamma turbulence model, we have $\alpha > \beta$ in most scenarios. Therefore, without loss of generality, we assume $\alpha > \beta$ in the study of diversity order and coding gain of this chapter. The results for $\alpha < \beta$ can also be readily derived as the parameters α and β are symmetric in the Gamma-Gamma model.

6.4.1 MRC Analysis

Coherent Systems With MRC: In a given OWC channel, the first term $(\overline{\gamma}_c)^{-[p+L\beta+q(\alpha-\beta)]}|_{q=0}$ decreases more rapidly than the other terms $(\overline{\gamma}_c)^{-[p+L\beta+q(\alpha-\beta)]}|_{q\neq 0}$ in (6.21) for the same p values as $\overline{\gamma}_c$ increases. As a result, when $\overline{\gamma}_c$ approaches ∞, the leading term in (6.21) becomes dominant. One can directly obtain the asymptotic BER in large SNR regimes for coherent OWC systems to be

$$P_{c,MRC}^{asym} = \frac{[\Gamma(\alpha)a_0(\alpha,\beta)]^L \Gamma(L\beta+\frac{1}{2})}{2\sqrt{\pi}\Gamma(L\beta+1)} \left(\frac{\overline{\gamma}_c}{2}\right)^{-L\beta}. \tag{6.37}$$

Thus, the diversity order and coding gain are obtained as $G_d = L\beta$ and

$$G_c = \left[\frac{2^{L\beta-1}[\Gamma(\alpha)a_0(\alpha,\beta)]^L\Gamma(L\beta+\frac{1}{2})}{\sqrt{\pi}\Gamma(L\beta+1)}\right]^{-\frac{1}{L\beta}} \tag{6.38}$$

respectively.

SIM Systems With MRC: From (6.27), we can similarly find the asymptotic BER in large SNR regimes for SIM systems as

$$P_{s,MRC}^{asym} = \frac{2^{L(\frac{\beta}{2}-1)-1}\left[a_0(\alpha,\beta)\Gamma\left(\frac{\beta}{2}\right)\right]^L\Gamma\left(\frac{L\beta}{2}+\frac{1}{2}\right)}{\sqrt{\pi}\Gamma\left(\frac{L\beta}{2}+1\right)}\left[\frac{\alpha\beta\overline{\gamma}_s}{(\alpha+1)(\beta+1)}\right]^{-\frac{L\beta}{2}}. \tag{6.39}$$

The diversity order and coding gain are found, respectively, to be $G_d = \frac{L\beta}{2}$ and

$$G_c = \frac{\alpha\beta}{(\alpha+1)(\beta+1)}\left[\frac{2^{L(\frac{\beta}{2}-1)-1}[a_0(\alpha,\beta)\Gamma(\frac{\beta}{2})]^L\Gamma(\frac{L\beta}{2}+\frac{1}{2})}{\sqrt{\pi}\Gamma(\frac{L\beta}{2}+1)}\right]^{-\frac{2}{L\beta}}. \tag{6.40}$$

6.4.2 EGC Analysis

Similarly, through (6.31) and (6.35) asymptotic BERs in large SNR regimes for coherent and SIM EGC systems can be found to be

$$P_{c,EGC}^{asym} = \frac{2^{L-2}b_0(\alpha,\beta)\Gamma(L\beta)\Gamma(L\beta+\frac{1}{2})}{\sqrt{\pi}\Gamma(L\beta+1)\Gamma(2L\beta)}\left(\frac{\overline{\gamma}_c}{2}\right)^{-L\beta} \tag{6.41}$$

and

$$P_{s,EGC}^{asym} = \frac{\Gamma(\frac{L\beta+1}{2})[\Gamma(\beta)a_0(\alpha,\beta)]^L}{2L\sqrt{\pi}\beta\Gamma(L\beta)}\left[\frac{\alpha\beta\overline{\gamma}_s}{2L(\alpha+1)(\beta+1)}\right]^{-\frac{L\beta}{2}} \tag{6.42}$$

respectively. Therefore, we find that the diversity order and coding gain for coherent EGC systems are $G_d = L\beta$ and

$$G_c = \left[\frac{2^{[L(\beta+1)-2]} b_0(\alpha,\beta)\Gamma(L\beta)\Gamma(L\beta+\frac{1}{2})}{\sqrt{\pi}\Gamma(L\beta+1)\Gamma(2L\beta)}\right]^{-\frac{1}{L\beta}} \tag{6.43}$$

respectively. The diversity order and coding gain for SIM EGC systems are found to be $G_d = \frac{L\beta}{2}$ and

$$G_c = \frac{\alpha\beta}{(\alpha+1)(\beta+1)}\left[\frac{(2L)^{\frac{L\beta}{2}-1}\Gamma\left(\frac{L\beta+1}{2}\right)[\Gamma(\beta)a_0(\alpha,\beta)]^L}{\sqrt{\pi}\beta\Gamma(L\beta)}\right]^{-\frac{2}{L\beta}} \tag{6.44}$$

respectively.

6.5 SC with DPSK and NCFSK

6.5.1 Error Rates for DSPK and NCFSK

The average BER for DPSK and NCFSK in turbulence-free channels is given by $0.5\exp(-\rho\gamma)$ where $\rho = 1/2$ for DPSK and $\rho = 1/4$ for NCFSK [100].

Coherent Systems With SC: The average BER of coherent SC systems with Gamma-Gamma turbulence can be shown to be

$$P_{c,SC} = \frac{1}{2}\int_0^\infty \exp(-\rho\overline{\gamma}_{c,SC}I_m)[F_I(I_m)]^{L-1} f_I(I_m)dI_m \tag{6.45}$$

where $I_m = \max\{I_{s,l}, l = 1,\cdots,L\}$ and $F_{I_s}(\cdot)$ denotes the CDF of the Gamma-Gamma RV. To assist the closed-form error rate derivation, we express the PDF of I_m, i.e., $f_{I_m}(I_m) = [F_I(I_m)]^{L-1} f_I(I_m)$,

in terms of a power series as (the detailed derivation of the PDF of I_m is given in Appendix D)

$$f_{I_m}(I_m) = \sum_{k=0}^{L-1} \binom{L-1}{k} \left[\sum_{p=0}^{\infty} e_p(L-k-1,k,\alpha,\beta) I_m^{p+(L-k)\beta+k\alpha-1} + \sum_{p=0}^{\infty} e_p(L-k-1,k,\beta,\alpha) I_m^{p+(L-k)\alpha+k\beta-1} \right] \tag{6.46}$$

where $e_p(\cdot,\cdot,\cdot,\cdot)$ is defined in (D.5) of Appendix D. We can then obtain the BER solution based on (6.45) by

$$\begin{aligned} P_{c,SC} =& \frac{L}{2} \sum_{k=0}^{L-1} \binom{L-1}{k} \sum_{p=0}^{\infty} e_p(L-1-k,k,\alpha,\beta) \int_0^{\infty} \exp(-\rho\overline{\gamma}_c I_m) I_m^{p+(L-1-k)\beta+k\alpha+\beta-1} dI_m \\ &+ \frac{L}{2} \sum_{k=0}^{L-1} \binom{L-1}{k} \sum_{p=0}^{\infty} e_p(L-1-k,k,\beta,\alpha) \int_0^{\infty} \exp(-\rho\overline{\gamma}_c I_m) I_m^{p+(L-1-k)\alpha+k\beta+\alpha-1} dI_m. \end{aligned} \tag{6.47}$$

Using an integral property [93, Eq. 3.326(2)], we obtain the BER in a closed-form as

$$\begin{aligned} P_{c,SC} = \frac{L}{2} \sum_{k=0}^{L-1} \binom{L-1}{k} \Bigg\{ & \sum_{p=0}^{\infty} e_p(L-1-k,k,\alpha,\beta) \Gamma(p+(L-k)\beta+k\alpha) (\rho\overline{\gamma}_c)^{-[p+(L-k)\beta+k\alpha]} \\ &+ \sum_{p=0}^{\infty} e_p(L-1-k,k,\beta,\alpha) \Gamma(p+(L-k)\beta+k\alpha) (\rho\overline{\gamma}_c)^{-[p+(L-k)\alpha+k\beta]} \Bigg\}. \end{aligned} \tag{6.48}$$

SIM Systems With SC: Using the SC combiner output SNR expression, we express the average BER as

$$P_{s,SC} = \frac{1}{2} \int_0^{\infty} \exp\left(-\frac{\rho\alpha\beta\overline{\gamma}_s}{(\alpha+1)(\beta+1)} I_m^2 \right) f_{I_m}(I_m) dI_m \tag{6.49}$$

where $I_m^2 = \max\{I_{s,l}^2, l = 1,\cdots,L\}$. Again, using the series expansion expression of $f_{I_m}(I_m)$ in

(6.46), we can find the BER solution by

$$P_{s,SC} = \frac{L}{2}\sum_{k=0}^{L-1}\binom{L-1}{k}\sum_{p=0}^{\infty} e_p(L-1-k,k,\alpha,\beta)\int_0^{\infty}\exp\left(\frac{-\rho\alpha\beta\overline{\gamma}_s I_m^2}{(\alpha+1)(\beta+1)}\right) I_m^{p+(L-k)\beta+k\alpha-1} dI_m$$
$$+\frac{L}{2}\sum_{k=0}^{L-1}\binom{L-1}{k}\sum_{p=0}^{\infty} e_p(L-1-k,k,\beta,\alpha)\int_0^{\infty}\exp\left(\frac{-\rho\alpha\beta\overline{\gamma}_s I_m^2}{(\alpha+1)(\beta+1)}\right) I_m^{p+(L-k)\alpha+k\beta-1} dI_m. \tag{6.50}$$

Finally, we obtain the closed-form BER expression for SIM SC systems as

$$P_{s,SC} = \frac{L}{4}\sum_{k=0}^{L-1}\binom{L-1}{k}$$
$$\times\left\{\sum_{p=0}^{\infty} e_p(L-1-k,k,\alpha,\beta)\Gamma\left(\frac{p+(L-k)\beta+k\alpha}{2}\right)\left[\frac{\rho\alpha\beta\overline{\gamma}_s}{(\alpha+1)(\beta+1)}\right]^{-\frac{p+(L-k)\beta+k\alpha}{2}}\right.$$
$$\left.+\sum_{p=0}^{\infty} e_p(L-1-k,k,\beta,\alpha)\Gamma(p+(L-k)\alpha+k\beta)\left[\frac{\rho\alpha\beta\overline{\gamma}_s}{(\alpha+1)(\beta+1)}\right]^{-\frac{p+(L-k)\alpha+k\beta}{2}}\right\}. \tag{6.51}$$

6.5.2 Diversity Order and Coding Gain for SC Reception

When $\alpha > \beta$ and $\overline{\gamma}_c$ or $\overline{\gamma}_s$ approach ∞, the leading terms in (6.48) or (6.51) become dominant, and one obtains the asymptotic BERs in large SNR regimes for coherent and SIM OWC systems, respectively, as

$$P_c^{asym} = \frac{L}{2}e_0(L-1,0,\alpha,\beta)\Gamma(L\beta)(\rho\overline{\gamma}_c)^{-L\beta} \tag{6.52}$$

and

$$P_s^{asym} = \frac{L}{4}e_0(L-1,0,\alpha,\beta)\Gamma\left(\frac{L\beta}{2}\right)\left[\frac{\rho\alpha\beta}{(\alpha+1)(\beta+1)}\overline{\gamma}_s\right]^{-\frac{L\beta}{2}}. \tag{6.53}$$

The diversity order and coding gain for coherent systems with SC are then found to be

$$G_d = L\beta \tag{6.54}$$

and

$$G_c = \rho \left[\frac{Le_0(L-1,0,\alpha,\beta)\Gamma(L\beta)}{2} \right]^{-\frac{1}{L\beta}} \tag{6.55}$$

respectively. The diversity order and coding gain for SIM systems with SC are found to be

$$G_d = \frac{L\beta}{2} \tag{6.56}$$

and

$$G_c = \frac{\rho\alpha\beta}{(\alpha+1)(\beta+1)} \left[\frac{Le_0(L-1,0,\alpha,\beta)\Gamma(\frac{L\beta}{2})}{4} \right]^{-\frac{2}{L\beta}} \tag{6.57}$$

respectively.

The asymptotic analyses performed for both coherent and subcarrier system can provide a efficient ways to evaluation the error rate performance for given OWC links in the large SNR regimes.

In the following section, we will link the average SNR to the average transmitted optical power for a fair performance comparison between coherent and subcarrier OWC systems. The comparison is carried out in terms of the average transmitted optical power because the noise sources are fundamentally different in coherent and subcarrier systems. Coherent systems are dominated by LO-induced shot noise, while subcarrier modulated systems are dominated by background and thermal noises.

6.6 Performance Comparison Under Average Transmitted Optical Power Constraints

We compare the coherent and subcarrier OWC receivers performance in terms of the same average transmitted optical power constraints. In order to perform such a comparison, we assume that the two systems have the same path loss. This implies that the same average transmitted optical power P_t will result in the same average received optical power $\overline{P}_s$, i.e., $\overline{P}_s = gP_t$ where g denotes a path loss factor being the same for both systems. To evaluate the error rate performance, we need to link the average SNRs with the average received optical power. In the following, we assume that the bit duration $T = 1/\Delta f$ and parameter A are the same for the coherent and SIM systems.

By recalling the average SNR definition for coherent OWC systems, we have

$$\overline{\gamma}_c = E[\gamma_c] = \frac{2R^2 P_{LO}}{2qRP_{LO}\Delta f}\overline{P}_s = \frac{Rg}{q\Delta f}P_t \tag{6.58}$$

where $\overline{P}_s = E[P_s] = AE[I]$. With the average SNR definition for subcarrier OWC systems, we have

$$\begin{aligned}\overline{\gamma}_s = E[\gamma_s] =& \frac{(RA\xi)^2}{2\Delta f(qRAI_b + 2k_b T_k F_n/R_L)}E[I^2] \\ =& \frac{(R\xi)^2}{2\Delta f(qRAI_b + 2k_b T_k F_n/R_L)}E[P_s^2].\end{aligned} \tag{6.59}$$

Using (1.4), we find the relation between average SNR and average received optical power as

$$\overline{\gamma}_s = \frac{(R\xi g)^2\left(1+\frac{1}{\alpha}\right)\left(1+\frac{1}{\beta}\right)}{2\Delta f(qRAI_b + 2k_b T_k F_n/R_L)}P_t^2. \tag{6.60}$$

By substituting (6.58) and (6.60) into (6.21), (6.27), (6.31), (6.35), (6.48) and (6.51), we can readily evaluate system performance in terms of average transmitted optical power for MRC, EGC and SC receivers.

From (6.58) and (6.60), for a given average transmitted optical power constraint, it is seen that the coherent OWC system is robust to variation in receiver temperature/ambient-irradiance, but the SIM OWC system is sensitive to these link parameters.

6.7 Numerical Results

In this section, we present numerical case studies on the error rate performance comparison for coherent and SIM OWC systems subject to the same average transmitted power constraints. Our series solutions[8] are verified by exact error rates calculated based on analytical expressions in (6.16), (6.24), [99, Eq. (38)], (6.32), (6.45), and (6.49) which have been confirmed by Monte Carlo simulations. We consider the following turbulent OWC scenarios where the path loss factor is empirically expressed in terms of visibility [101] and the turbulence strength is assumed to increase with propagation distance [63], [102]: 1) a 2 km haze optical channel (in strong turbulence) with 4.3 dB/km path loss; 2) a 900 m light smoke optical channel (in moderate turbulence) with 9.56 dB/km path loss; 3) a 700 m light fog optical channel (in weak-to-moderate turbulence) with 11.5 dB/km path loss.

Numerical plots are presented for BER versus average transmitted optical power where the modulation index is $\xi = 0.9$, the photodetector responsivity is $R = 0.75$ A/W, $R_L = 50\ \Omega$, and $T = 1$ ns (i.e., approximate transmission rate of 1 Gb/s [102]). For a SIM system, the noise is dominated by thermal noise with a typical noise variance of 3.3×10^{-13} A^2 at room temperature being higher than the background noise variance[9] typically on the order of 10^{-16} to 10^{-14} A^2. Assuming a typical local oscillator power around 10^{-2} W [104], the local oscillator-induced shot noise[10] variance is 5×10^{-12} A^2.

[8] All series error rates are calculated using the first 31 terms.

[9] Outdoor OWC applications have background radiation power on the order of several microWatts for scattered sunlight by clouds or fog, hundreds of microWatts for reflected sunlight [103]. Here we ignore the direct sunlight which may induce up to several milliWatts background radiation power, because statistically such a case can occur less than one hour per year [103].

[10] A large local oscillator power (typically from a few to tens of milliWatts) is desired to eliminate thermal/background noise effects in coherent links.

We first consider turbulence-free OWC links. The BER results for BPSK and DPSK/NCFSK modulated systems in the absence of turbulence are evaluated through

$$P_{\text{turbulence-free}} = Q\left(\sqrt{\gamma}\right) \tag{6.61}$$

and

$$P_{\text{turbulence-free}} = \frac{1}{2}\exp(-\rho\gamma) \tag{6.62}$$

where γ represents γ_c or γ_s for the coherent system or the SIM system, respectively. A substitution of (6.58) and (6.59) into these two expressions gives the BER solutions as a function of average transmitted optical power for turbulence-free OWC links.

The turbulence-free results for BPSK systems are shown in Fig. 6.1. The coherent OWC system is seen to substantially outperform the SIM system. For example, when the average transmitted optical power is -45 dBm, the SIM system BER is 10^{-1} while the coherent system BER is 10^{-3}. To achieve the same error rate of 10^{-9}, the SIM system needs -14.5 dBm average transmitted optical power while the coherent system only needs -38.5 dBm average transmitted optical power.

The receiver sensitivity[11] difference between coherent and SIM systems in the absence of turbulence can be found as 24 dB. This sensitivity improvement obtained for the coherent OWC system compared to the SIM system is consistent with the sensitivity improvement of a analogous coherent heterodyne fiber link [105]. Though an experimental implementation may have a higher optical device loss [74] and other noises/distortions neglected here, our theoretical comparison result can be used as a benchmark for OWC system designing. The performance improvement for the coherent system obtained here is mainly because a sufficiently large LO power in coherent optical systems will eliminate the effects of thermal and background noises. The increased LO power does not impact the coherent receiver performance[12] as both signal power and LO-induced shot

[11] In optics literature, receiver sensitivity is defined as the received number of photons or optical power required to achieve a specified BER (typically 10^{-9}).

[12] Amplified noise is ignored here. Also, we note that the sensitivity of a SIM receiver is degraded as a DC bias must be added to keep the transmitted optical signal non-negative.

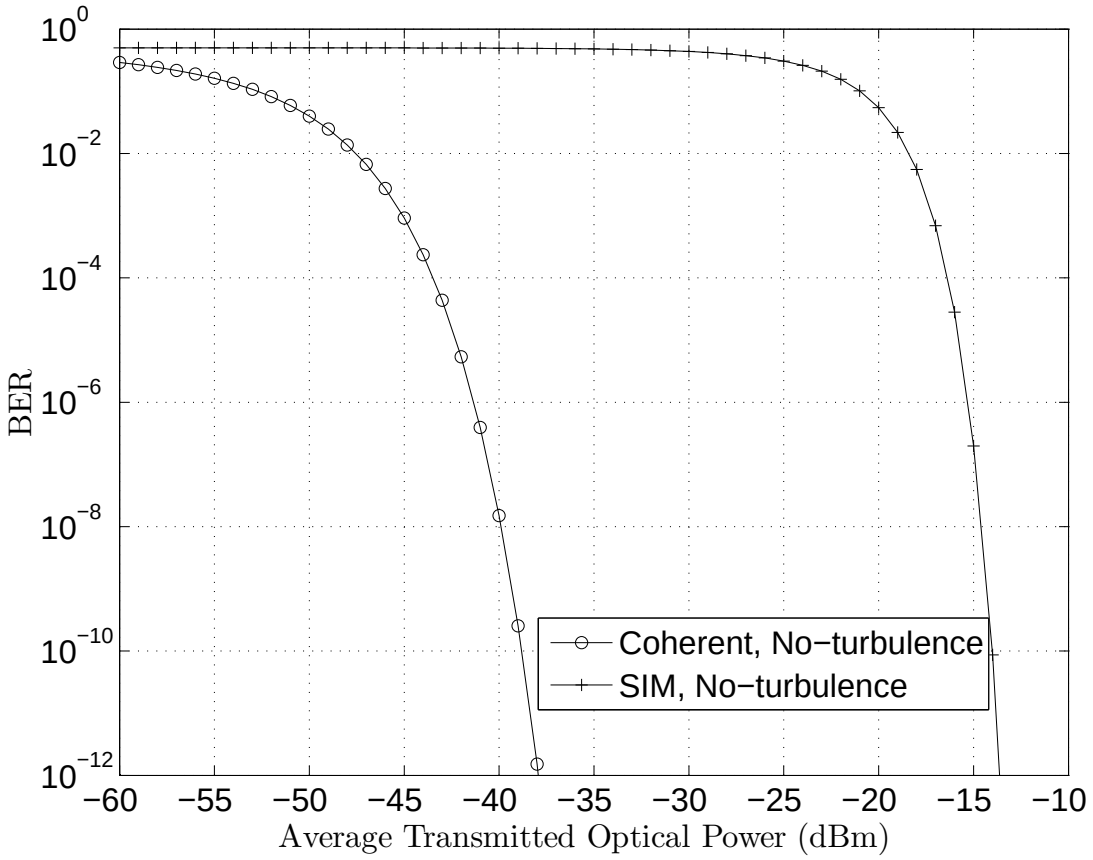

Figure 6.1: BER comparison of subcarrier and coherent BPSK optical communication links subject to the same average transmitted optical power through turbulence-free channels.

noise variance are proportional to P_{LO}. It should be noted, however, that the exact performance gap between coherent and SIM OWC systems will vary with system parameters, e.g., temperature, receiver branch number, etc.

In these turbulence channels, the receiver sensitivity improvement from the SIM to coherent receiver can be found to be around 30 dB. It can be shown that this sensitivity difference is insensitive to changes in the turbulence levels as long as the smaller channel parameter β value is small (e.g., less than 3.5). For instance, the sensitivity difference will only change by less than 1.4 dB for β value varies from 1 to 3. In the special case of K-distributed turbulence, where $\beta = 1$, this sensitivity difference is independent of the turbulence level changes.

We now present the BER comparison considering dual-branch ($L = 2$) optical wireless links. In Fig. 6.2, the BERs of subcarrier and coherent optical BPSK systems are compared when MRC or EGC reception is employed in strong and moderate turbulence channels. It is seen that the coherent system outperforms the subcarrier system. For example, at an average transmitted optical power of 2 dBm over the strong turbulence channel, a dual-branch coherent MRC link gives a BER performance of 10^{-12}, while a SIM MRC link gives a BER performance of 10^{-5}. The BER differences between subcarrier and coherent systems are increasingly noticeable when moving from strong turbulence to moderate turbulence. Figure 6.3 shows a similar BER comparison in a weak-to-moderate turbulence channel with the coherent system again outperforming the SIM system. For instance, with a -2 dBm average transmitted optical power, the coherent EGC system can achieve a BER performance of 3×10^{-15} in a weak-to-moderate turbulence channel, while the SIM EGC system can only attain a BER performance of 1.2×10^{-5}. In addition, it is seen from Figs. 6.2 and 6.3 that the OWC EGC system has a close error rate performance to that of the OWC MRC system in all three turbulence channels.

BERs for DPSK with SC are shown in Fig. 6.4 for strong, moderate and weak-to-moderate turbulence channels. The coherent optical link results show a substantial advantage in the error performance over the subcarrier link in a comparison of reduced complexity DPSK-based SC sys-

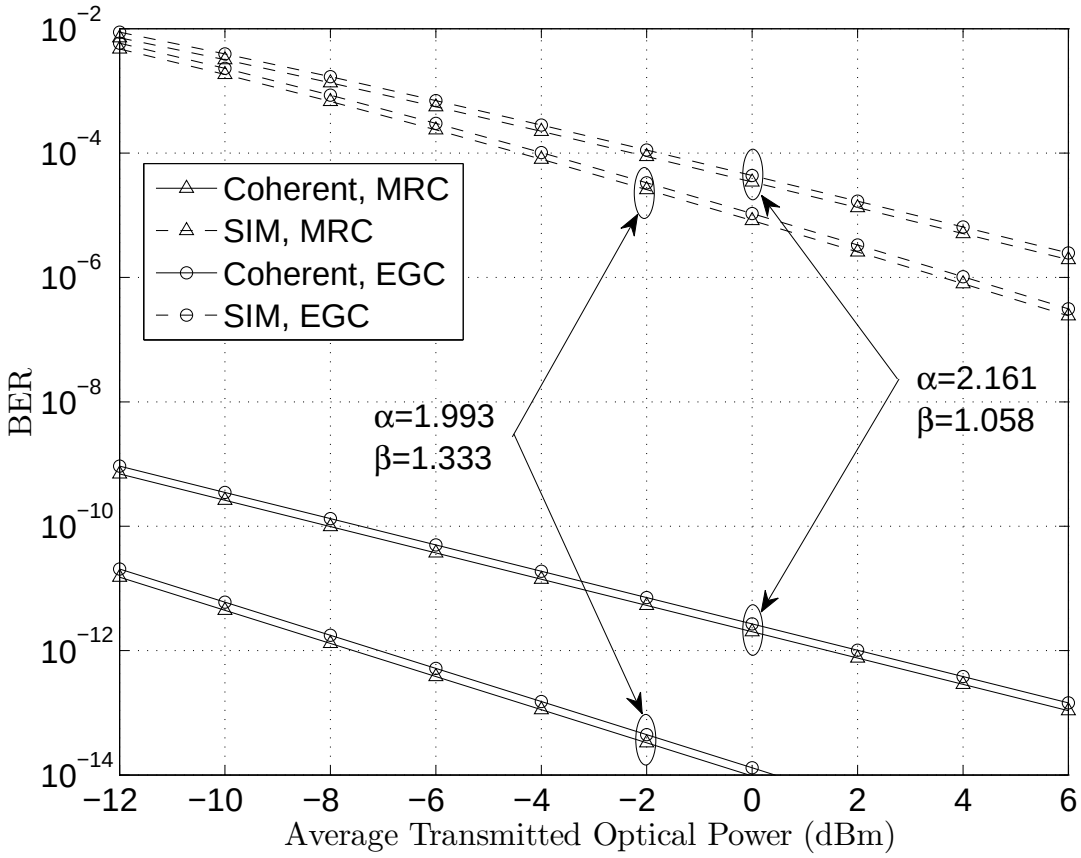

Figure 6.2: BER comparison of subcarrier and coherent BPSK optical communication links subject to the same average transmitted optical power with MRC/EGC over 2 km strong ($\alpha = 2.161$, $\beta = 1.058$) and 900 m moderate ($\alpha = 1.993, \beta = 1.333$) turbulence channels.

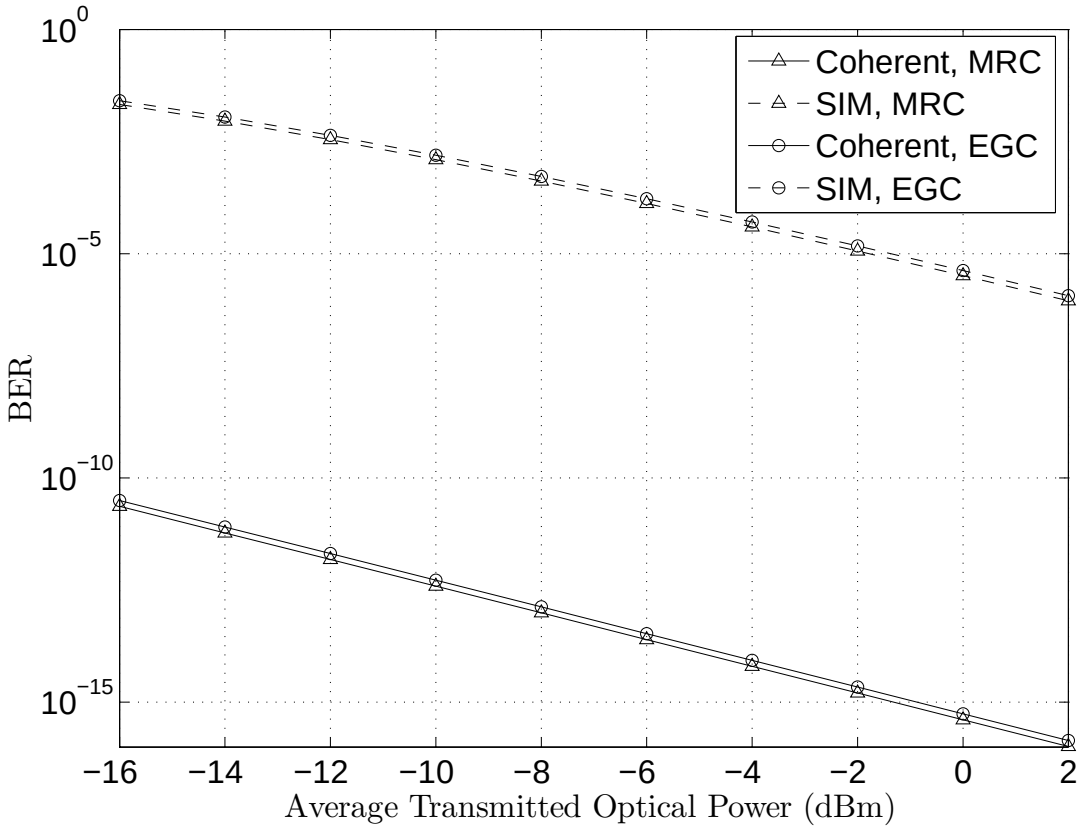

Figure 6.3: BER comparison of subcarrier and coherent BPSK optical communication links subject to the same average transmitted optical power with MRC/EGC over a 700 m weak-to-moderate ($\alpha = 2.314, \beta = 1.820$) turbulence channel.

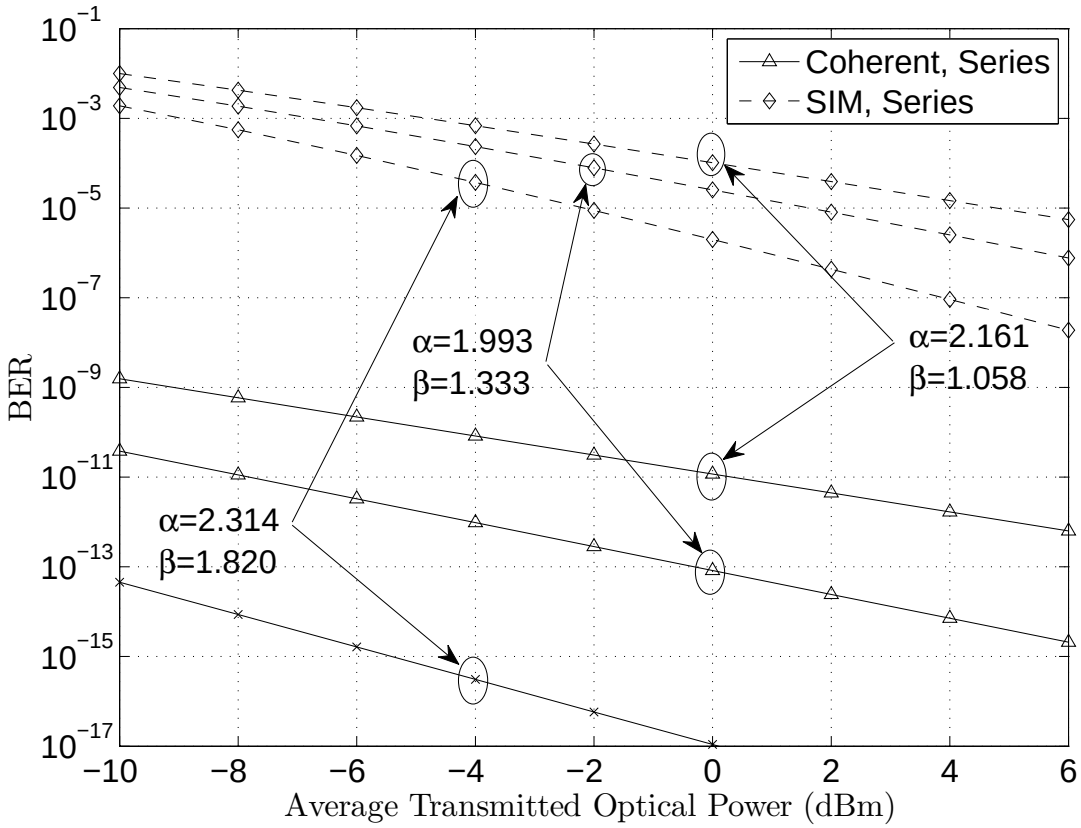

Figure 6.4: BER comparison of DPSK subcarrier and coherent optical communication links subject to the same average transmitted optical power with SC over 2 km strong ($\alpha = 2.161$, $\beta = 1.058$), 900 m moderate ($\alpha = 1.993, \beta = 1.333$) and 700 m weak-to-moderate ($\alpha = 2.314$, $\beta = 1.820$) turbulence channels.

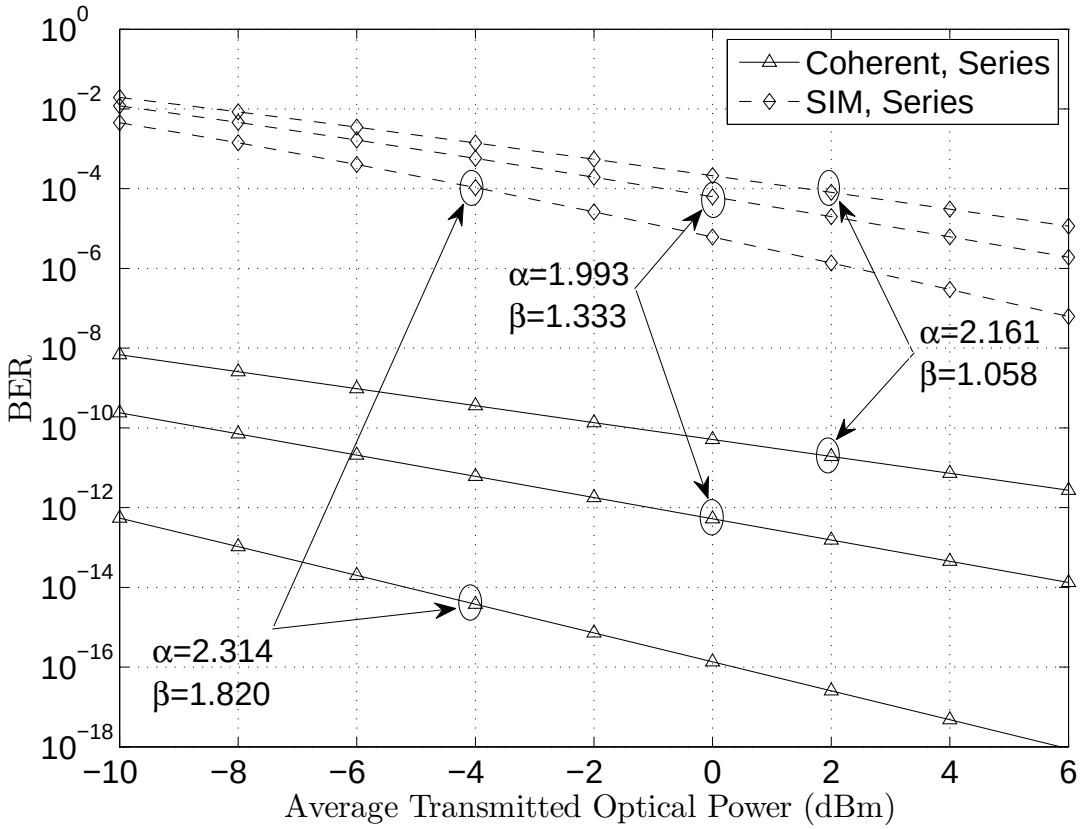

Figure 6.5: BER comparison of NCFSK subcarrier and coherent optical communication links subject to the same average transmitted optical power with SC over 2 km strong ($\alpha = 2.161$, $\beta = 1.058$), 900 m moderate ($\alpha = 1.993, \beta = 1.333$) and 700 m weak-to-moderate ($\alpha = 2.314$, $\beta = 1.820$) turbulence channels.

tems. Such benefits are more clear as the average transmitted optical power increases. For instance, at an average transmitted optical power of -8 dBm in moderate turbulence, the coherent DPSK system has an average BER on the order of 10^{-11} and the SIM DPSK system has an average BER on the order of 10^{-3} (differing by 8 orders of magnitude). At an average transmitted optical power of 2 dBm in moderate turbulence, the coherent DPSK system has an average BER on the order of 10^{-14} and the SIM DPSK system has an average BER on the order of 10^{-5} (differing by 9 orders of magnitude).

Figure 6.5 plots BERs for NCFSK SC systems. Again, an increasingly noticeable performance gap is seen when the turbulence level reduces. We note that at the same average transmitted optical power, the coherent OWC system under the strong turbulence outperforms the SIM OWC system under all three turbulence conditions. For example, at an average transmitted optical power of 6 dBm, the coherent system has a BER of 2.7×10^{-12} in the 2 km strong turbulence channel, while the SIM system has BERs of 1.1×10^{-5}, 1.9×10^{-6} and 6.2×10^{-8} for strong, moderate and weak-to-moderate turbulence channels, respectively. This observation again confirms the usefulness of coherent OWC systems in combating atmospheric turbulence impacts.

6.8 Summary

In this chapter, we have compared coherent systems with SIM systems for optical communications in the Gamma-Gamma turbulence channels. Optical links employing BPSK have been analyzed with MRC and EGC receptions for both systems. Furthermore, DPSK and NCFSK are considered for coherent and SIM systems employing the SC reception scheme. Through the analytical analyses and numerical studies, the performance gaps between coherent and subcarrier systems have been quantified. As a result, significant improvements for coherent systems in error rate performance can be established over SIM systems with weak-to-strong turbulence.

Chapter 7

An $M \times N$ MIMO Architecture for Coherent Optical Wireless Communications

In this chapter, we propose a new architecture to achieve MIMO diversity for atmospheric coherent optical communication systems. Based on the proposed architecture, we study the system performance for MRC and EGC combining schemes. The error rates comparison shows improved system performance of coherent detection when implemented with the proposed MIMO OWC architecture.

7.1 A MIMO Architecture and Its Performance

7.1.1 MIMO System Model

We consider an uncoded coherent MIMO OWC system with M laser source transmitters and N destination receivers operating through atmospheric turbulence channels. The detailed block diagram of the proposed MIMO architecture is shown in Fig. 7.1. Here, M different optical carrier frequencies $\omega_1, \omega_2, \cdots, \omega_M$ are set for the M laser transmitters. As the coherence length for a optical wave propagating through atmosphere is on the order of centimeters, it is appropriate to assume independent turbulence in the $M \times N$ transmission links by placing transmitters and receivers sufficiently far apart (beyond the coherence length).

The nth receiver ($n = 1, 2, \cdots, N$) will have M arriving mixed beams. We can express the

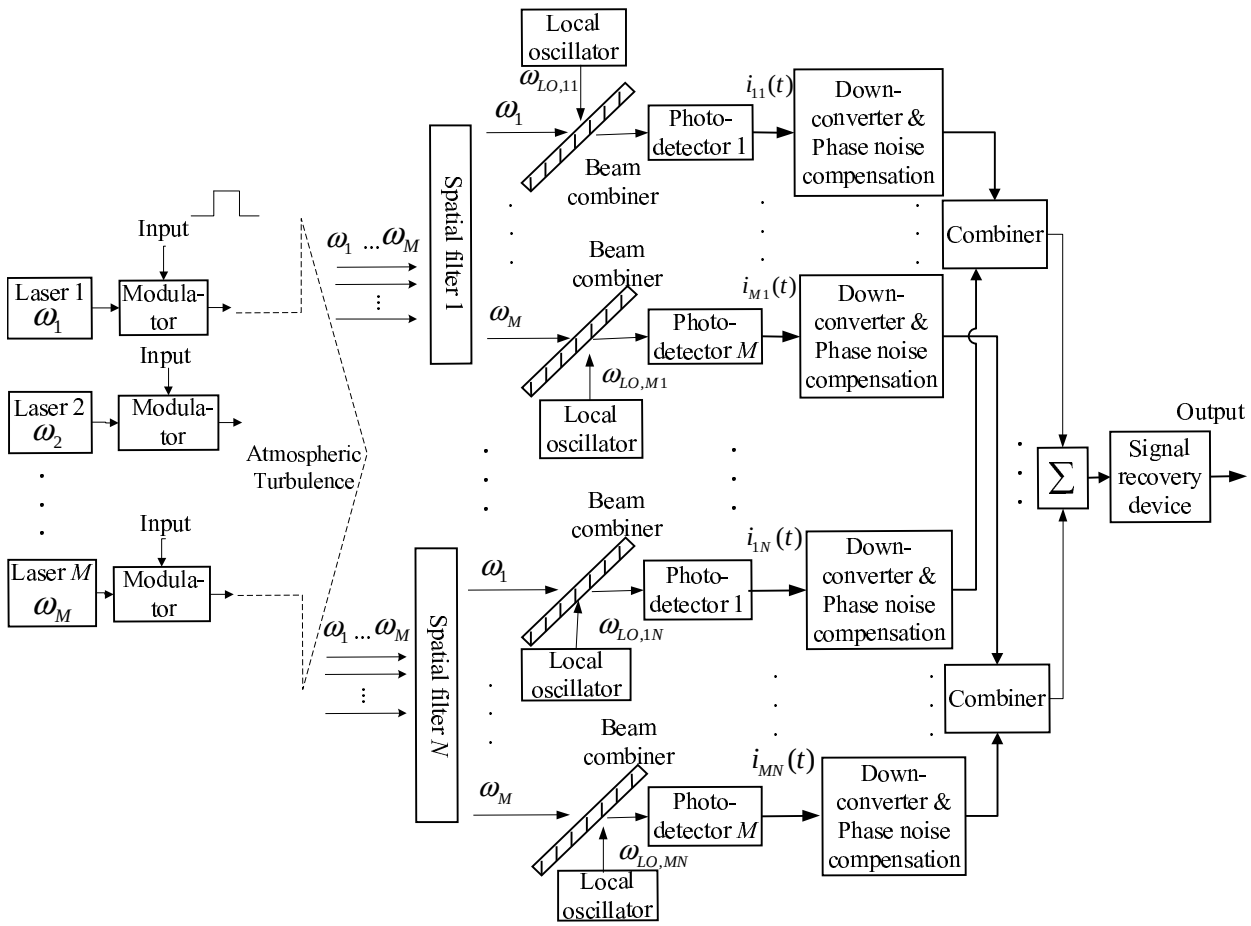

Figure 7.1: Block diagram of an $M \times N$ coherent optical MIMO architecture operating in atmospheric turbulence channels.

electric field of this composite beam as

$$e_n(t) = \sum_{m=1}^{M} E_{s,mn} \exp(j\omega_m t + j\phi + j\phi_{st,m}(t)) \tag{7.1}$$

where $E_{s,mn}$ is the received electric field amplitude of the nth receiver from the mth transmitter, ϕ represents the phase modulated information, and $\phi_{st,mn}(t)$ is the accumulated phase noise induced on the mth transmitter signal (from the laser source and its turbulence channel) arriving at the nth receiver. Since the composite beam electric field expression in (7.1) has distinct transmit frequencies, we apply a wavelength-selective spatial filter [106] to separate the incident optical signal beam according to the transmitter carrier frequencies. A beam combiner is then used to combine each of the M transmitter beams with its corresponding LO beam. Note that M photodetectors are included in the nth receiver to convert the M optical beams into M photocurrents. The resulting layout is detailed in Fig. 7.1.

As shown in Fig. 7.1, $M \times N$ optical beams are summed with their respective LO beams. Following the signal flow, we can then express the combining using the electric field expression

$$e_{sum,mn}(t) = E_{s,mn} \exp(j\omega_m t + j\phi + j\phi_{st,m}(t)) + E_{LO} \exp(j\omega_{LO,mn} t + j\phi_{LO,mn}(t)) \tag{7.2}$$

where $\omega_{LO,mn}$ and $\phi_{LO,mn}(t)$ respectively denote the mth LO[13] frequency and phase noise of the nth receiver. Here, the LO power P_{LO} is the same for all beam combiners. After the optoelectronic conversion with sufficiently small photodetector areas, the photocurrent at the mth photodetector output of the nth receiver can be expressed as $i_{mn}(t) = i_{dc,mn} + i_{ac,mn}(t) + w_{mn}(t)$ where $i_{dc,mn} = R(P_{s,mn} + P_{LO})$ and $i_{ac,mn}(t) = 2R\sqrt{P_{s,mn}P_{LO}}\cos(\omega_{IF,mn}t + \phi + \phi_{s,mn}(t))$ represent, respectively, the DC and AC terms, and $w_{mn}(t)$ is a zero-mean AWGN process due to shot noise. Here, $P_{s,mn}$ is the received optical signal power between the mth transmitter and the nth receiver, P_{LO} denotes

[13]Though a subscript mn is used for LOs and $M \times N$ LOs are shown in Fig. 7.1, the mth LO beam can be reused in N receivers to reduce receiver size and implementation cost.

the LO power, $\phi_{s,mn}(t)$ denotes the accumulated phase noise between the mth transmitter and the output of its corresponding photodetector at the nth receiver (including laser phase noise as well as turbulence phase noise), and $\omega_{IF,mn} = \omega_m - \omega_{LO,mn}$ is the intermediate frequency of the mth AC photocurrent for the nth receiver. Since atmospheric turbulence has a relatively slow variation in the optical channel, when compared to the high optical data rates [63], [30], phase noise from the turbulence and the narrow-linewidth lasers changes slowly and can be fully compensated with a co-transmitted carrier's phase estimation circuit (e.g., through an embedded DSP unit). After combining and demodulating through an electrical demodulator, the sampled electrical signal at the output of the receiver can be used to recover the transmitted data.

7.1.2 Average Error Rate Studies

To start the error rate analyses, we define the average SNR in a single branch as $\overline{\gamma} = RA/(q\Delta f)$ where A is the photodetector area and Δf is the NEB for each identical photodetector. We consider BPSK using MRC (for $N \geq 2$) and EGC implementations with heterodyne detection. From $P_{s,mn} = AI_{s,mn}$ where $I_{s,mn}$ is the irradiance between the mth transmitter and the nth receiver, we can express the BER via the alternative expression of the Gaussian Q-function in (3.9) as

$$P_e = \frac{1}{\pi}\int_0^{\frac{\pi}{2}}\int_0^{\infty} \exp\left(-\frac{\gamma}{2\sin^2\theta}\right) f_\gamma(\gamma)d\gamma d\theta \tag{7.3}$$

where $f_\gamma(\cdot)$ is the PDF of the instantaneous SNR at the input of the signal recovery device using MRC or EGC schemes. These respective SNRs are found to be $\gamma_{\text{MRC}} = \overline{\gamma}\left(\sum_{m=1}^{M}\sum_{n=1}^{N} I_{s,mn}\right)$ and $\gamma_{\text{EGC}} = \overline{\gamma}\left(\sum_{m=1}^{M}\sum_{n=1}^{N}\sqrt{I_{s,mn}}\right)^2/(MN)$. To facilitate the ensuing BER analysis, we make use of a series expansion of the modified Bessel function of the second kind and the fact that the PDF of the RV $Y = \sqrt{I_s}$ is $f_Y(y) = 2yf_{I_s}(y^2)$. We find that the PDF of Y is

$$f_Y(y) = 2\sum_{p=0}^{\infty}\left[a_p(\alpha,\beta)y^{2(p+\beta)-1} + a_p(\beta,\alpha)y^{2(p+\alpha)-1}\right] \tag{7.4}$$

where $a_p(\alpha,\beta)$ is defined in (6.20). To determine the PDF of γ_{EGC}, we will make use of the MGF of a RV X defined as $M_X(s) = E[\exp(sX)]$. As $\{\sqrt{I_{s,mn}}, m = 1,\cdots,M; n = 1,\cdots,N\}$ are i.i.d., the MGF of $I_g = \sum_{m=1}^{M}\sum_{n=1}^{N}\sqrt{I_{s,mn}}$ can be written as $M_{I_g}(s) = [M_Y(s)]^{MN}$. Thus, the MGF of I_g can be obtained in closed-form as

$$M_{I_g}(s) = 2^{MN}\sum_{i=0}^{MN}\binom{MN}{i}\sum_{p=0}^{\infty}\frac{\lambda_p^{[MN-i]}(\alpha,\beta,2)*\lambda_p^{[i]}(\beta,\alpha,2)}{(-s)^{p+MN\beta+i(\alpha-\beta)}} \tag{7.5}$$

where $\lambda_p(\alpha,\beta,x) = a_p(\alpha,\beta)\Gamma(xp+x\beta)$. Therefore, we find the PDF of I_g as

$$f_{I_g}(I) = 2^{MN}\sum_{i=0}^{MN}\binom{MN}{i}\sum_{p=0}^{\infty}I^{p+MN\beta+i(\alpha-\beta)-1}\frac{\lambda_p^{[MN-i]}(\alpha,\beta,2)*\lambda_p^{[i]}(\beta,\alpha,2)}{\Gamma(p+MN\beta+i(\alpha-\beta))}. \tag{7.6}$$

Utilizing the relationship $\gamma_{\text{EGC}} = \overline{\gamma}I_g^2/(MN)$, one can derive the PDF for γ_{EGC} from (7.6) as

$$f_\gamma(\gamma_{\text{EGC}}) = \frac{2^{MN}}{2\overline{\gamma}}\sum_{i=0}^{MN}\binom{MN}{i}\sum_{p=0}^{\infty}\frac{\lambda_p^{[MN-i]}(\alpha,\beta,2)*\lambda_p^{[i]}(\beta,\alpha,2)}{\Gamma(2\kappa_p(\alpha,\beta,MN,i))}MN\left(\frac{\gamma_{\text{EGC}}MN}{\overline{\gamma}}\right)^{\kappa_p(\alpha,\beta,MN,i)-1} \tag{7.7}$$

where $\kappa_p(\alpha,\beta,MN,i) = p+MN\beta+i(\alpha-\beta)$. Using a similar method, we find the PDF of γ_{MRC} as

$$f_\gamma(\gamma_{\text{MRC}}) = \frac{1}{\overline{\gamma}}\sum_{i=0}^{MN}\binom{MN}{i}\sum_{p=0}^{\infty}\frac{\lambda_p^{[MN-i]}(\alpha,\beta,1)*\lambda_p^{[i]}(\beta,\alpha,1)}{\Gamma(\kappa_p(\alpha,\beta,MN,i))}\left(\frac{\gamma_{\text{MRC}}}{\overline{\gamma}}\right)^{\kappa_p(\alpha,\beta,MN,i)-1}. \tag{7.8}$$

Substituting (7.7) and (7.8) into (7.3) and using the integral identities [93, Eqs. 3.478(2), 3.621(1)], we obtain closed-form BER expressions for EGC and MRC schemes, respectively, as

$$\begin{aligned} P_b^{\text{EGC}} = &\sum_{i=0}^{MN}\binom{MN}{i}\sum_{p=0}^{\infty}\frac{\lambda_p^{[MN-i]}(\alpha,\beta,2)*\lambda_p^{[i]}(\beta,\alpha,2)}{\Gamma(2\kappa_p(\alpha,\beta,MN,i))}\Gamma(\kappa_p(\alpha,\beta,MN,i)) \\ &\times B\left(\frac{1}{2},\kappa_p(\alpha,\beta,MN,i)+\frac{1}{2}\right)\frac{2^{MN-2}}{\pi}\left(\frac{\overline{\gamma}}{2MN}\right)^{-\kappa_p(\alpha,\beta,MN,i)} \end{aligned} \tag{7.9}$$

and

$$P_b^{\text{MRC}} = \sum_{i=0}^{MN} \binom{MN}{i} \sum_{p=0}^{\infty} \frac{\lambda_p^{[MN-i]}(\alpha,\beta,1) * \lambda_p^{[i]}(\beta,\alpha,1)}{2\pi} \times B\left(\frac{1}{2}, \kappa_p(\alpha,\beta,MN,i) + \frac{1}{2}\right) \left(\frac{\overline{\gamma}}{2}\right)^{-\kappa_p(\alpha,\beta,MN,i)}. \tag{7.10}$$

Note that the BER expressions in (7.9) and (7.10) are rapidly converging solutions with increasing p and/or $\overline{\gamma}$. The obtained BER results in (7.9) and (7.10) only involve the Gamma and Beta functions and can be readily computed with standard scientific software.

7.1.3 Outage Probability Studies

The outage probability is an important performance criterion for a given MIMO OWC system and was defined in (3.20). Using (7.7), (7.8) and (3.20), we derive outage probabilities for EGC and MRC, respectively, as

$$P_{outage}^{\text{EGC}}(\Lambda) = 2^{MN} \sum_{i=0}^{MN} \binom{MN}{i} \sum_{p=0}^{\infty} \frac{\lambda_p^{[MN-i]}(\alpha,\beta,2) * \lambda_p^{[i]}(\beta,\alpha,2)}{\Gamma(2\kappa_p(\alpha,\beta,MN,i)+1)} \left(\frac{\Lambda MN}{\overline{\gamma}}\right)^{\kappa_p(\alpha,\beta,MN,i)} \tag{7.11}$$

and

$$P_{outage}^{\text{MRC}}(\Lambda) = \sum_{i=0}^{MN} \binom{MN}{i} \sum_{p=0}^{\infty} \frac{\lambda_p^{[MN-i]}(\alpha,\beta,1) * \lambda_p^{[i]}(\beta,\alpha,1)}{\Gamma(\kappa_p(\alpha,\beta,MN,i)+1)} \left(\frac{\gamma_{\text{MRC}}}{\overline{\gamma}}\right)^{\kappa_p(\alpha,\beta,MN,i)}. \tag{7.12}$$

By investigating (7.9), (7.10), (7.11) and (7.12), we find the terms decrease rapidly with the increasing values of average SNR and/or index p. In large SNR regimes, the term corresponding to the largest exponent of $\overline{\gamma}$ becomes dominant in the series solutions. Therefore, we can find from the error rate expressions that the diversity order of the proposed MIMO architecture is $MN \min\{\alpha,\beta\}$ for coherent OWC systems with either an EGC or MRC implementation.

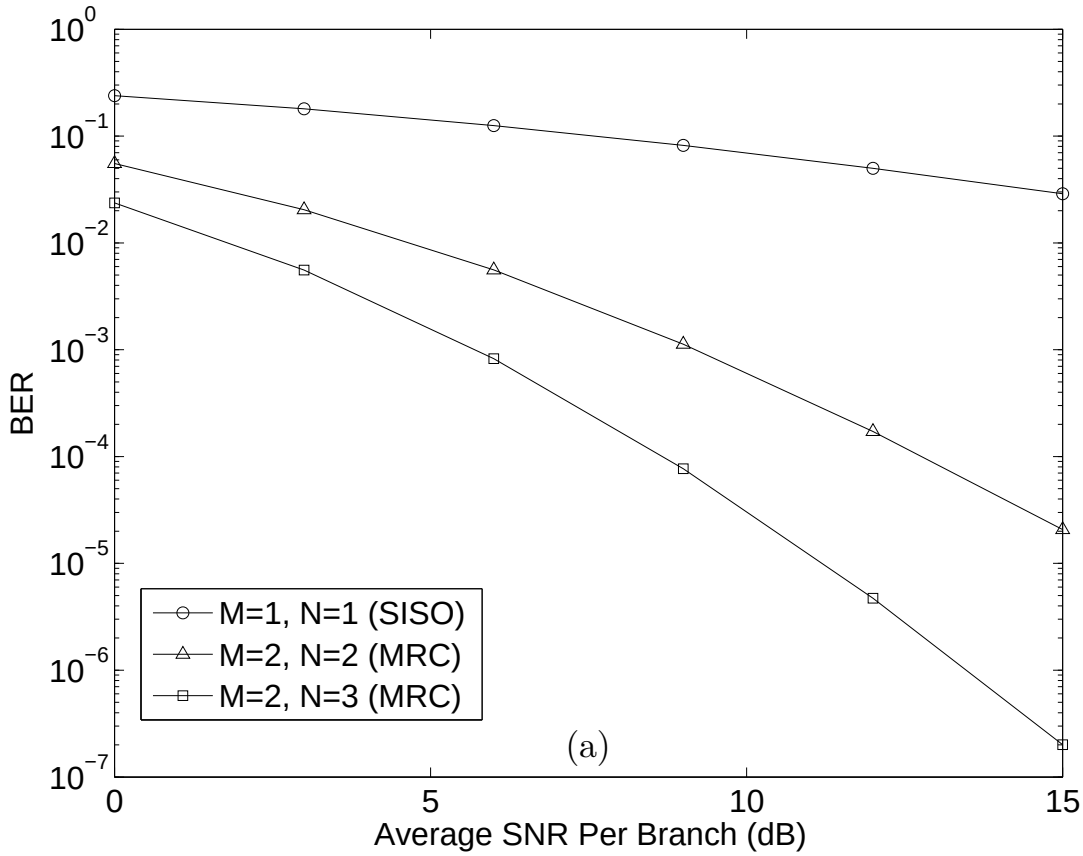

Figure 7.2: BERs for coherent SISO and MIMO using the MRC scheme in the strongly turbulent Gamma-Gamma turbulence channels ($\alpha = 2.23, \beta = 1.70$).

7.2 Numerical Examples

In this section, we present numerical case studies for BERs and outage probabilities with simulation results[14] of the proposed coherent MIMO system.

Figure 7.2 compares the BER curves for BPSK modulated optical signals for SISO and MIMO with MRC reception in a Gamma-Gamma distributed turbulence channel with the channel parameters $\alpha = 2.23, \beta = 1.70$. The BER performance improves as the number of transmitter/receiver antennas increases. It is readily seen that a simple 2×3 MIMO transmission can significantly

[14] We use the first 21 terms in our error rate solutions and have confirmed the solutions by Monte Carlo simulations.

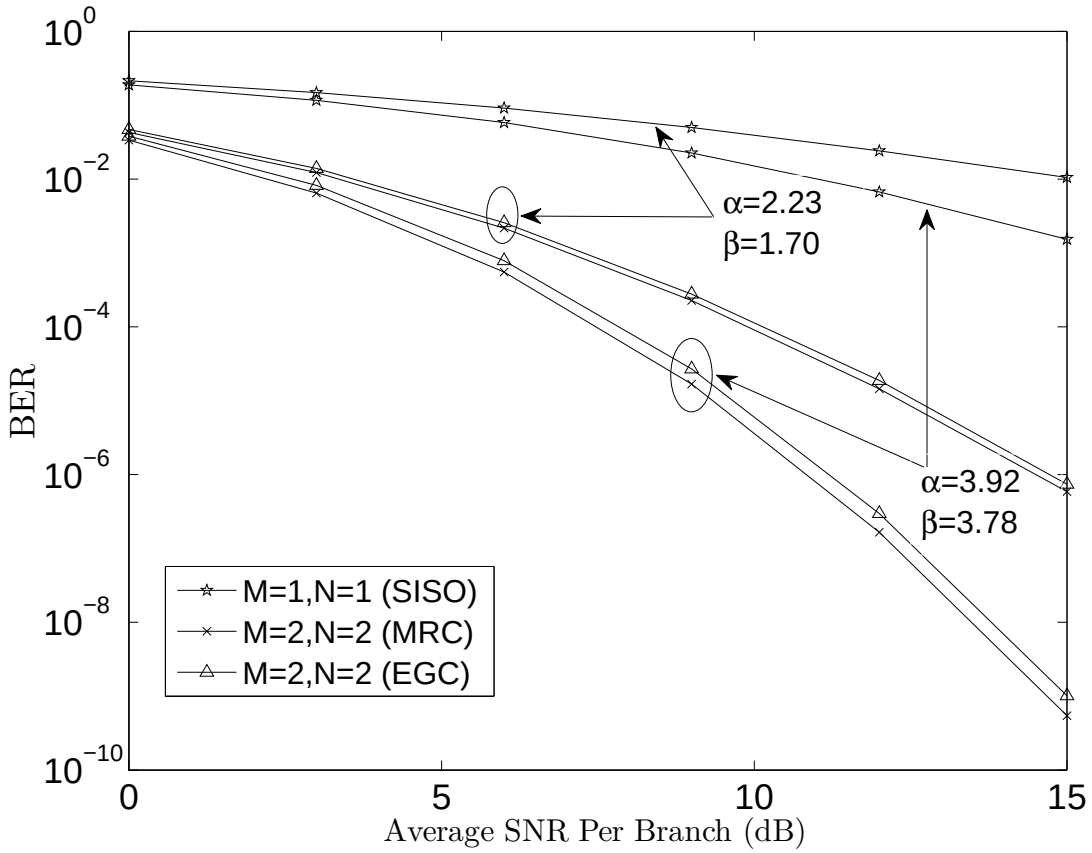

Figure 7.3: Performance comparison between coherent MIMO MRC and MIMO EGC in Gamma-Gamma turbulence channels with weak ($\alpha = 3.92, \beta = 3.78$) and strong turbulence conditions ($\alpha = 2.23, \beta = 1.70$).

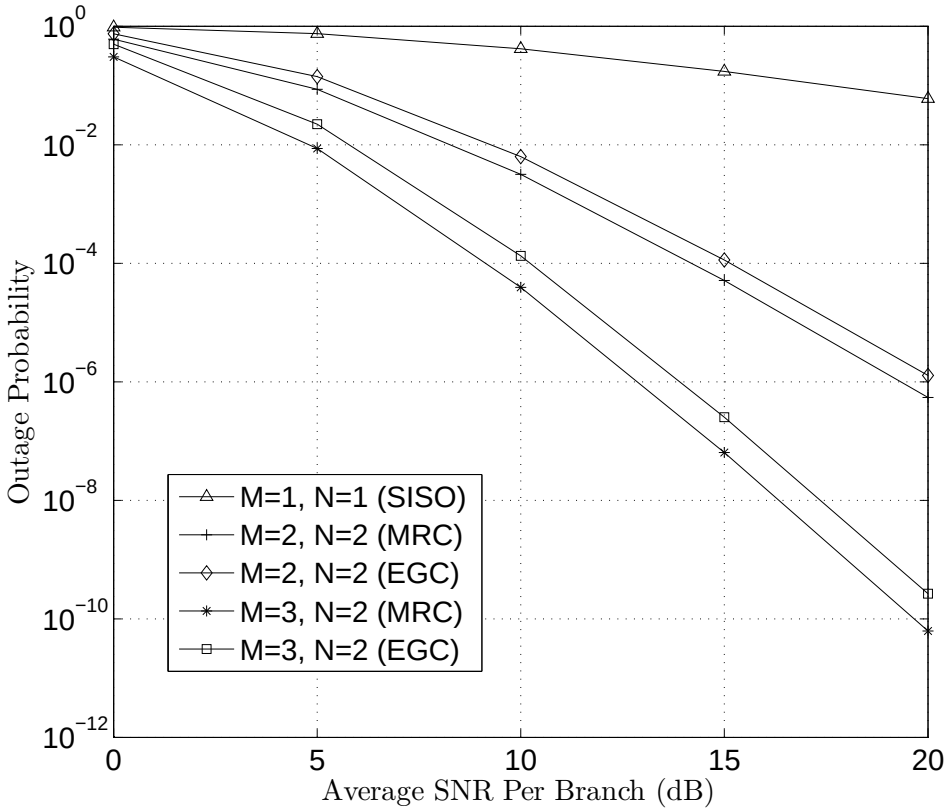

Figure 7.4: Outage probability for coherent SISO and MIMO using MRC/EGC reception in strongly turbulent Gamma-Gamma turbulence channels ($\alpha = 2.15, \beta = 1.06$) with an outage threshold of $\Lambda = 6$ dB.

mitigate the effects of atmospheric turbulence. For instance, at an average SNR of 15 dB, the SISO system has a BER of 2.8×10^{-2} while the 2×3 MIMO system has a BER of 1.9×10^{-7}.

Figure 7.3 plots the BER curves for BPSK modulated optical signals for SISO and MIMO with MRC/EGC receptions in Gamma-Gamma distributed turbulence channels. At both weak and strong turbulence levels, the error performances of MIMO systems are substantially improved as the transmitter/receiver numbers increase compared to the corresponding SISO cases. A 2×2 MIMO EGC transmission can also overcome the effects of atmospheric turbulence. For instance, at an average SNR of 15 dB, the SISO system has a BER of 1.5×10^{-3} while the 2×2 MIMO EGC system has a BER of 7.9×10^{-10} under a weak turbulence condition.

The outage probability curves are shown in Fig. 7.4 for coherent MIMO systems in strong turbulence. A 3×2 MIMO implementation is seen to improve the outage probability by nine orders of magnitude (from 6×10^{-2} to 6×10^{-11}) when compared to SISO for an average SNR of 20 dB. It is observed from both Figs. 7.3 and 7.4 that the performance of MIMO EGC systems, with lower cost and complexity, is close to that of the more complex MIMO MRC systems.

While we have only presented a basic architecture for coherent MIMO in this chapter, a further performance improvement could be created by employing polarization multiplexing in the coherent MIMO OWC system. By applying different states of polarization to the transmitter lasers, we can double the degree of freedom at the transmitter.

7.3 Summary

In this chapter, we have proposed a new MIMO architecture for coherent OWC systems. The BER and outage probability performance of such an OWC MIMO link have been studied for various turbulence conditions and compared to the performance of a coherent SISO link. It was found that the proposed coherent MIMO operation can successfully mitigate atmospheric turbulence with both MRC and EGC, and can significantly outperform coherent SISO systems.

Chapter 8

Space-Time Coding for Coherent Optical Wireless Communication Systems

In this chapter, we propose two new space-time coded optical systems for coherent detection. We first propose two 2×1 systems and then generalize them to 2×2 systems. Our performance analysis show that the space-time coding (STC) technique can indeed realize dual transmitter diversity for coherent FSO communications and achieve full diversity gain.

8.1 Optical Wireless STBC System Models

In this section, we present two coherent space-time coded OWC architectures for operation with atmospheric turbulence channels.

8.1.1 2×1 Alamouti-Type Space-Time Coded Communication: System 1

We first propose an Alamouti-type STBC coherent MPSK OWC system with 2 transmitters and 1 receiver in which the same carrier frequency ω is used. The system structure is shown in Fig. 8.1. We comment that a straightforward Alamouti decoding will not give the desired signals in coherent OWC links over atmospheric turbulence. Additional processing is required and it is detailed as follows.

At the output of the transmitters, we have the modulated electric field from the first transmitter

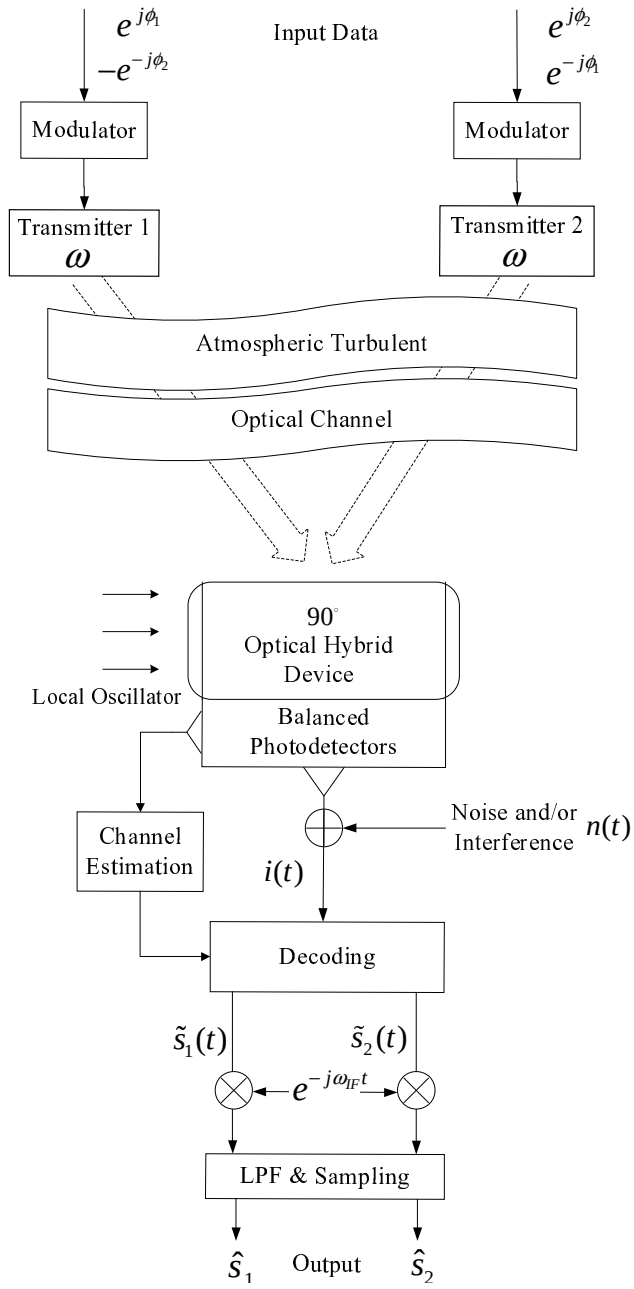

Figure 8.1: Structure of a 2×1 Alamouti-type STBC single-wavelength OWC system using coherent detection.

for the first and the second symbol durations, respectively, as[15]

$$e_1^{(1)}(t) = E_0 \exp(j\omega t + j\phi_1 + j\phi_{t,1}) \tag{8.1}$$

and

$$e_1^{(2)}(t) = -E_0 \exp(j\omega t - j\phi_2 + j\phi_{t,1}) \tag{8.2}$$

where $\phi_i, i = 1,2$ denotes the modulated phase information, and $\phi_{t,1}$ denotes the phase noise arisen within the first transmitter. For the second transmitter, we have the modulated electric field in the first and the second symbol durations as

$$e_2^{(1)}(t) = E_0 \exp(j\omega t + j\phi_2 + j\phi_{t,2}) \tag{8.3}$$

and

$$e_2^{(2)}(t) = E_0 \exp(j\omega t - j\phi_1 + j\phi_{t,2}) \tag{8.4}$$

respectively. In (8.3) and (8.4), $\phi_{t,2}$ denotes the phase noise arisen within the second transmitter.

Following the notational convention used in (8.1)−(8.4), we use subscript $n \in \{1,2\}$ to denote elements corresponding to the first and second transmitters, and we use superscripts with parentheses to denote the corresponding first and second symbol durations. For example, we let $i_1(t)$ and $i_2(t)$ denote the receiver photocurrent from the first and second transmitters, respectively, and let $i_1^{(1)}(t)$ and $i_1^{(2)}(t)$ denote the photocurrents received from the first transmitter during the first and second symbol durations, respectively.

The mixed optical signals at the input of the beam combiner can be written as[16]

$$e_{\text{mix}}^{(1)}(t) = E_{s,1} \exp(j\omega t + j\phi_1 + j\phi_{tc,1}) + E_{s,2} \exp(j\omega t + j\phi_2 + j\phi_{tc,2}) \tag{8.5}$$

[15]Using a narrow linewidth laser, we can assume that the transmitter laser phase noises $\phi_{t,i}$ for $i = 1,2$ are constant over two consecutive symbol periods.

[16]For analytical convenience, we will use complex notations in the ensuing analysis.

and

$$e_{\text{mix}}^{(2)}(t) = -E_{s,1}\exp(j\omega t - j\phi_2 + j\phi_{tc,1}) + E_{s,2}\exp(j\omega t - j\phi_1 + j\phi_{tc,2}) \tag{8.6}$$

where $E_{s,n}$ is the received amplitude of the electric field from the nth transmitter, and $\phi_{tc,n}$ denotes the overall phase noise from the nth transmitter to the input of the coherent receiver. In obtaining (8.5) and (8.6), we have assumed optical phase noise and turbulence-induced fading remain constant for at least two consecutive symbol durations. This is a valid assumption because typical turbulence channel variations are slow (being on the order of milliseconds) when compared to the nanosecond symbol durations of the gigabit per second operational data rates in OWC applications.

At the beam combiner output, we denote the combined electric fields as

$$e_{\text{combine}}^{(1)}(t) = e_{\text{mix}}^{(1)}(t) + E_{LO}\exp(j\omega_{LO}t + j\phi_{LO}) \tag{8.7}$$

and

$$e_{\text{combine}}^{(2)}(t) = e_{\text{mix}}^{(2)}(t) + E_{LO}\exp(j\omega_{LO}t + j\phi_{LO}). \tag{8.8}$$

At the output of the 90° optical hybrid detector[17], we can express the converted photocurrent in

[17]Implementations and the detailed structure of an optical hybrid receiver can be found in [107]. In practice, two circuits can be used to process the real and imaginary parts separately.

the first symbol duration as

$$\begin{aligned} i^{(1)}(t) = {} & RP_{s,1} + RP_{s,2} + RP_{LO} + R\sqrt{P_{s,1}P_{s,2}}\exp(j(\phi_1-\phi_2)+j(\phi_{tc,1}-\phi_{tc,2})) \\ & + R\sqrt{P_{s,2}P_{s,1}}\exp(j(\phi_2-\phi_1)+j(\phi_{tc,2}-\phi_{tc,1})) + R\sqrt{P_{LO}}\exp(j\omega_{IF}t) \\ & \times\left[\sqrt{P_{s,1}}\exp(j\phi_1+j\phi_{tc,1}-j\phi_{LO})+\sqrt{P_{s,2}}\exp(j\phi_2+j\phi_{tc,2}-j\phi_{LO})\right] \\ & + R\sqrt{P_{LO}}\exp(-j\omega_{IF}t)\left[\sqrt{P_{s,1}}\exp(-j\phi_1-j\phi_{tc,1}+j\phi_{LO})\right. \\ & \left.+\sqrt{P_{s,2}}\exp(-j\phi_2-j\phi_{tc,2}+j\phi_{LO})\right] + n^{(1)}(t) \end{aligned} \tag{8.9}$$

where $P_{s,n}$ denotes the power of the received signal sent from the nth transmitter, $\phi_{tr,n}$ is the total phase noise within the nth coherent OWC link, and $n^{(1)}(t)$ is an AWGN process due to shot noise with variance σ_n^2.

From (8.6) and (8.8), we find the converted photocurrent in the second symbol duration as

$$\begin{aligned} i^{(2)}(t) = {} & RP_{s,1} + RP_{s,2} + RP_{LO} - R\sqrt{P_{s,1}P_{s,2}}\exp(-j(\phi_1-\phi_2)+j(\phi_{tc,2}-\phi_{tc,1})) \\ & - R\sqrt{P_{s,2}P_{s,1}}\exp(-j(\phi_2-\phi_1)+j(\phi_{tc,1}-\phi_{tc,2})) + R\sqrt{P_{LO}}\exp(j\omega_{IF}t) \\ & \times\left[\sqrt{P_{s,2}}\exp(-j\phi_1+j\phi_{tc,2}-j\phi_{LO})-\sqrt{P_{s,1}}\exp(-j\phi_2+j\phi_{tc,1}-j\phi_{LO})\right] \\ & + R\sqrt{P_{LO}}\exp(-j\omega_{IF}t)\left[\sqrt{P_{s,2}}\exp(j\phi_1-j\phi_{tc,2}+j\phi_{LO})\right. \\ & \left.-\sqrt{P_{s,1}}\exp(j\phi_2-j\phi_{tc,1}+j\phi_{LO})\right] + n^{(2)}(t) \end{aligned} \tag{8.10}$$

where $n^{(2)}(t)$ is an AWGN process with variance σ_n^2 and it is statistically independent of $n^{(1)}(t)$. After filtering out DC components in (8.9) and (8.10), the filtered photocurrents can be expressed as

$$\begin{aligned} \tilde{i}^{(1)}(t) = {} & R\sqrt{P_{LO}}\exp(j\omega_{IF}t)\left[\sqrt{P_{s,1}}\exp(j\phi_1+j\phi_{tc,1}-j\phi_{LO})\right. \\ & \left.+\sqrt{P_{s,2}}\exp(j\phi_2+j\phi_{tc,2}-j\phi_{LO})\right] \\ & + R\sqrt{P_{LO}}\exp(-j\omega_{IF}t)\left[\sqrt{P_{s,1}}\exp(-j\phi_1-j\phi_{tc,1}+j\phi_{LO})\right. \\ & \left.+\sqrt{P_{s,2}}\exp(-j\phi_2-j\phi_{tc,2}+j\phi_{LO})\right] + \tilde{n}^{(1)}(t) \end{aligned} \tag{8.11}$$

and

$$\begin{aligned}\tilde{i}^{(2)}(t) = R\sqrt{P_{LO}}\exp(j\omega_{IF}t)\left[\sqrt{P_{s,2}}\exp(-j\phi_1 + j\phi_{tc,2} - j\phi_{LO}) - \right.\\ \left.\sqrt{P_{s,1}}\exp(-j\phi_2 + j\phi_{tc,1} - j\phi_{LO})\right]\\ + R\sqrt{P_{LO}}\exp(-j\omega_{IF}t)\left[\sqrt{P_{s,2}}\exp(j\phi_1 - j\phi_{tc,2} + j\phi_{LO})\right.\\ \left.-\sqrt{P_{s,1}}\exp(j\phi_2 - j\phi_{tc,1} + j\phi_{LO})\right] + \tilde{n}^{(2)}(t)\end{aligned} \tag{8.12}$$

where $\tilde{n}^{(1)}(t)$ and $\tilde{n}^{(2)}(t)$ are two filtered AWGN processes. According to the Alamouti decoding approach, the reconstructed two signals can be expressed as

$$\begin{cases} \tilde{s}_1 = h_1^*\tilde{i}^{(1)}(t) + h_2[\tilde{i}^{(2)}(t)]^* \\ \tilde{s}_2 = h_2^*\tilde{i}^{(1)}(t) - h_1[\tilde{i}^{(2)}(t)]^* \end{cases} \tag{8.13}$$

where the superscript * denotes the complex conjugate, $h_1 = \sqrt{P_{LO}P_{s,1}}\exp(j\phi_{tc,1} - j\phi_{LO})$ and $h_2 = \sqrt{P_{LO}P_{s,2}}\exp(j\phi_{tc,2} - j\phi_{LO})$ are two complex quantities which are assumed to be known from the estimation device [108], [109]. Substituting (8.11) and (8.12) into (8.13) yields

$$\begin{aligned}\tilde{s}_1(t) = RP_{LO}\exp(j\omega_{IF}t)\left\{P_{s,1}\exp(j\phi_1) + \sqrt{P_{s,1}P_{s,2}}\exp(j\phi_2 + j(\phi_{tc,2} - \phi_{tc,1}))\right\}\\ + RP_{LO}\exp(-j\omega_{IF}t)\Big\{P_{s,1}\exp(-j\phi_1 - 2j\phi_{tc,1} + 2j\phi_{LO})\\ + \sqrt{P_{s,1}P_{s,2}}\exp(-j\phi_2 - j(\phi_{tc,1} + \phi_{tc,2}) + 2j\phi_{LO})\Big\}\\ + RP_{LO}\exp(j\omega_{IF}t)\left\{P_{s,2}\exp(j\phi_1) - \sqrt{P_{s,2}P_{s,1}}\exp(j\phi_2 - j(\phi_{tc,1} - \phi_{tc,2}))\right\}\\ + RP_{LO}\exp(-j\omega_{IF}t)\Big\{P_{s,2}\exp(-j\phi_1 + 2j\phi_{tc,2} - 2j\phi_{LO})\\ - \sqrt{P_{s,1}P_{s,2}}\exp(-j\phi_2 + j(\phi_{tc,1} + \phi_{tc,2}) - 2j\phi_{LO})\Big\}\\ + h_1^*\tilde{n}^{(1)}(t) + h_2[\tilde{n}^{(2)}(t)]^*\end{aligned} \tag{8.14}$$

and

$$\begin{aligned}
\tilde{s}_2(t) = {} & RP_{LO}\exp(j\omega_{IF}t)\left\{\sqrt{P_{s,1}P_{s,2}}\exp(j\phi_1 + j(\phi_{tc,1}-\phi_{tc,2})) + P_{s,2}\exp(j\phi_2)\right\} \\
& + RP_{LO}\exp(-j\omega_{IF}t)\left\{\sqrt{P_{s,1}P_{s,2}}\exp(-j\phi_1 - j(\phi_{tc,1}+\phi_{tc,2}) + 2j\phi_{LO})\right. \\
& \left. + P_{s,2}\exp(-j\phi_2 - 2j\phi_{tc,2} + 2j\phi_{LO})\right\} \\
& - RP_{LO}\exp(j\omega_{IF}t)\left\{\sqrt{P_{s,2}P_{s,1}}\exp(j\phi_1 - j(\phi_{tc,2}-\phi_{tc,1})) - P_{s,1}\exp(j\phi_2)\right\} \\
& - RP_{LO}\exp(-j\omega_{IF}t)\left\{\sqrt{P_{s,2}P_{s,1}}\exp(-j\phi_1 + j(\phi_{tc,2}+\phi_{tc,1}) - 2j\phi_{LO})\right. \\
& \left. - P_{s,2}\exp(-j\phi_2 + 2j\phi_{tc,1} - 2j\phi_{LO})\right\} \\
& + h_2^*\tilde{n}^{(1)}(t) - h_1[\tilde{n}^{(2)}(t)]^*.
\end{aligned} \tag{8.15}$$

By observing (8.14) and (8.15), we note that those terms containing $\exp(-j\omega_{IF}t)$ are corrupted by phase noises so that they are of little use in signal reconstruction. To recover the desired signals, we multiply $\exp(-j\omega_{IF}t)$ to both (8.14) and (8.15) and filter out the high frequency components. As a result, we obtain the desired signals containing only $\exp(j\phi_1)$ or $\exp(j\phi_2)$ as

$$\begin{aligned}
\hat{s}_1(t) = {} & RP_{LO}[P_{s,1}\exp(j\phi_1) + \sqrt{P_{s,1}P_{s,2}}\exp(j\phi_2 + j(\phi_{tc,2}-\phi_{tc,1}))] \\
& + RP_{LO}[P_{s,2}\exp(j\phi_1) - \sqrt{P_{s,1}P_{s,2}}\exp(j\phi_2 - j(\phi_{tc,1}-\phi_{tc,2}))] \\
& + \underbrace{h_1^* n^{(1)}(t)\exp(-j\omega_{IF}t) + h_2[n^{(2)}(t)]^*\exp(-j\omega_{IF}t)}_{z_1(t)} \\
& = RP_{LO}\exp(j\phi_1)\underbrace{[P_{s,1}+P_{s,2}]}_{S_s} + z_1(t)
\end{aligned} \tag{8.16}$$

and

$$\begin{aligned}\hat{s}_2(t) &= RP_{LO}[\sqrt{P_{s,1}P_{s,2}}\exp(j\phi_1 + j(\phi_{tc,1} - \phi_{tc,2})) + P_{s,2}\exp(j\phi_2)] \\ &\quad - RP_{LO}[\sqrt{P_{s,2}P_{s,1}}\exp(j\phi_1 - j(\phi_{tc,2} - \phi_{tc,1})) - P_{s,1}\exp(j\phi_2)] \\ &\quad + \underbrace{h_2^* n^{(1)}(t)\exp(-j\omega_{IF}t) - h_1[n^{(2)}(t)]^*\exp(-j\omega_{IF}t)}_{z_2(t)} \\ &= RP_{LO}\exp(j\phi_2)\underbrace{[P_{s,1} + P_{s,2}]}_{S_s} + z_2(t).\end{aligned} \tag{8.17}$$

In (8.16) and (8.17), $z_1(t)$ and $z_2(t)$ denote two filtered AWGN processes. At the output of an electrical demodulator, we find the first reconstructed signal as

$$\hat{s}_1 = RP_{LO}\exp(j\phi_1)S_s + z_1 \tag{8.18}$$

where $S_s = P_{s,1} + P_{s,2}$ is the summed receiving optical signal power, z_1 is a zero-mean Gaussian RV with variance σ_z^2. Similarly, we obtain the second reconstructed signal as

$$\hat{s}_2 = RP_{LO}\exp(j\phi_2)S_s + z_2 \tag{8.19}$$

where z_2 is an AWGN term having the same variance σ_z^2 as z_1.

The SNR at the input of the demodulator of an optical receiver is defined as the ratio of the time-averaged AC photocurrent power to the total noise variance, and it can be calculated as

$$\gamma = \frac{R^2 P_{LO}^2 S_s^2}{2S_s q R P_{LO}^2 \Delta f} = \frac{R(P_{s,1} + P_{s,2})}{2q\Delta f} = \frac{\overline{\gamma}}{2}\underbrace{\sum_{n=1}^{2} I_{s,n}}_{Y} \tag{8.20}$$

where we have used the relationship $P_{s,n} = AI_{s,n}$, and $\overline{\gamma} = \frac{RA}{q\Delta f}$ is defined as the average SNR.

8.1.2 2×1 Alamouti-Type Space-Time Coded Communication: System 2

An alternative STBC system using coherent detection can be achieved with two distinct carrier frequencies at the transmitters. The resulting system block diagram is shown in Fig. 8.2.

Following the signal flow in Fig. 8.2, we express the received electric fields from the nth transmitter as

$$\begin{cases} e_1^{(1)}(t) = E_{s,1}\exp(j\omega_1 t + j\phi_1 + j\phi_{tc,1}) \\ e_1^{(2)}(t) = -E_{s,1}\exp(j\omega_1 t - j\phi_2 + j\phi_{tc,1}) \\ e_2^{(1)}(t) = E_{s,2}\exp(j\omega_2 t + j\phi_2 + j\phi_{tc,2}) \\ e_2^{(2)}(t) = E_{s,2}\exp(j\omega_2 t - j\phi_1 + j\phi_{tc,2}) \end{cases} \tag{8.21}$$

where $\omega_n, n = 1,2$ denotes the optical carrier frequency of the nth transmitter.

After filtering out the DC photocurrent and down-conversion processing, we can express the baseband-equivalent signal at the output of the receiver photodetectors during the two symbol intervals as

$$\begin{cases} i_1^{(1)}(t) = \sqrt{2}R\sqrt{P_{s,1}P_{LO}}\exp(j\phi_1)\exp(j\phi_{tr,1}) + n_1^{(1)}(t) \\ i_1^{(2)}(t) = -\sqrt{2}R\sqrt{P_{s,1}P_{LO}}\exp(-j\phi_2)\exp(j\phi_{tr,1}) + n_1^{(2)}(t) \\ i_2^{(1)}(t) = \sqrt{2}R\sqrt{P_{s,2}P_{LO}}\exp(j\phi_2)\exp(j\phi_{tr,2}) + n_2^{(1)}(t) \\ i_2^{(2)}(t) = \sqrt{2}R\sqrt{P_{s,2}P_{LO}}\exp(-j\phi_1)\exp(j\phi_{tr,2}) + n_2^{(2)}(t) \end{cases} \tag{8.22}$$

where $P_{s,n}$ denotes the power of the received signal sent from the nth transmitter, $\phi_{tr,n}$ is the total phase noise within the nth OWC link, $n_n^{(1)}(t)$ and $n_n^{(2)}(t)$ are i.i.d. AWGN processes due to shot noise. Then the photocurrent containing only $s_1 = \exp(j\phi_1)$ can be constructed by combining the received photocurrent as

$$\begin{aligned} \tilde{i}_1(t) = {} & \sqrt{2}R(P_{LO}P_{s,1} + P_{LO}P_{s,2})\exp(j\phi_1) + \sqrt{2}RP_{LO}\sqrt{P_{s,1}P_{s,2}}g^2(t)\exp(j\phi_2)\exp(j(\phi_{tc,2} - \phi_{tc,1})) \\ & - \sqrt{2}RP_{LO}\sqrt{P_{s,2}P_{s,1}}g^2(t)\exp(j\phi_2)\exp(-j(\phi_{tc,1} - \phi_{tc,2})) \\ & + \sqrt{P_{s,1}P_{LO}}\exp(j\phi_{tc,1})[n_1^{(1)}(t) + n_2^{(1)}(t)] + \sqrt{P_{s,2}P_{LO}}\exp(j\phi_{tc,2})[n_1^{(2)}(t) + n_2^{(2)}(t)]. \end{aligned} \tag{8.23}$$

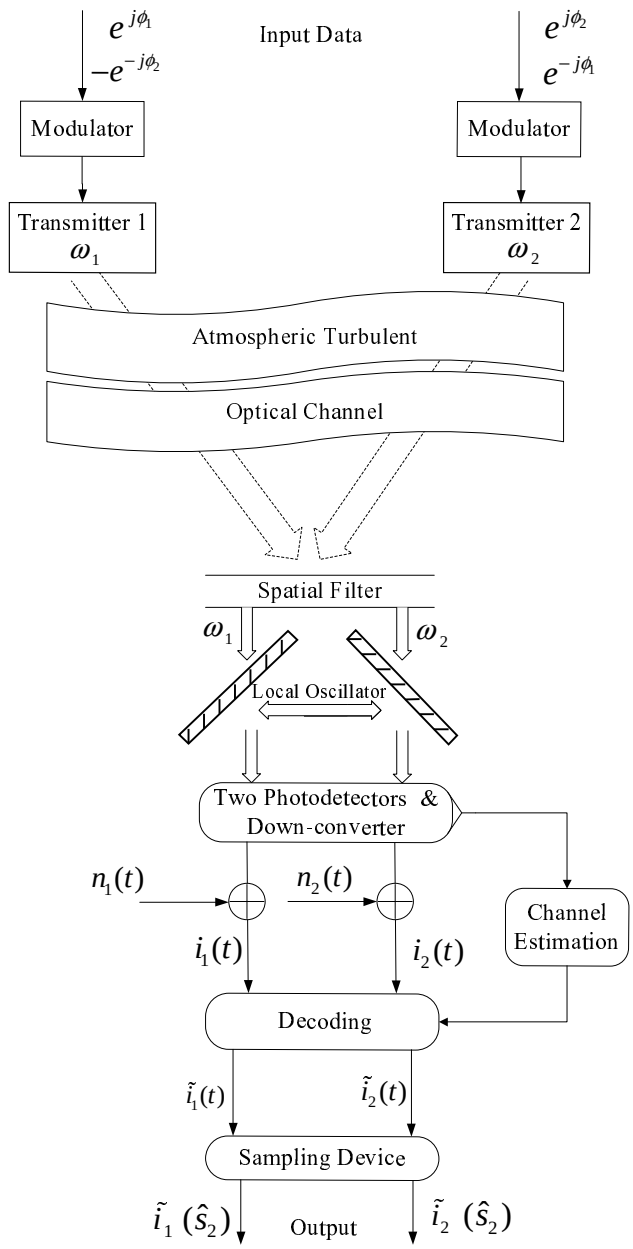

Figure 8.2: Structure of a 2×1 Alamouti-type STBC multiple-wavelength OWC system using coherent detection.

We can further simplify (8.23) to be

$$\begin{aligned}\tilde{i}_1(t) = \sqrt{2}R(\underbrace{P_{LO}P_{s,1} + P_{LO}P_{s,2}}_{S})\exp(j\phi_1) \\ + \underbrace{\sqrt{P_{s,1}P_{LO}}\exp(j\phi_{tc,1})[n_1^{(1)}(t) + n_2^{(1)}(t)] + \sqrt{P_{s,2}P_{LO}}\exp(j\phi_{tc,2})[n_1^{(2)}(t) + n_2^{(2)}(t)]}_{v_1(t)}.\end{aligned} \tag{8.24}$$

After the use of an electrical demodulator, the sampled signal can be found as

$$\tilde{i}_1 = \sqrt{2}RS\exp(j\phi_1) + v_1 \tag{8.25}$$

where $S = P_{LO}\left(\sum_{n=1}^{2} P_{s,n}\right)$, and v_1 is an AWGN term having variance $\sigma_{v_1}^2$. Similarly, we can construct the photocurrent containing only $s_2 = \exp(j\phi_2)$ to be

$$\begin{aligned}\tilde{i}_2(t) = \sqrt{2}R(\underbrace{P_{LO}P_{s,1} + P_{LO}P_{s,2}}_{S})\exp(j\phi_2) \\ + \underbrace{\sqrt{P_{s,2}P_{LO}}\exp(-j\phi_{tc,2})[n_1^{(1)}(t) + n_2^{(1)}(t)] - \sqrt{P_{s,1}P_{LO}}\exp(j\phi_{tc,1})[n_1^{(2)}(t) + n_2^{(2)}(t)]}_{v_2(t)}\end{aligned} \tag{8.26}$$

and its sampled signal is

$$\tilde{i}_2 = \sqrt{2}RS\exp(j\phi_2) + v_2 \tag{8.27}$$

where v_2 is an AWGN term having variance $\sigma_{v_2}^2$. The SNR at the input of the demodulator in the optical receiver can be found as

$$\gamma = \frac{2R^2S^2}{4qRP_{LO}\Delta f S} = \frac{R(P_{LO}P_{s,1} + P_{LO}P_{s,2})}{2qP_{LO}\Delta f} = \frac{\overline{\gamma}}{2}\underbrace{\sum_{n=1}^{2} I_{s,n}}_{Y}. \tag{8.28}$$

We note that the SNR in (8.28) has the same expression as that derived in (8.20). We will use this SNR expression in our performance analysis presented in the following section.

8.2 Error Rate Analysis for 2×1 Space-Time Coded Systems

8.2.1 Symbol Error Rate Analysis

In a coherent OWC turbulence link, the average SER of MPSK can be expressed as [68]

$$P_e = \frac{1}{\pi}\int_0^{\frac{(M-1)\pi}{M}} M_Y\left(-\frac{\sin^2(\pi/M)}{2\sin^2\theta}\frac{\overline{\gamma}}{2}\right)d\theta. \tag{8.29}$$

We can write the MGF of $Y = \sum_{n=1}^{2} I_{s,n}$ defined in (8.20) or (8.28) as $M_Y(s) = [M_{I_{s,n}}(s)]^2$. From (6.19), this MGF can be expressed as

$$M_Y(s) = \sum_{m=0}^{2}\binom{2}{m}\sum_{p=0}^{\infty} b_p(2-m,m,\alpha,\beta)(-s)^{-p-2\beta-m(\alpha-\beta)} \tag{8.30}$$

where $b_p(x,y,\alpha,\beta) = a_p^{[x]}(\alpha,\beta) * a_p^{[y]}(\beta,\alpha)$. Substituting (8.30) into (8.29), we can find the SER for an Alamouti-coded OWC system with coherent detection as

$$\begin{aligned} P_{e,M} &= \frac{1}{\pi}\sum_{m=0}^{2}\binom{2}{m}\sum_{p=0}^{\infty} b_p(2-m,m,\alpha,\beta)\,(\mu_M\overline{\gamma})^{-p-2\beta-m(\alpha-\beta)}\int_0^{\frac{(M-1)\pi}{M}}(\sin^2\theta)^{p+2\beta+m(\alpha-\beta)}d\theta \\ &= \frac{1}{\pi}\sum_{m=0}^{2}\binom{2}{m}\sum_{p=0}^{\infty} b_p(2-m,m,\alpha,\beta)\,(\mu_M\overline{\gamma})^{-p-2\beta-m(\alpha-\beta)}\,\varphi\left(p+2\beta+m(\alpha-\beta),\frac{M-1}{M}\right) \end{aligned} \tag{8.31}$$

where we define $\mu_M = \frac{\sin^2(\frac{\pi}{M})}{4}$. In deriving (8.31), we have also used the integral identity [110]

$$\begin{aligned}\varphi(x,\eta_a) &= \int_0^{\eta_a\pi} \sin^{2x}\theta d\theta \\ &= \left[\frac{\pi^{3/2}\sec(\pi x)}{2\Gamma(x+1)\Gamma\left(\frac{1}{2}-x\right)} - \cos(\eta_a\pi)\,{}_2F_1\left(\frac{1}{2},\frac{1}{2}-x,\frac{3}{2};\cos^2\eta_a\pi\right)\right].\end{aligned} \tag{8.32}$$

Note that when $M=2$, i.e., BPSK modulation, $\varphi\left(x,\frac{1}{2}\right)$ reduces to

$$\varphi\left(x,\frac{1}{2}\right) = \frac{\sqrt{\pi}\Gamma(x+\frac{1}{2})}{2\Gamma(x+1)} = \frac{1}{2}B\left(\frac{1}{2},x+\frac{1}{2}\right). \tag{8.33}$$

Therefore, we can find the average BER for Alamouti-coded coherent systems using BPSK as

$$\begin{aligned}P_{e,2} =& \frac{1}{2\pi}\sum_{m=0}^{2}\binom{2}{m}\sum_{p=0}^{\infty} b_p(2-m,m,\alpha,\beta) \\ &\times B\left(\frac{1}{2},p+2\beta+m(\alpha-\beta)+\frac{1}{2}\right)\left(\frac{\overline{\gamma}}{4}\right)^{-p-2\beta-m(\alpha-\beta)}.\end{aligned} \tag{8.34}$$

When QPSK modulation is considered, we can derive the average SER for Alamouti coded coherent systems using QPSK as

$$\begin{aligned}P_{e,4} =& \frac{1}{2\pi}\sum_{m=0}^{2}\binom{2}{m}\sum_{p=0}^{\infty} b_p(2-m,m,\alpha,\beta) \\ &\times\left[B\left(\frac{1}{2},p+2\beta+m(\alpha-\beta)+\frac{1}{2}\right)-\varphi\left(p+2\beta+m(\alpha-\beta),\frac{3}{4}\right)\right] \\ &\times\left(\frac{\overline{\gamma}}{8}\right)^{-p-2\beta-m(\alpha-\beta)}\end{aligned} \tag{8.35}$$

where $\varphi\left(x,\frac{3}{4}\right)$ is obtained by making use of the Gaussian hypergeometric function definition as

$$\begin{aligned}\varphi\left(x,\frac{3}{4}\right) &= \int_0^{\frac{\pi}{4}}\sin^{2x}\theta d\theta = 2^{-x-\frac{3}{2}}\int_0^1 y^{x-\frac{1}{2}}\left(1-\frac{y}{2}\right)^{-\frac{1}{2}}dy \\ &= \frac{\sqrt{2}\,{}_2F_1\left(\frac{1}{2},x+\frac{1}{2},x+\frac{3}{2};\frac{1}{2}\right)}{2^{x+1}(2x+1)}.\end{aligned} \tag{8.36}$$

The error rate solutions derived in (8.31), (8.33) and (8.35) contain only the Gamma function and the Gaussian hypergeometric function, and thus they can be rapidly calculated with standard MATLAB or Maple software.

8.2.2 Truncation Error Analysis

For practical evaluation of system performance, the infinite summation presented in the error rate solutions must be approximated by finite terms. As a result, a truncation error will be present due to the elimination of infinite terms.

In order to examine the accuracy of the series solutions with finite terms, we define the truncation error from an elimination of all terms after the first $J+1$ terms as

$$\varepsilon_{J,M} = \sum_{m=0}^{2} \binom{2}{m} \sum_{p=J+1}^{\infty} u_p(\alpha,\beta,m,M) \left(\frac{1}{\mu_M \overline{\gamma}}\right)^p \tag{8.37}$$

where $u_p(\cdot,\cdot,\cdot,\cdot)$ is defined as

$$u_p(x,y,m,M) = \frac{\varphi\left(p+2y+m(x-y), \frac{M-1}{M}\right)}{\pi} b_p(2-m,m,x,y) \left(\frac{1}{\mu_M \overline{\gamma}}\right)^{2y+m(x-y)}. \tag{8.38}$$

Making use of a Taylor series expansion $\frac{x^{J+1}}{1-x} = x^{J+1}(1+x+x^2+\cdots+x^n+\cdots)$, we can simplify the summation term in (8.37) and obtain an upper bound for truncation error in (8.37) as

$$\varepsilon_{J,M} \leq \frac{2}{\pi(\mu_M \overline{\gamma}-1)} \left(\frac{1}{\mu_M \overline{\gamma}}\right)^J \sum_{m=0}^{2} \frac{\max\limits_{p>J} \left\{u_p(\alpha,\beta,m,M)\right\}}{m!(2-m)!}. \tag{8.39}$$

In deriving (8.39) we have also used the identity

$$\binom{2}{m} = \frac{2}{m!(2-m)!}. \tag{8.40}$$

In order to prove that (8.39) is a decaying upper bound, we need to prove that the maxi-

mum value of $u_p(\alpha,\beta,m,M)$ exists. It can be shown that the term $b_p(2-m,m,\alpha,\beta)$ decreases with increasing p values and will approach zero as $p \to \infty$. From (8.32), we note that the term $\varphi\left(p+2y+m(x-y),\frac{M-1}{M}\right)$ is finite for any value of the index p. We conclude that the term $u_p(\alpha,\beta,m,M)$ becomes zero as $p \to \infty$. As a result, there must exist a J_0 where the maximum value of $u_p(\alpha,\beta,m,M)$ exists when $J \geq J_0$. Therefore, the truncation error decreases as the value of J increases. Furthermore, we note from (8.39) that the truncation error diminishes with increasing SNR values. The derived series solutions with finite terms are therefore highly accurate in large SNR regimes.

8.2.3 Asymptotic Analysis

The asymptotic error rate of a digital communication system in fading channels can be obtained with diversity order G_d and coding gain G_c as $P_e^{asym} \approx (G_c\overline{\gamma})^{-G_d}$. For the proposed Alamouti-type STBC OWC systems using coherent detection, we observe that the infinite summation terms appearing in (8.31), (8.33) and (8.35) diminish rapidly with increasing $\overline{\gamma}$. This implies that the derived series solutions with finite terms can be highly accurate in large SNR regimes.

Since the terms in (8.31) also decrease with the increasing index p ($p \in \mathbf{N}$), the dominant term in the SER solution only contains $(\mu_M\overline{\gamma})^{-2\min\{\alpha,\beta\}}$. As a result, when $\overline{\gamma}$ approaches ∞, the leading term when $p=0$ in (8.31) becomes the dominant term. Therefore, we obtain the asymptotic SER approximation in large SNR regimes for MPSK modulated Alamouti-type STBC systems over the Gamma-Gamma turbulence channels as

$$P_{e,M}^{asym} \approx \frac{[a_0(\alpha,\beta)]^2\varphi\left(2\min\{\alpha,\beta\},\frac{M-1}{M}\right)}{\pi}(\mu_M\overline{\gamma})^{-2\min\{\alpha,\beta\}}. \tag{8.41}$$

Though the closed-form expressions of asymptotic error rates show that the diversity order is $G_d = 2\min\{\alpha,\beta\}$, which only depends on the smaller channel parameter, the convergence of the asymptotic error rate depends on the absolute difference between α and β in the Gamma-

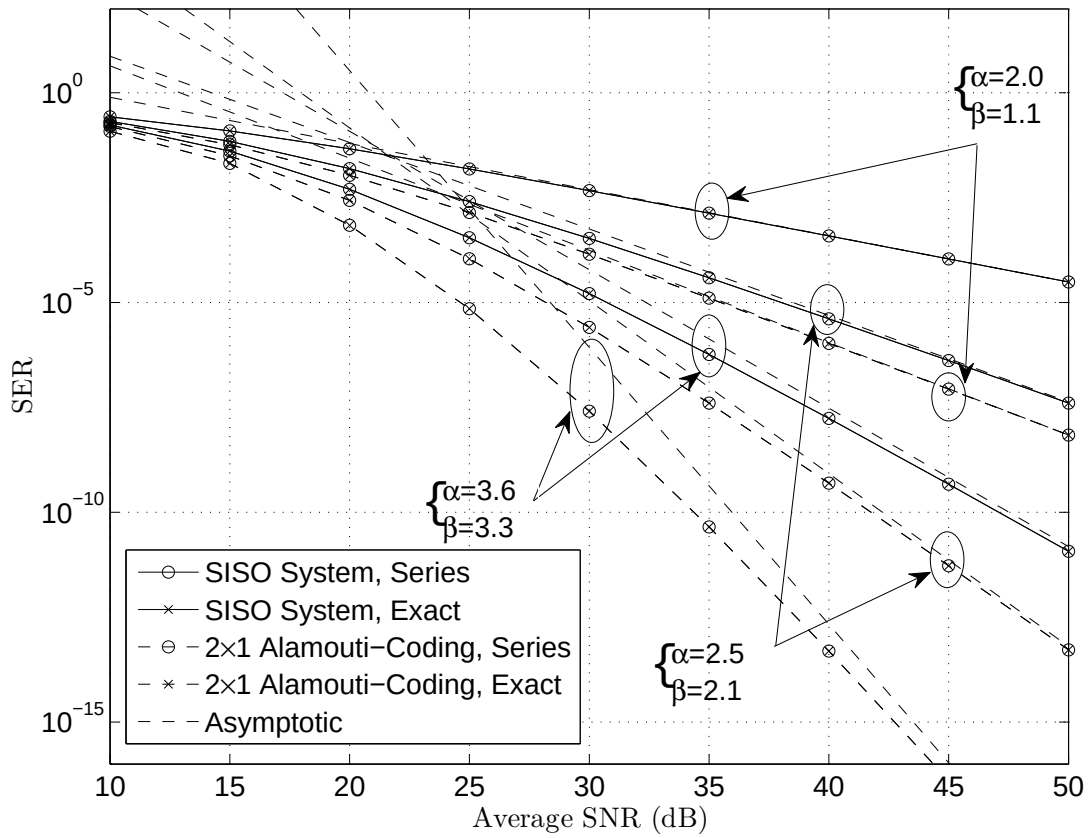

Figure 8.3: SERs of Alamouti-type STBC 2×1 and SISO OWC systems with 8PSK modulation using coherent detection over the Gamma-Gamma turbulence channels with $J = 36$.

Gamma turbulence channels. When the absolute difference between α and β is small, the leading term containing $(\mu_M \overline{\gamma})^{-2\min\{\alpha,\beta\}}$ (when $p = 0$) decreases at a similar rate to that of the second leading term containing $(\mu_M \overline{\gamma})^{-(\alpha+\beta)}$ (when $p = 0$) as $\overline{\gamma}$ increases. Thus, the asymptotic error rates obtained in (8.41) will slowly converge to the exact error rates. The asymptotic error rates approach the exact error rates rapidly when the difference of $|\alpha - \beta|$ is large. Such asymptotic error rate behavior will be observed from our numerical examples.

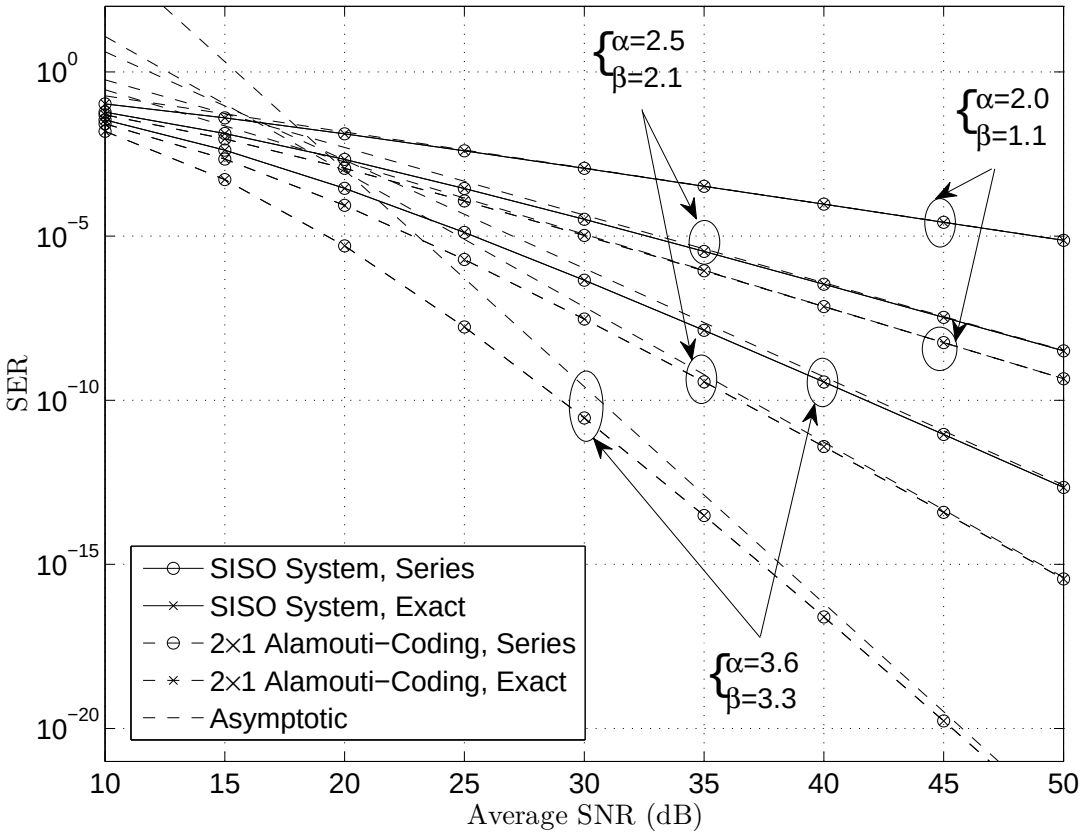

Figure 8.4: SERs of Alamouti-type STBC 2×1 and SISO OWC systems with QPSK modulation using coherent detection over the Gamma-Gamma turbulence channels with $J = 36$.

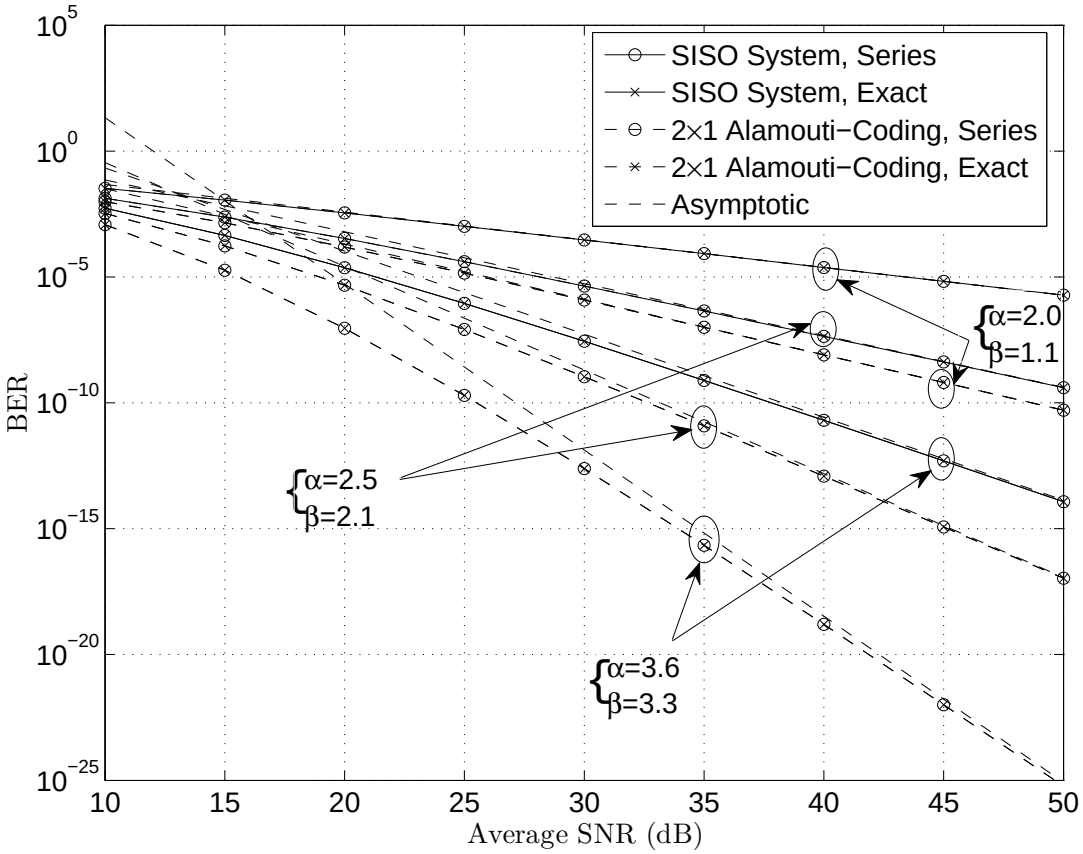

Figure 8.5: BERs of Alamouti-type STBC 2×1 and SISO OWC systems with BPSK modulation using coherent detection over the Gamma-Gamma turbulence channels with $J = 36$.

8.2.4 Numerical Examples

In this section, we present error rate curves for the Alamouti-type STBC coded optical systems using coherent detection over the Gamma-Gamma turbulence channels. The series error rates are computed by eliminating the infinite terms after calculating the first $J+1$ terms. The exact error rates are calculated from numerical integration through $P_e = \int_0^\infty P_e(\gamma) f_\gamma(\gamma) d\gamma$ where $P_e(\gamma)$ is the conditional error probability and $f_\gamma(\gamma)$ denotes the PDF of the receiver instantaneous SNR.

SER curves for 8PSK-modulated signals with Alamouti-type STBC using coherent detection are presented in Fig. 8.3 for weak ($\alpha = 3.6, \beta = 3.3$), medium ($\alpha = 2.5, \beta = 2.1$), and strong ($\alpha = 2.0, \beta = 1.1$) turbulence conditions. The series SERs are compared with the exact SERs, and excellent agreement is seen between these two types of SER curves. This validates our series solutions. Asymptotic error rates are also shown to agree with our analytical error rate results when the average SNR is large. The results show that our proposed Alamouti-type STBC systems using coherent detection can effectively mitigate the turbulence impacts. A substantial SER improvement can be found in moving from the SISO system to the 2×1 Alamouti-type STBC coded systems. For example, when $\alpha = 3.6$ and $\beta = 3.3$ and at 35 dB SNR, a SISO coherent system has an error rate of 10^{-6}, while an Alamouti 2×1 system achieves an error rate of 10^{-10}.

Figure 8.4 compares the series SER and exact SER for QPSK-modulated OWC systems using coherent detection. Again, excellent agreement is observed from the SER plots in Fig. 8.4 between our series solutions and exact SERs. Agreement between asymptotic and exact SERs also becomes clear as the average SNR increases. As expected, the asymptotic SER approaches the exact SER much faster in the case of $\alpha = 2.0$ and $\beta = 1.1$ (parameters α and β having a large difference) than the case of $\alpha = 3.6$ and $\beta = 3.3$ (parameters α and β having a small difference). A substantial SER improvement can also be seen for the SISO system compared to the 2×1 Alamouti systems. At an average SNR of 35 dB in a turbulent channel with parameters $\alpha = 2.5$ and $\beta = 2.1$, a SISO coherent system has a SER of 3×10^{-5}, while an Alamouti 2×1 system achieves a SER of 3×10^{-10}.

From the presented numerical examples, we conclude that the two proposed Alamouti-type STBC OWC systems using coherent detection can indeed improve the error rate performance, beyond that of SISO OWC systems, in a wide range of turbulence conditions. Furthermore, the derived simple series error rate solutions are found to be efficient and easy to use.

8.3 2×2 Alamouti-Type Space-Time Coded MIMO Communication: System 1

The performance of optical wireless communication systems may need to be further enhanced for situations where higher diversity orders are required. For example, the BER in Fig. 8.5 for coherent STC systems under strong turbulence conditions requires higher transmitted power to achieve 10^{-9} (e.g., at 50 dB SNR). In this case, both multiple transmitters and receivers can be employed for the STC links.

We can extend the proposed systems in Section 8.1 to 2×2 systems. Figure 8.6 describes the structure of a 2×2 STC-coded MIMO system using a single carrier frequency. The encoding is the same as the single coherent receiver case. Note that the two receivers should be sufficiently far apart within the beam spot but beyond the coherence length.

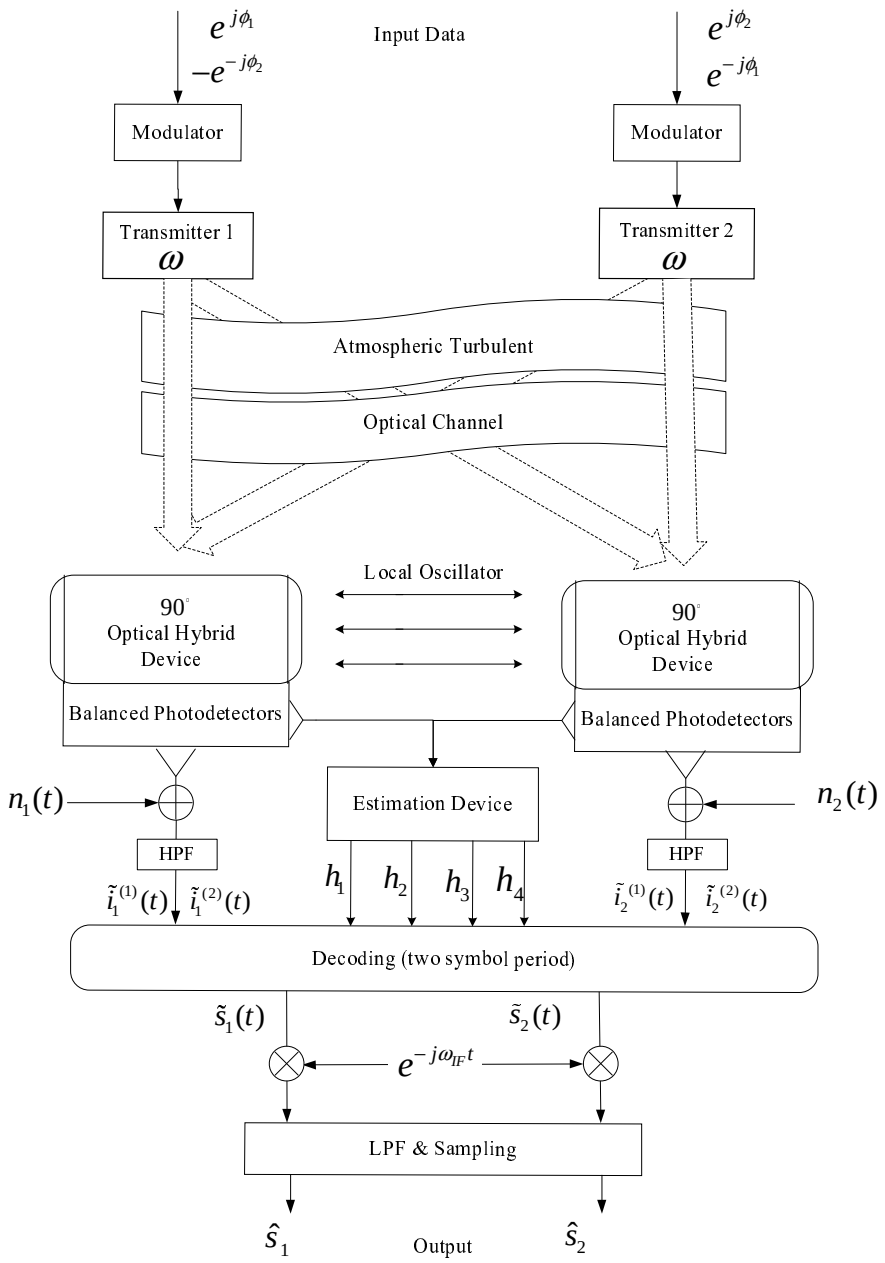

Figure 8.6: Structure of a 2×2 Alamouti-type STBC single-wavelength OWC system using coherent detection.

At the receivers, the received electric fields can be written as

$$\begin{cases} e_{11}^{(1)}(t) = E_{s,11}\exp(j\omega t + j\phi_1 + j\phi_{tc,11}) \\ e_{21}^{(1)}(t) = E_{s,21}\exp(j\omega t + j\phi_2 + j\phi_{tc,21}) \\ e_{12}^{(1)}(t) = E_{s,12}\exp(j\omega t + j\phi_1 + j\phi_{tc,12}) \\ e_{22}^{(1)}(t) = E_{s,22}\exp(j\omega t + j\phi_2 + j\phi_{tc,22}) \\ e_{11}^{(2)}(t) = -E_{s,11}\exp(j\omega t - j\phi_2 + j\phi_{tc,11}) \\ e_{21}^{(2)}(t) = E_{s,21}\exp(j\omega t - j\phi_1 + j\phi_{tc,21}) \\ e_{12}^{(2)}(t) = -E_{s,12}\exp(j\omega t - j\phi_2 + j\phi_{tc,12}) \\ e_{22}^{(2)}(t) = E_{s,22}\exp(j\omega t - j\phi_1 + j\phi_{tc,22}) \end{cases} \tag{8.42}$$

where $\{n;l\} \in \{1,2;1,2\}$, $E_{s,nl}$ is the received amplitude of the electric field from the nth transmitter to the lth coherent receiver, and $\phi_{tc,nl}$ denotes the overall phase noise from the nth transmitter to the input of the lth coherent receiver.

After combining with the LO[18], the electric fields (at the first and second symbol intervals) become

$$\begin{aligned} e_{\text{combine},R1}^{(1)}(t) = {} & E_{s,11}\exp(j\omega t + j\phi_1 + j\phi_{tc,11}) \\ & + E_{s,21}\exp(j\omega t + j\phi_2 + j\phi_{tc,21}) + E_{LO}\exp(j\omega_{LO}t + j\phi_{LO}) \end{aligned} \tag{8.43}$$

$$\begin{aligned} e_{\text{combine},R1}^{(2)}(t) = {} & -E_{s,11}\exp(j\omega t - j\phi_2 + j\phi_{tc,11}) \\ & + E_{s,21}\exp(j\omega t - j\phi_1 + j\phi_{tc,21}) + E_{LO}\exp(j\omega_{LO}t + j\phi_{LO}) \end{aligned} \tag{8.44}$$

[18]Only one beam combiner is needed for two receivers. To keep the LO phase noise the same for all receiving branches, one LO is used for the two receivers. This also reduces the implementation and operational costs.

$$
\begin{aligned}
e^{(1)}_{\text{combine},R2}(t) = {} & E_{s,12}\exp(j\omega t + j\phi_1 + j\phi_{tc,12}) \\
& + E_{s,22}\exp(j\omega t + j\phi_2 + j\phi_{tc,22}) + E_{LO}\exp(j\omega_{LO}t + j\phi_{LO})
\end{aligned}
\tag{8.45}
$$

and

$$
\begin{aligned}
e^{(2)}_{\text{combine},R2}(t) = {} & -E_{s,12}\exp(j\omega t - j\phi_2 + j\phi_{tc,12}) \\
& + E_{s,22}\exp(j\omega t - j\phi_1 + j\phi_{tc,22}) + E_{LO}\exp(j\omega_{LO}t + j\phi_{LO})
\end{aligned}
\tag{8.46}
$$

where the subscripts "$\cdot_{R1}$" and "$\cdot_{R2}$" respectively denote the processed signals in the first and second receivers. Thus, after the optoelectronic conversion and filtering out of the DC components, we find the photocurrents containing the useful signals as

$$
\begin{aligned}
\tilde{i}^{(1)}_{R1}(t) = {} & R\sqrt{P_{LO}}\exp(j\omega_{IF}t)\left[\sqrt{P_{s,11}}\exp(j\phi_1 + j\phi_{tc,11} - j\phi_{LO}) + \sqrt{P_{s,21}}\exp(j\phi_2 + j\phi_{tc,21} - j\phi_{LO})\right] \\
& + R\sqrt{P_{LO}}\exp(-j\omega_{IF}t)\left[\sqrt{P_{s,11}}\exp(-j\phi_1 - j\phi_{tc,11} + j\phi_{LO})\right. \\
& \left. + \sqrt{P_{s,21}}\exp(-j\phi_2 - j\phi_{tc,21} + j\phi_{LO})\right] + \tilde{n}^{(1)}_{R1}(t)
\end{aligned}
\tag{8.47}
$$

$$
\begin{aligned}
\tilde{i}^{(2)}_{R1}(t) = {} & R\sqrt{P_{LO}}\exp(j\omega_{IF}t)\left[\sqrt{P_{s,21}}\exp(-j\phi_1 + j\phi_{tc,21} - j\phi_{LO}) - \sqrt{P_{s,11}}\exp(-j\phi_2 + j\phi_{tc,11} - j\phi_{LO})\right] \\
& + R\sqrt{P_{LO}}\exp(-j\omega_{IF}t)\left[\sqrt{P_{s,21}}\exp(j\phi_1 - j\phi_{tc,21} + j\phi_{LO})\right. \\
& \left. - \sqrt{P_{s,11}}\exp(j\phi_2 - j\phi_{tc,11} + j\phi_{LO})\right] + \tilde{n}^{(2)}_{R1}(t)
\end{aligned}
\tag{8.48}
$$

$$\begin{aligned}\tilde{i}_{R2}^{(1)}(t) = {} & R\sqrt{P_{LO}}\exp(j\omega_{IF}t)\left[\sqrt{P_{s,12}}\exp(j\phi_1 + j\phi_{tc,12} - j\phi_{LO}) + \sqrt{P_{s,22}}\exp(j\phi_2 + j\phi_{tc,22} - j\phi_{LO})\right] \\ & + R\sqrt{P_{LO}}\exp(-j\omega_{IF}t)\left[\sqrt{P_{s,12}}\exp(-j\phi_1 - j\phi_{tc,12} + j\phi_{LO})\right. \\ & \left. + \sqrt{P_{s,22}}\exp(-j\phi_2 - j\phi_{tc,22} + j\phi_{LO})\right] + \tilde{n}_{R2}^{(1)}(t)\end{aligned} \tag{8.49}$$

and

$$\begin{aligned}\tilde{i}_{R2}^{(2)}(t) = {} & R\sqrt{P_{LO}}\exp(j\omega_{IF}t)\left[\sqrt{P_{s,22}}\exp(-j\phi_1 + j\phi_{tc,22} - j\phi_{LO}) - \sqrt{P_{s,12}}\exp(-j\phi_2 + j\phi_{tc,12} - j\phi_{LO})\right] \\ & + R\sqrt{P_{LO}}\exp(-j\omega_{IF}t)\left[\sqrt{P_{s,22}}\exp(j\phi_1 - j\phi_{tc,22} + j\phi_{LO})\right. \\ & \left. - \sqrt{P_{s,12}}\exp(j\phi_2 - j\phi_{tc,12} + j\phi_{LO})\right] + \tilde{n}_{R2}^{(2)}(t)\end{aligned} \tag{8.50}$$

where $\tilde{n}_{R1}^{(1)}(t)$, $\tilde{n}_{R1}^{(2)}(t)$, $\tilde{n}_{R2}^{(1)}(t)$ and $\tilde{n}_{R2}^{(2)}(t)$ are filtered AWGN processes representing the receiver shot noises. In the 2×2 case, we can formulate the signals through

$$\begin{cases} \tilde{s}_1 = \exp(-j\omega_{IF}t)\left\{h_1^*\tilde{i}_{R1}^{(1)}(t) + h_2[\tilde{i}_{R1}^{(2)}(t)]^* + h_3^*\tilde{i}_{R2}^{(1)}(t) + h_4[\tilde{i}_{R2}^{(2)}(t)]^*\right\} \\ \tilde{s}_2 = \exp(-j\omega_{IF}t)\left\{h_2^*\tilde{i}_{R1}^{(1)}(t) - h_1[\tilde{i}_{R1}^{(2)}(t)]^* + h_4^*\tilde{i}_{R2}^{(1)}(t) - h_3[\tilde{i}_{R2}^{(2)}(t)]^*\right\} \end{cases} \tag{8.51}$$

where h_1, h_2, h_3 and h_4 are

$$\begin{cases} h_1 = \sqrt{P_{LO}P_{s,11}}\exp(-j\phi_{tc,11} + j\phi_{LO}) \\ h_2 = \sqrt{P_{LO}P_{s,21}}\exp(j\phi_{tc,21} - j\phi_{LO}) \\ h_3 = \sqrt{P_{LO}P_{s,12}}\exp(-j\phi_{tc,12} + j\phi_{LO}) \\ h_4 = \sqrt{P_{LO}P_{s,22}}\exp(j\phi_{tc,22} - j\phi_{LO}) \end{cases} \tag{8.52}$$

which are estimated complex quantities as shown in Fig. 8.6 and are assumed to be known. After the appropriate signal combining according to (8.51), the desired signals can be obtained by

filtering out the remaining high frequency components and become

$$\begin{aligned}
\hat{s}_1(t) = & RP_{LO}\left[P_{s,11}\exp(j\phi_1) + P_{s,21}\exp(j\phi_1) + \sqrt{P_{s,11}P_{s,21}}\exp(j\phi_2 + j(\phi_{tc,21} - \phi_{tc,11}))\right. \\
& \left. -\sqrt{P_{s,11}P_{s,21}}\exp(j\phi_2 - j(\phi_{tc,11} - \phi_{tc,21}))\right] \\
& + RP_{LO}\left[P_{s,12}\exp(j\phi_1) + \sqrt{P_{s,12}P_{s,22}}\exp(j\phi_2 - j(\phi_{tc,12} - \phi_{tc,22})) + P_{s,22}\exp(j\phi_1)\right. \\
& \left. -\sqrt{P_{s,12}P_{s,22}}\exp(j\phi_2 + j(\phi_{tc,22} - \phi_{tc,12}))\right] \\
& + \underbrace{\{h_1^* n_{R1}^{(1)}(t) + h_2[n_{R1}^{(2)}(t)]^* + h_3^* n_{R2}^{(1)}(t) + h_4[n_{R2}^{(2)}(t)]^*\}\exp(-j\omega_{IF}t)}_{z_{m,1}(t)} \\
= & RP_{LO}\exp(j\phi_1)\underbrace{[P_{s,11} + P_{s,21} + P_{s,12} + P_{s,22}]}_{S_{s,m}} + z_{m,1}(t)
\end{aligned} \tag{8.53}$$

and

$$\begin{aligned}
\hat{s}_2(t) = & RP_{LO}\left[\sqrt{P_{s,21}P_{s,11}}\exp(j\phi_1 + j(\phi_{tc,11} - \phi_{tc,21})) + P_{s,21}\exp(j\phi_2)\right. \\
& \left. -\sqrt{P_{s,11}P_{s,21}}\exp(j\phi_1 - j(\phi_{tc,21} - \phi_{tc,11})) + P_{s,11}\exp(j\phi_2)\right] \\
& - RP_{LO}\left[\sqrt{P_{s,22}P_{s,12}}\exp(j\phi_1 + j(\phi_{tc,22} - \phi_{tc,12})) + P_{s,22}\exp(j\phi_2)\right. \\
& \left. -\sqrt{P_{s,22}P_{s,12}}\exp(j\phi_1 - j(\phi_{tc,12} - \phi_{tc,22})) + P_{s,12}\exp(j\phi_2)\right] \\
& + \underbrace{\{h_2^* n_{R1}^{(1)}(t) - h_1[n_{R1}^{(2)}(t)]^* + h_4^* n_{R2}^{(1)}(t) - h_3[n_{R2}^{(2)}(t)]^*\}\exp(-j\omega_{IF}t)}_{z_{m,2}(t)} \\
= & RP_{LO}\exp(j\phi_2)\underbrace{[P_{s,21} + P_{s,11} + P_{s,22} + P_{s,12}]}_{S_{s,m}} + z_{m,2}(t).
\end{aligned} \tag{8.54}$$

After demodulating with an electrical demodulator, we find the reconstructed signals as

$$\hat{s}_1 = RP_{LO}\exp(j\phi_1)S_{s,m} + z_{m,1} \tag{8.55}$$

and

$$\hat{s}_2 = RP_{LO}\exp(j\phi_2)S_{s,m} + z_{m,2} \tag{8.56}$$

where $S_{s,m} = \sum_{n=1}^{2}\sum_{l=1}^{2} P_{s,nl}$ is the summed received optical signal power, and $z_{m,1}$ and $z_{m,2}$ are two Gaussian RVs. The SNR at the input of the demodulator can be calculated as

$$\gamma = \frac{\overline{\gamma}}{2}\underbrace{\sum_{n=1}^{2}\sum_{l=1}^{2} I_{s,nl}}_{Y_m} \tag{8.57}$$

where $I_{s,nl}$ is the lth received signal irradiance from the nth transmitter.

8.4 2 × 2 Alamouti-Type Space-Time Coded MIMO Communication: System 2

In this section, we generalize the 2×1 multiple-wavelength system to a 2×2 MIMO system with coherent detection. The proposed 2×2 system is described in Fig. 8.7.

The encoding processes at the two transmitters are the same as that of the single receiver case described in Section 8.1.2. After filtering and down-converting, we can write the received baseband

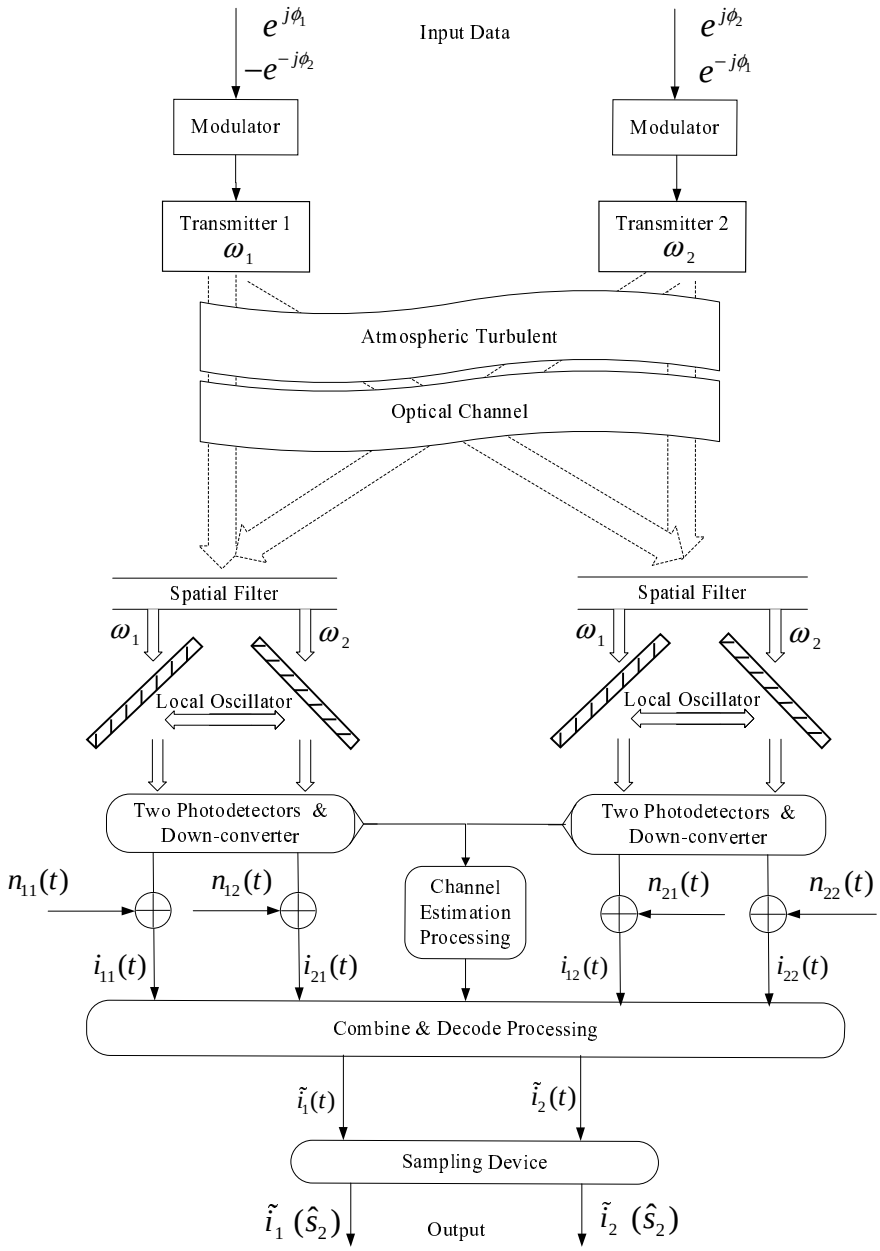

Figure 8.7: Structure of a 2×2 Alamouti-type STBC multiple-wavelength OWC system using coherent detection.

equivalent signal as

$$\begin{cases} i_{11}^{(1)}(t) = \sqrt{2}R\sqrt{P_{s,11}P_{LO}}\exp(j\phi_1)\exp(j\phi_{tr,11}) + n_{11}^{(1)}(t) \\ i_{11}^{(2)}(t) = -\sqrt{2}R\sqrt{P_{s,11}P_{LO}}\exp(-j\phi_2)\exp(j\phi_{tr,11}) + n_{11}^{(2)}(t) \\ i_{21}^{(1)}(t) = \sqrt{2}R\sqrt{P_{s,21}P_{LO}}\exp(j\phi_2)\exp(j\phi_{tr,21}) + n_{21}^{(1)}(t) \\ i_{21}^{(2)}(t) = \sqrt{2}R\sqrt{P_{s,21}P_{LO}}\exp(-j\phi_1)\exp(j\phi_{tr,21}) + n_{21}^{(2)}(t) \\ i_{12}^{(1)}(t) = \sqrt{2}R\sqrt{P_{s,12}P_{LO}}\exp(j\phi_1)\exp(j\phi_{tr,12}) + n_{12}^{(1)}(t) \\ i_{12}^{(2)}(t) = -\sqrt{2}R\sqrt{P_{s,12}P_{LO}}\exp(j\phi_2)\exp(j\phi_{tr,12}) + n_{12}^{(2)}(t) \\ i_{22}^{(1)}(t) = \sqrt{2}R\sqrt{P_{s,22}P_{LO}}\exp(j\phi_2)\exp(j\phi_{tr,22}) + n_{22}^{(2)}(t) \\ i_{22}^{(2)}(t) = \sqrt{2}R\sqrt{P_{s,22}P_{LO}}\exp(j\phi_1)\exp(j\phi_{tr,22}) + n_{22}^{(2)}(t) \end{cases} \tag{8.58}$$

where $P_{s,nl}$ denotes the power of the lth received signal transmitted from the nth laser source, $\phi_{tr,nl}$ is the total phase noise within the OWC link from the nth transmitter to the lth receiver, $n_{nl}^{(1)}(t)$ and $n_{nl}^{(2)}(t)$ denote complex AWGN processes having the same variance σ_n^2. Then the photocurrent containing only $s_1 = \exp(j\phi_1)$ can be constructed by combining the received photocurrent as

$$\begin{aligned} \tilde{i}_1(t) = \sqrt{2}R &\underbrace{\left(\sum_{n=1}^{2}\sum_{l=1}^{L} P_{LO}P_{s,nl}\right)}_{S_M}\exp(j\phi_1) \\ &+ \underbrace{\sqrt{P_{s,11}P_{LO}}\exp(j\phi_{tc,11})[n_{11}^{(1)}(t) + n_{21}^{(1)}(t)] + \sqrt{P_{s,21}P_{LO}}\exp(j\phi_{tc,21})[n_{11}^{(2)}(t) + n_{21}^{(2)}(t)]}_{v_{11}(t)} \\ &+ \underbrace{\sqrt{P_{s,12}P_{LO}}\exp(j\phi_{tc,12})[n_{12}^{(1)}(t) + n_{22}^{(1)}(t)] + \sqrt{P_{s,22}P_{LO}}\exp(j\phi_{tc,22})[n_{12}^{(2)}(t) + n_{22}^{(2)}(t)]}_{v_{12}(t)}. \end{aligned} \tag{8.59}$$

Similarly, we can construct the photocurrent containing only $s_2 = \exp(\phi_2)$ as

$$\begin{aligned}\tilde{i}_2(t) = \sqrt{2}R\left(\sum_{n=1}^{2}\sum_{l=1}^{2} P_{LO}P_{s,nl}\right)\exp(j\phi_2) \\ + \underbrace{\sqrt{P_{s,21}P_{LO}}\exp(-j\phi_{tc,21})[n_{11}^{(2)}(t)+n_{21}^{(2)}(t)] - \sqrt{P_{s,11}P_{LO}}\exp(j\phi_{tc,11})[n_{11}^{(1)}(t)+n_{21}^{(1)}(t)]}_{v_{21}(t)} \\ + \underbrace{\sqrt{P_{s,22}P_{LO}}\exp(-j\phi_{tc,22})[n_{12}^{(2)}(t)+n_{22}^{(2)}(t)] - \sqrt{P_{s,12}P_{LO}}\exp(j\phi_{tc,12})[n_{12}^{(1)}(t)+n_{22}^{(1)}(t)]}_{v_{22}(t)}.\end{aligned} \tag{8.60}$$

After demodulating through an electrical demodulator, we can find the sampled signals for transmitted data recovery as

$$\tilde{i}_1 = \sqrt{2}R\left(\sum_{n=1}^{2}\sum_{l=1}^{2} P_{LO}P_{s,nl}\right)\exp(j\phi_1) + \underbrace{\sum_{l=1}^{2} v_{1l}}_{w_{m,1}} \tag{8.61}$$

and

$$\tilde{i}_1 = \sqrt{2}R\left(\sum_{n=1}^{2}\sum_{l=1}^{2} P_{LO}P_{s,nl}\right)\exp(j\phi_1) + \underbrace{\sum_{l=1}^{2} v_{2l}}_{w_{m,2}} \tag{8.62}$$

where $w_{m,1}$ and $w_{m,2}$ denote two Gaussian RVs. Therefore, the instantaneous SNR at the input of the demodulator becomes

$$\gamma = \frac{\overline{\gamma}}{2}\underbrace{\sum_{n=1}^{2}\sum_{l=1}^{2} I_{s,nl}}_{Y_m} \tag{8.63}$$

which is identical to (8.57).

8.5 System Performance Studies of the 2× 2 Links

We can readily obtain the MGF of Y_m as

$$M_{Y_m}(s) = \sum_{m=0}^{4} \binom{4}{m} \sum_{p=0}^{\infty} b_p(4-m,m,\alpha,\beta)(-s)^{-p-4\beta-m(\alpha-\beta)}. \tag{8.64}$$

Replacing $M_Y(\cdot)$ by $M_{Y_m}(\cdot)$ in (8.29), we can find the SER for an Alamouti-coded OWC system with coherent detection as

$$P_{e,M} = \frac{1}{\pi} \sum_{m=0}^{4} \binom{4}{m} \sum_{p=0}^{\infty} b_p(4-m,m,\alpha,\beta)\,(\mu_M\overline{\gamma})^{-p-4\beta-m(\alpha-\beta)}\,\varphi\left(p+4\beta+m(\alpha-\beta),\frac{M-1}{M}\right). \tag{8.65}$$

From (8.65), we can obtain the closed-form asymptotic error rate for 2×2 MIMO MSPK OWC systems as

$$P_{e,M}^{asym} \approx \frac{[a_0(\alpha,\beta)]^4\varphi\left(4\min\{\alpha,\beta\},\frac{M-1}{M}\right)}{\pi}\,(\mu_M\overline{\gamma})^{-4\min\{\alpha,\beta\}}. \tag{8.66}$$

We note that the diversity order for 2×2 systems is $4\min\{\alpha,\beta\}$, which is twice the diversity order for 2×1 systems studied in Section 8.2.3 as expected.

In Fig. 8.8, we plot the BER curves for SISO, 2×1 and 2×2 coherent FSO systems employing BPSK signaling under a strong turbulence condition ($\alpha = 2.05, \beta = 1.11$). We note a substantial error performance enhancement when comparing the 2×2 link to the SISO link. Furthermore, a 22 dB average SNR improvement can be found at a BER of 10^{-10} when moving from the 2×1 systems to the 2×2 systems.

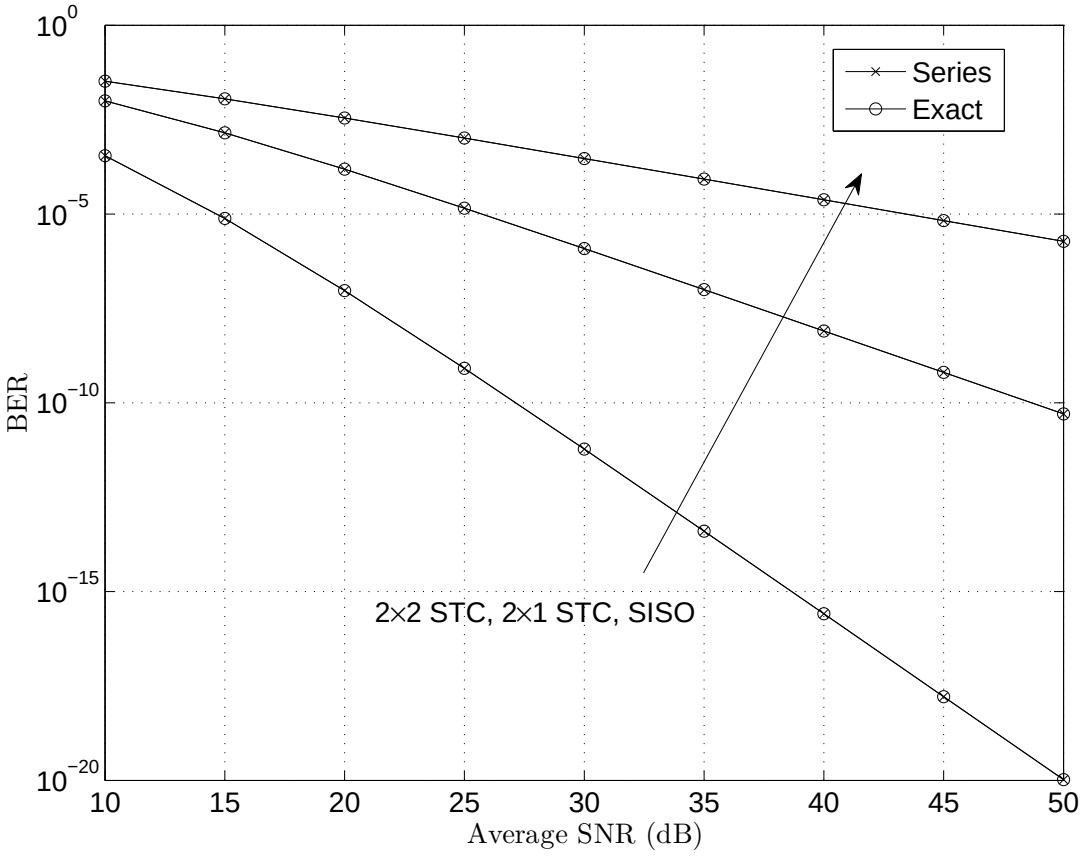

Figure 8.8: BERs of Alamouti-type STBC 2×2 and SISO OWC systems with BPSK modulation using coherent detection over the Gamma-Gamma turbulence channels with $J = 36$.

8.6 Comparison of Alamouti Coding and Repetition Coding

This section first compares the BER performance between the Alamouti STC coherent system and a repetition coded coherent system with single transmitter frequency. We then compare the BER performance between the Alamouti STC coherent system and the repetition coded coherent system with multiple transmitter frequencies described in Section 7.1.1.

Considering a 2×1 coherent BPSK link with single transmitter frequency, we can find the photocurrent at the output of the photodetector as

$$\begin{aligned} i(t) = {} & RP_{s,1} + RP_{s,2} + R\sqrt{P_{s,1}P_{s,2}}\exp(j\phi_{tc,1} - j\phi_{tc,2}) + R\sqrt{P_{s,1}P_{s,2}}\exp(-j\phi_{tc,1} + j\phi_{tc,2}) + RP_{LO} + \\ & 2R\sqrt{P_{s,1}P_{LO}}\cos(\omega_{IF}t + \phi + \underbrace{\phi_{tc,1} - \phi_{LO}}_{\phi_{rc,1}}) + 2R\sqrt{P_{s,2}P_{LO}}\cos(\omega_{IF}t + \phi + \underbrace{\phi_{tc,2} - \phi_{LO}}_{\phi_{rc,2}}) + n(t) \end{aligned} \tag{8.67}$$

where the phase ϕ denotes the encoded data bit.

After filtering out the DC components and down-converting, the baseband equivalent signal is

$$\tilde{i} = \sqrt{2}R\sqrt{AP_{LO}}\left[\sqrt{I_{s,1}}\exp(j\phi_{rc,1}) + \sqrt{I_{s,2}}\exp(j\phi_{rc,2})\right]\exp(j\phi) + \tilde{n} \tag{8.68}$$

where $\tilde{n}$ represents the filtered AWGN noise. Without loss of generality, we can assume the phase noise $\phi_{rc,1}$ is compensated and construct the real part signal as

$$\tilde{i}_r = \Re\{\tilde{i}\exp(-j\phi_{rc,1})\} = \sqrt{2}R\sqrt{AP_{LO}}\cos\phi\left[\sqrt{I_{s,1}} + \sqrt{I_{s,2}}\cos(\phi_{rc,2} - \phi_{rc,1})\right] + \tilde{n}_r \tag{8.69}$$

where we define $\Delta\phi = |\phi_{rc,2} - \phi_{rc,1}| \in [0, \pi]$ as the absolute difference in phase noises between the first and second transmission branches, and $\tilde{n}_r = \Re\{\tilde{n}\exp(-\phi_{rc,1})\}$ is a Gaussian RV. Note that no matter how perfect the phase compensation is performed, the term $\Delta\phi$ will be present in the

reconstructed signal. In this case, we can derive the SNR at the input of a demodulator as

$$\gamma_{rc}^{s} = \overline{\gamma}\left[\sqrt{I_{s,1}} + \sqrt{I_{s,2}}\cos(\Delta\phi)\right]^2. \tag{8.70}$$

The receiver SNRs of the repetition coded system with multiple transmitter frequencies and the Alamouti coded system can be shown to be

$$\gamma_{rc}^{m} = \frac{\overline{\gamma}}{2}\left(\sqrt{I_{s,1}} + \sqrt{I_{s,2}}\right)^2 \tag{8.71}$$

and

$$\gamma_{ac} = \frac{\overline{\gamma}}{2}(I_{s,1} + I_{s,2}) \tag{8.72}$$

respectively. We can obtain the BER expression for Alamouti coded systems as

$$P_{e,ac} = \frac{1}{\pi}\sum_{m=0}^{2}\binom{2}{m}\sum_{p=0}^{\infty} b_p(2-m,m,\alpha,\beta)\varphi\left(p+2\beta+m(\alpha-\beta),\frac{1}{2}\right)\left(\frac{\overline{\gamma}}{4}\right)^{-p-2\beta-m(\alpha-\beta)} \tag{8.73}$$

and obtain the BER expressions for repetition coded systems as

$$P_{e,rc}^{s} = \frac{1}{4\pi}\int_{-\infty}^{\infty}\Re\left\{F(\omega)\Phi_z^*\left(\frac{g_{rc}\omega}{\sqrt{2}}\right)\Phi_{z_d}^*\left(\frac{g_{rc}\omega}{\sqrt{2}}\right)\right\}d\omega \tag{8.74}$$

and

$$\begin{aligned} P_{e,rc}^{m} =& \frac{1}{\pi}\sum_{m=0}^{2}\binom{2}{m}\sum_{p=0}^{\infty}\frac{\lambda_p^{[2-m]}(\alpha,\beta,2) * \lambda_p^{[m]}(\beta,\alpha,2)}{\Gamma(2(p+2\beta+m(\alpha-\beta)))}\Gamma(p+2\beta+m(\alpha-\beta)) \\ &\times B\left(\frac{1}{2},p+2\beta+m(\alpha-\beta)+\frac{1}{2}\right)\left(\frac{\overline{\gamma}}{4}\right)^{-p-2\beta-m(\alpha-\beta)}. \end{aligned} \tag{8.75}$$

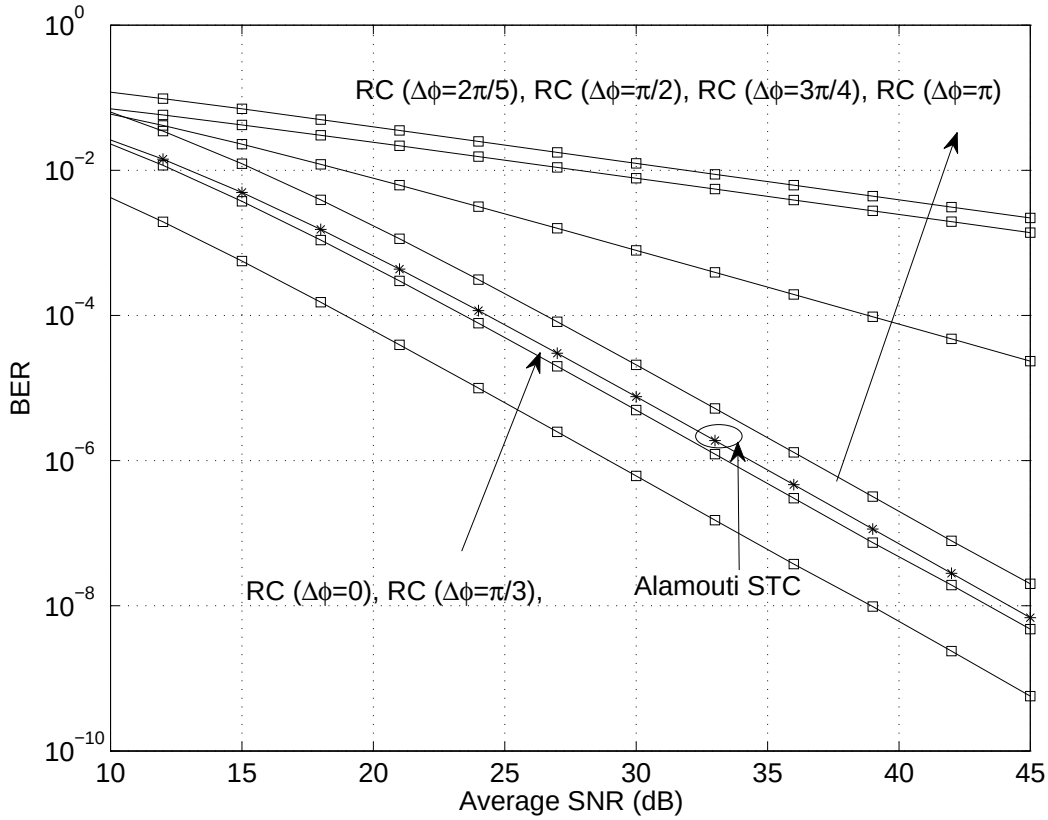

Figure 8.9: BER comparison of Alamouti coded and repetition coded systems using single transmitter frequency with BPSK modulation over the Gamma-Gamma turbulence channels with $\alpha = 2.33, \beta = 1.03$.

In (8.74), we have $\Phi_z(\cdot)$ derived in (5.18)-(5.20), $\Phi_{z_d}(x) = \Phi_z(\cos(\Delta\phi)x)/|\cos\Delta\phi|$, $\digamma(\cdot)$ is the Fourier transform of the complementary error function given in (5.26), and $g_{rc} \triangleq \sqrt{RA/(2q\Delta f)}$.

Figure 8.9 compares the BER performance of Alamouti coded and repetition coded 2×1 systems in strong turbulence ($\alpha = 2.33, \beta = 1.03$) for single transmitter frequency. It is shown that the Alamouti coded system can outperform the repetition coded system when $\Delta\phi$ is large (e.g., $2\pi/5 \lesssim \Delta\phi \leq \pi$). For example, when $\Delta\phi = 2\pi/5$, the Alamouti coded system outperforms the repetition coded system, while both systems achieve the same diversity order of $2\min\{\alpha, \beta\}$. As $\Delta\phi$ increases to $\pi/2$ and beyond, the repetition coded system suffers severe error rate performance degradation due to losses in diversity order, and performs inferior to the Alamouti coded system.

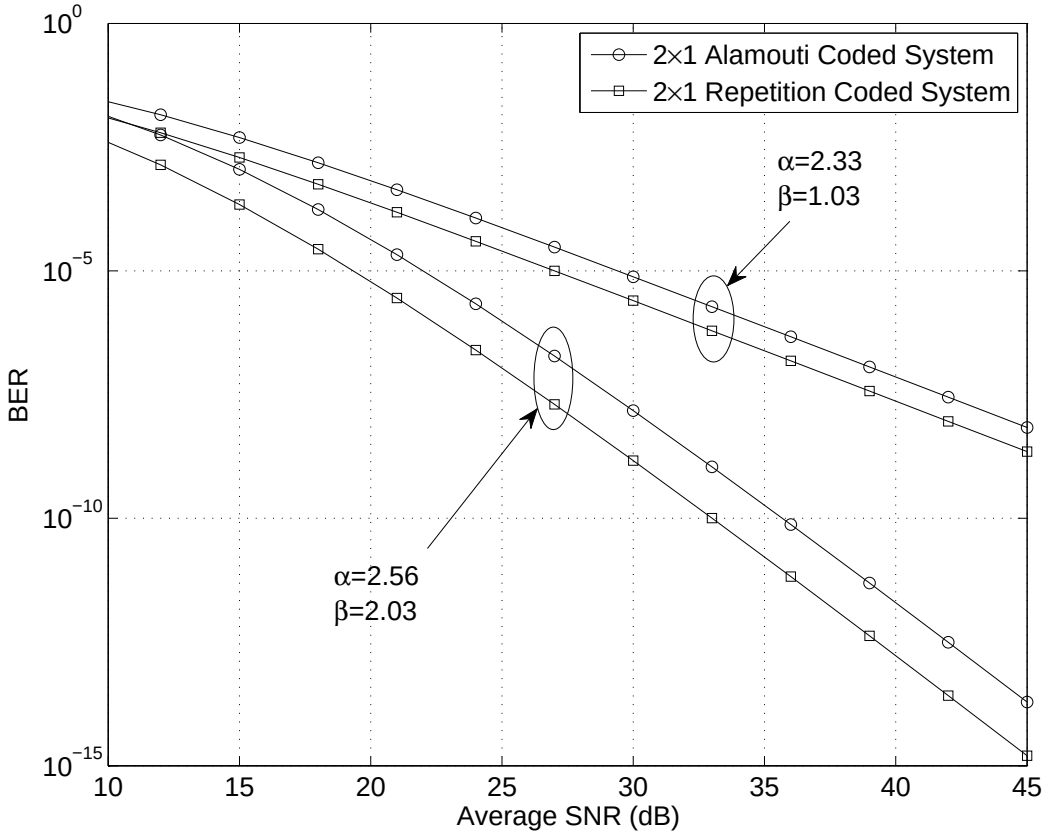

Figure 8.10: BER comparison of Alamouti coded and repetition coded systems using multiple distinct transmitter frequencies with BPSK modulation over the Gamma-Gamma turbulence channels.

This observation is in contrast to direct detection based systems where it has been previously discovered in [79] that the repetition coded systems *always* outperform orthogonal STBC systems using IM/DD.

Figure 8.10 compares the BER performance of Alamouti coded and repetition coded 2×1 systems in strong ($\alpha = 2.04, \beta = 1.10$) and moderate ($\alpha = 2.56, \beta = 2.03$) turbulence conditions. It is shown that the repetition coded system with two distinct transmitter frequencies can outperform the Alamouti coded system though both systems achieve the same diversity order of $2\min\{\alpha, \beta\}$. For example, when the BER level is 10^{-10}, there is a 2.9 dB SNR penalty for the Alamouti coded system with respect to the repetition coded system when $\alpha = 2.56, \beta = 2.03$. This suggests that the repetition code is a preferred choice when multiple distinct transmitter frequencies are used for a coherent OWC system.

8.7 Summary

In this chapter, transmit diversity has been explored for coherent OWC applications through the use of space-time codes. We have proposed two novel STBC systems for coherent optical wireless links over atmospheric turbulence channels. The error rate performance of OWC links employing these structures has been studied with PSK modulations. A truncation error analysis demonstrates that the derived error rate solutions allow a highly accurate and efficient estimation of the error rate performance for coherent STBC systems. Our study has demonstrated that the STC can be used to realize dual transmitter diversity and achieve full diversity order. The Alamouti-type coherent FSO system shows superior performance over a repetition coded system when operating on a single carrier frequency.

Chapter 9

Conclusions

In this chapter, we summarize the contributions of this dissertation and propose some future work on topics related to coherent optical wireless communications.

9.1 Summary of Contributions

In this thesis, we addressed several challenges that researchers and engineers face in performance evaluation and system designing of OWC systems utilizing coherent detection. Due to the random statistics of the coherent OWC links, we proposed several effective techniques and architectures for improving the link performance by mitigating the turbulence-induced fading and phase noise impacts. Analytical analyses and numerical studies have verified the performance enhancements from our proposed systems. We demonstrated the superior performance of coherent OWC links over SIM OWC links in weak-to-strong turbulence. We also contributed to the realization of space-time coding to the coherent OWC links. The specific contributions of this thesis are summarized as follows.

In Chapter 3, we derived closed-form MGF expressions of the K-distributed turbulence and carried out an exact BER analysis. We derived the diversity order and coding gain of coherent OWC links through the K-distributed turbulence channels. The diversity order was found to be unity. Our numerical results suggested that a powerful turbulence (fading) mitigation technique must be applied to achieve reliable optical communication links under strong turbulence conditions.

In Chapter 4, we used spatial diversity techniques to mitigate strong turbulence impacts. Coherent OWC systems employing MRC, EGC and SC were investigated. Our error rate performance

study showed that a three-branch MRC diversity link can improve the coherent system performance by five orders of magnitude compared to a SISO link. The three-branch EGC receiver was shown to have a comparable performance to that of the more complicated MRC receiver, with a BER of 10^{-8} at a 30 dB SNR. We also found that the diversity order for MRC, EGC and SC are the same, and are equal to the sum of the diversity order offered by each individual branch.

In Chapter 5, we studied the error rate performance for coherent EGC systems with imperfect phase noise compensation. Our investigation revealed that the performance impairment caused by imperfect phase noise compensation can be kept especially small, being less than 0.5 dB SNR for the same BER, when the standard deviation of the phase noise compensation error is below twenty degrees. Furthermore, we proposed DPSK with postdetection EGC, which does not require CSI, as an alternative to BPSK with EGC. Our numerical results demonstrated that the postdetection EGC scheme can be an effective diversity technique when the phase noise compensation error for the EGC scheme is large.

In Chapter 6, we presented a detailed comparison of two error-floor-free OWC systems: coherent detection and SIM based BPSK systems. We investigated the BER performance of these two types of OWC links over the Gamma-Gamma turbulence channels. The asymptotic analyses were also performed for coherent and SIM OWC links employing MRC, EGC and SC. A performance comparison in terms of the error rates versus average transmitted optical power is presented for variety of turbulence conditions. Our numerical results confirmed that the BER of coherent OWC system is superior to that of SIM systems (e.g., a BER improvement of six orders of magnitude under strong turbulence conditions). In addition, we found that the sensitivity improvement in moving from a SIM to coherent receiver is 24 dB in the absence of turbulence. The benefit of using coherent system becomes even larger in the presence of turbulence, with an approximately 30 dB sensitivity improvement found for a coherent system compared to a SIM system.

In Chapter 7, we introduced a coherent optical MIMO architecture that can be used to further enhance the coherent system performance by combating the atmospheric turbulence effects. To

validate the proposed architecture, we carried out BER studies for both MRC and EGC schemes for systems employing the proposed architecture. Our numerical example demonstrated that a BER of 10^{-9} can be achieved at an average SNR of 15 dB through the use of a 2×2 MIMO architecture in coherent OWC applications under weak turbulence conditions. The simple SISO architecture can only provide an approximate BER of 10^{-3} at the same SNR.

In Chapter 8, we proposed two new coherent OWC STC systems for operation in atmospheric turbulence channels. In designing such systems, we considered transmitter phase noise, turbulence-induced fading, turbulence-induced phase noise, and receiver LO phase noise. The proposed STC systems were particularly useful in exploiting the transmit diversity. The SER performance of the proposed systems employing MPSK was analyzed using a series expansion approach for the Gamma-Gamma turbulence. We also carried out a convergence performance analysis for the obtained series solutions. Based on the analysis, we demonstrated the efficiency and accuracy of our series solutions. The performance analyses showed that the proposed STC OWC systems can effectively improve the coherent optical link performance. The numerical results for an 8PSK 2×1 coherent link showed two to three orders of magnitude SER improvements over weak-to-strong turbulence channels. In addition, through comparisons of Alamouti and repetition coded coherent systems, we studied the error rate performance for these two kinds of transmit diversity systems using single or multiple carrier frequencies. The Alamouti STC system was shown to be a viable choice for coherent systems using single carrier frequency.

9.2 Suggested Future Research

OWC systems deployed in dense urban areas may be subject to pointing errors due to building sway. Therefore, the pointing accuracy becomes increasingly important as the propagation distance increases. It has been shown that the diversity order of FSO systems can be independent of pointing errors [46]. However, large SNR values may be required to achieve reliable link performance in

these cases. This will make the OWC systems less power efficient. One could therefore study the pointing accuracy impacts on coherent MIMO OWC links and relate the system performance with practical system designing parameters such as beam waist and propagation distance. The recently proposed building sway model, namely Hoyt distribution [111], can be considered in the study because the Hoyt model takes the jitter in both vertical and horizontal directions into account. Such results can be useful for the engineering community in designing beam control devices/terminals.

For practical reasons, real-time estimation of the instantaneous SNR may be difficult or impractical. Therefore, a simplified selection based combining scheme can be employed for practical OWC systems. Traditional selection diversity systems must choose the branch with the largest instantaneous SNR. To reduce the complexity, one can therefore introduce the signal-plus-noise (S+N) selection scheme to OWC links. The S+N scheme simply selects the branch having the largest photocurrent. Such a scheme is equivalent to traditional SC if the noise power is equal for all the branches because the branch with the largest SNR will have the largest S+N value. Coherent detection with S+N selection diversity can be explored in future research. A theoretical error rate analysis as well as asymptotic analysis for S+N systems would be worthwhile to investigate.

The use of optical coherent detection provides additional mechanisms to improve the optical channel capacity. These improvements can be made by implementing polarized modulation (i.e., polarized phase-shift keying) and polarized transmission (i.e., polarization multiplexing). Future work can explore this idea for coherent OWC systems. There are certain challenges that must be addressed for these polarization-based systems. In particular, the time-varying nature of turbulence channels may lead to an imperfectly maintained state of polarization. This issue needs to be investigated for practical polarization-based coherent OWC systems.

Bibliography

[1] H. Willebrand and B. Ghuman, *Free Space Optics: Enabling Optical Connectivity in Today's Networks*. Indianapolis: Sams Publishing, 2002.

[2] R. Ramaswami, "Optical fiber communication: from transmission to networking," *IEEE Communications Magazine*, vol. 40, no. 5, pp. 138–147, May 2002.

[3] D. Kedar and S. Arnon, "Urban optical wireless communication networks: the main challenges and possible solutions," *IEEE Communications Magazine*, vol. 42, no. 5, pp. S2–S7, May 2004.

[4] A. G. Bell, "Upon the production and reproduction of sound by light," *Journal of the Society of Telegraph Engineers*, vol. 9, no. 34, pp. 404–426, 1880.

[5] D. Killinger, "Free space optics for laser communication through the air," *Optics and Photonics News*, vol. 13, no. 10, pp. 36–42, Oct. 2002.

[6] F. Goodwin, "A review of operational laser communication systems," *Proceedings of the IEEE*, vol. 58, no. 10, pp. 1746–1752, Oct. 1970.

[7] V. W. S. Chan, "Space coherent optical communication systems – an introduction," *IEEE/OSA Journal of Lightwave Technology*, vol. 5, no. 4, pp. 633–637, Apr. 1987.

[8] K. Kiasaleh, "Performance of APD-based, PPM free-space optical communication systems in atmospheric turbulence," *IEEE Transactions on Communications*, vol. 53, no. 9, pp. 1455–1461, Sept. 2005.

[9] L. Hanzo, H. Haas, S. Imre, D. O'Brien, M. Rupp, and L. Gyongyosi, "Wireless myths, realities, and futures: From 3G/4G to optical and quantum wireless," *Proceedings of the IEEE*, vol. 100, no. 10, pp. 1853–1888, May 2012.

[10] Q. Liu, C. Qiao, G. Mitchell, and S. Stanton, "Optical wireless communication networks for first- and last-mile broadband access," *Journal of Optical Networking*, vol. 4, no. 12, pp. 807–828, Dec. 2005.

[11] B. He and R. Schober, "Bit-interleaved coded modulation for hybrid RF/FSO systems," *IEEE Transactions on Communications*, vol. 57, no. 12, pp. 3753–3763, Dec. 2009.

[12] O. Awwad, A. Al-Fuqaha, B. Khan, and G. Brahim, "Topology control schema for better QoS in hybrid RF/FSO mesh networks," *IEEE Transactions on Communications*, vol. 60, no. 5, pp. 1398–1406, May 2012.

[13] S. A. Clough, F. X. Kneizys, E. P. Shettle, and G. P. Anderson, "Atmospheric radiance and transmittance - FASCOD2," in *Proceedings of the 6th Conference on Atmospheric Radiation*. American Meteorological Society, May 1986, pp. 141–144.

[14] G. P. Anderson, *et al.*, "MODTRAN4: radiative transfer modeling for remote sensing," in *Proceedings of SPIE*, 2000, vol. 4049, pp. 176–183.

[15] E. Ip, A. P. T. Lau, D. J. F. Barros, and J. M. Kahn, "Coherent detection in optical fiber systems," *Optics Express*, vol. 16, no. 2, pp. 753–791, Jan. 2008.

[16] G. Li, "Recent advances in coherent optical communication," *Advances in Optics and Photonics*, vol. 1, no. 2, pp. 279–307, Apr. 2009.

[17] S. Karp, R. Gagliadi, S. E. Moran, and L. B. Scotts, *Optical Channels*. Plenum Press, 1988.

[18] J. Barry and E. Lee, "Performance of coherent optical receivers," *Proceedings of the IEEE*, vol. 78, no. 8, pp. 1369–1394, Aug. 1990.

[19] M. Z. Win, C.-C. Chen, and R. A. Scholtz, "Optical phase-locked loop for an amplitude modulated communications link using solid-state lasers," *IEEE Journal on Selected Areas in Communications*, vol. 13, no. 3, pp. 569–576, Apr. 1995.

[20] L. Andrews, R. Phillips, and C. Hopen, *Laser Beam Scintillation with Applications*. SPIE Press, 2001.

[21] E. Kemp, B. Felton, and R. Alliss, "Estimating the refractive index structure-function and related optical seeing parameters with the WRFARW," in *Proceedings of National Center for Atmospheric Research WRF User Workshop*, 2008, pp. P9.30 (1–3).

[22] J. Paul B. MacCready, "The inertial subrange of atmospheric turbulence," *J. Geophys. Res.*, vol. 67, no. 3, pp. 1051–1059, Mar. 1962.

[23] J. Goodman, *Statistical Optics*. Wiley, 1985.

[24] J. C. Ricklin, S. M. Hammel, F. D. Eaton, and S. L. Lachinova, "Atmospheric channel effects on free-space laser communication," *Journal of Optical and Fiber Communications Research*, vol. 3, no. 2, pp. 111–158, Apr. 2006.

[25] L. C. Andrews, R. L. Phillips, C. Y. Hopen, and M. A. Al-Habash, "Theory of optical scintillation," *Journal of the Optical Society of America A*, vol. 16, no. 6, pp. 1417–1429, June 1999.

[26] D. O'Brien and M. Katz, "Optical wireless communications within fourth-generation wireless systems," *Journal of Optical Networking*, vol. 4, no. 6, pp. 312–322, June 2005.

[27] V. W. S. Chan, "Free-space optical communications," *IEEE/OSA Journal of Lightwave Technology*, vol. 24, no. 12, pp. 4750–4762, Dec. 2006.

[28] WCAI, *Wireless Communications Association International*, [Online]. Available: http://www.wcai.com/.

[29] M. Loeschnigg, T. Plank, and E. Leitgeb, "Five years analysis of a free space optics link in Graz," in *Proceedings of the 6th European Conference on Antennas and Propagation*, Mar. 2012, pp. 1248–1251.

[30] E. J. Lee and V. W. S. Chan, "Part 1: Optical communication over the clear turbulent atmospheric channel using diversity," *IEEE Journal on Selected Areas in Communications*, vol. 22, no. 9, pp. 1896–1906, Nov. 2004.

[31] X. Zhu, J. M. Kahn, and J. Wang, "Mitigation of turbulence-induced scintillation noise in free-space optical links using temporal-domain detection techniques," *IEEE Photonics Technology Letters*, vol. 15, no. 4, pp. 623–625, Apr. 2003.

[32] E. Jakeman and P. N. Pusey, "Significance of K distributions in scattering experiments," *Physical Review Letters*, vol. 40, no. 9, pp. 546–550, Feb. 1978.

[33] R. L. Phillips and L. C. Andrews, "Universal statistical model for irradiance fluctuations in a turbulent medium," *Journal of the Optical Society of America*, vol. 72, no. 7, pp. 864–870, July 1982.

[34] G. Osche, *Optical Detection Theory for Laser Applications*. Wiley-Interscience, 2002.

[35] A. García-Zambrana, "Error rate performance for STBC in free-space optical communications through strong atmospheric turbulence," *IEEE Communications Letters*, vol. 11, no. 5, pp. 390–392, May 2007.

[36] M. A. Al-Habash, L. C. Andrews, and R. L. Phillips, "Mathematical model for the irradiance probability density function of a laser beam propagating through turbulent media," *Optical Engineering*, vol. 40, no. 8, pp. 1554–1562, Aug. 2001.

[37] J. H. Churnside and S. F. Clifford, "Log-normal Rician probability-density function of optical scintillations in the turbulent atmosphere," *Journal of the Optical Society of America A*, vol. 4, no. 10, pp. 1923–1930, Oct. 1987.

[38] J. H. Churnside and R. G. Frehlich, "Experimental evaluation of log-normally modulated Rician and *IK* models of optical scintillation in the atmosphere," *Journal of the Optical Society of America A*, vol. 6, no. 11, pp. 1760–1766, Nov. 1989.

[39] L. Andrews and R. Phillips, *Laser Beam Propagation Through Random Media*. SPIE Press, 2005.

[40] L. C. Andrews and R. L. Phillips, "I-K distribution as a universal propagation model of laser beams in atmospheric turbulence," *Journal of the Optical Society of America A*, vol. 2, no. 2, pp. 160–163, Feb. 1985.

[41] X. Zhu and J. M. Kahn, "Performance bounds for coded free-space optical communications through atmospheric turbulence channels," *IEEE Transactions on Communications*, vol. 51, no. 8, pp. 1233–1239, Aug. 2003.

[42] M. Uysal, S. M. Navidpour, and J. Li, "Error rate performance of coded free-space optical links over strong turbulence channels," *IEEE Communications Letters*, vol. 8, no. 10, pp. 635–637, Oct. 2004.

[43] M. Riediger, R. Schober, and L. Lampe, "Multiple-symbol detection for shot-noise limited free-space optical communications," in *Proceedings of IEEE Canadian Conference on Electrical and Computer Engineering*, Apr. 2007, pp. 908–911.

[44] S. Arnon, "Effects of atmospheric turbulence and building sway on optical wireless-communication systems," *Optics Letters*, vol. 28, no. 2, pp. 129–131, Jan. 2003.

[45] H. G. Sandalidis, T. A. Tsiftsis, and G. K. Karagiannidis, "Optical wireless communications with heterodyne detection over turbulence channels with pointing errors," *IEEE/OSA Journal of Lightwave Technology*, vol. 27, no. 20, pp. 4440–4445, Oct. 2009.

[46] A. García-Zambrana, B. Castillo-Vázquez, and C. Castillo-Vázquez, "Asymptotic error-rate analysis of FSO links using transmit laser selection over gamma-gamma atmospheric

turbulence channels with pointing errors," *Optics Express*, vol. 20, no. 3, pp. 2096–2109, Jan. 2012.

[47] M. Ibrahim and A. Ibrahim, "Performance analysis of optical receivers with space diversity reception," *IEE Proceedings-Communications*, vol. 143, no. 6, pp. 369–372, Dec. 1996.

[48] S. M. Navidpour, M. Uysal, and M. Kavehrad, "BER performance of free-space optical transmission with spatial diversity," *IEEE Transactions on Wireless Communications*, vol. 6, no. 8, pp. 2813–2819, Aug. 2007.

[49] S. G. Wilson, M. Brandt-Pearce, Q. Cao, and M. Baedke, "Optical repetition MIMO transmission with multipulse PPM," *IEEE Journal on Selected Areas in Communications*, vol. 23, no. 9, pp. 1901–1910, Sept. 2005.

[50] S. G. Wilson, M. Brandt-Pearce, Q. Cao, and J. H. Leveque, "Free-space optical MIMO transmission with q-ary PPM," *IEEE Transactions on Communications*, vol. 53, no. 8, pp. 1402–1412, Aug. 2005.

[51] T. Tsiftsis, H. Sandalidis, G. Karagiannidis, and M. Uysal, "Optical wireless links with spatial diversity over strong atmospheric turbulence channels," *IEEE Transactions on Wireless Communications*, vol. 8, no. 2, pp. 951–957, Feb. 2009.

[52] E. Bayaki, R. Schober, and R. Mallik, "Performance analysis of MIMO free-space optical systems in gamma-gamma fading," *IEEE Transactions on Communications*, vol. 57, no. 11, pp. 3415–3424, Nov. 2009.

[53] J. Li, J. Liu, and D. Taylor, "Optical communication using subcarrier PSK intensity modulation through atmospheric turbulence channels," *IEEE Transactions on Communications*, vol. 55, no. 8, pp. 1598–1606, Aug. 2007.

[54] W. Huang, J. Takayanagi, T. Sakanaka, and M. Nakagawa, "Atmospheric optical communication system using subcarrier PSK modulation," *IEICE Transactions on Communications*, vol. E76-B, no. 9, pp. 1169–1177, Sept. 1993.

[55] N. Letzepis and A. G. i Fabregas, "Outage analysis in MIMO free-space optical channels with pulse-position modulation," Tech. Rep. CUED/F-INFENG/TR 597, Department of Engineering, University of Cambridge., Feb. 2008.

[56] W. Popoola, Z. Ghassemlooy, J. Allen, E. Leitgeb, and S. Gao, "Free-space optical communication employing subcarrier modulation and spatial diversity in atmospheric turbulence channel," *IET Optoelectronics*, vol. 2, no. 1, pp. 16–23, Feb. 2008.

[57] W. Popoola and Z. Ghassemlooy, "BPSK subcarrier intensity modulated free-space optical communications in atmospheric turbulence," *IEEE/OSA Journal of Lightwave Technology*, vol. 27, no. 8, pp. 967–973, Apr. 2009.

[58] H. Samimi and P. Azmi, "Subcarrier intensity modulated free-space optical communications in K-distributed turbulence channels," *IEEE/OSA Journal of Optical Communications and Networking*, vol. 2, no. 8, pp. 625–632, Aug. 2010.

[59] N. Chatzidiamantis, A. Lioumpas, G. Karagiannidis, and S. Arnon, "Adaptive subcarrier PSK intensity modulation in free space optical systems," *IEEE Transactions on Communications*, vol. 59, no. 5, pp. 1368–1377, May 2011.

[60] X. Song, M. Niu, and J. Cheng, "Error rate of subcarrier intensity modulations for wireless optical communications," *IEEE Communications Letters*, vol. 16, no. 4, pp. 540–543, Apr. 2012.

[61] D. Fried, "Optical heterodyne detection of an atmospherically distorted signal wave front," *Proceedings of the IEEE*, vol. 55, no. 1, pp. 57–77, Jan. 1967.

[62] E. Lee and V. W. S. Chan, "Diversity coherent and incoherent receivers for free-space optical communication in the presence and absence of interference," *IEEE/OSA Journal of Optical Communications and Networking*, vol. 1, no. 5, pp. 463–483, Oct. 2009.

[63] K. Kiasaleh, "Performance of coherent DPSK free-space optical communication systems in K-distributed turbulence," *IEEE Transactions on Communications*, vol. 54, no. 4, pp. 604–607, Apr. 2006.

[64] T. Tsiftsis, "Performance of heterodyne wireless optical communication systems over gamma-gamma atmospheric turbulence channels," *Electronics Letters*, vol. 44, no. 5, pp. 372–373, Feb. 2008.

[65] A. Belmonte and J. M. Kahn, "Performance of synchronous optical receivers using atmospheric compensation techniques," *Optics Express*, vol. 16, no. 18, pp. 14151–14162, Sept. 2008.

[66] A. Belmonte and J. M. Kahn, "Capacity of coherent free-space optical links using atmospheric compensation techniques," *Optics Express*, vol. 17, no. 4, pp. 2763–2773, Feb. 2009.

[67] A. Belmonte and J. M. Kahn, "Capacity of coherent free-space optical links using diversity-combining techniques," *Optics Express*, vol. 17, no. 15, pp. 12601–12611, July 2009.

[68] M. Niu, J. Cheng, and J. F. Holzman, "Error rate analysis of M-ary coherent free-space optical communication systems with K-distributed turbulence," *IEEE Transactions on Communications*, vol. 59, no. 3, pp. 664–668, Mar. 2011.

[69] M. Niu, J. Cheng, and J. F. Holzman, "Exact error rate analysis of equal gain and selection diversity for coherent free-space optical systems on strong turbulence channels," *Optics Express*, vol. 18, no. 13, pp. 13915–13926, June 2010.

[70] A. Belmonte and J. Kahn, "Field conjugation adaptive arrays in free-space coherent laser communications," *IEEE/OSA Journal of Optical Communications and Networking*, vol. 3, no. 11, pp. 830–838, Nov. 2011.

[71] S. M. Aghajanzadeh and M. Uysal, "Diversity-multiplexing trade-off in coherent free-space optical systems with multiple receivers," *IEEE/OSA Journal of Optical Communications and Networking*, vol. 2, no. 12, pp. 1087–1094, Dec. 2010.

[72] J. Basak and B. Jalali, "Adaptive electronic linearization of a coherent heterodyne optical receiver," in *Proceedings of IEEE MTT-S International Microwave Symposium*, june 2006, pp. 18 –21.

[73] R. Lange, B. Smutny, B. Wandernoth, R. Czichy, and D. Giggenbach, "142 km, 5.625 Gbps free-space optical link based on homodyne BPSK modulation," in *Proceedings of SPIE*, 2006, vol. 6105, pp. 61050A(1–9).

[74] N. Cvijetic, D. Qian, J. Yu, Y.-K. Huang, and T. Wang, "Polarization-multiplexed optical wireless transmission with coherent detection," *IEEE/OSA Journal of Lightwave Technology*, vol. 28, no. 8, pp. 1218–1227, Apr. 2010.

[75] S. Alamouti, "A simple transmit diversity technique for wireless communications," *IEEE Journal on Selected Areas in Communications*, vol. 16, no. 8, pp. 1451–1458, Oct. 1998.

[76] V. Tarokh, H. Jafarkhani, and A. Calderbank, "Space-time block codes from orthogonal designs," *IEEE Transactions on Information Theory*, vol. 45, no. 5, pp. 1456–1467, July 1999.

[77] M. Simon and V. Vilnrotter, "Alamouti-type space-time coding for free-space optical communication with direct detection," *IEEE Transactions on Wireless Communications*, vol. 4, no. 1, pp. 35–39, Jan. 2005.

[78] J. Park, E. Lee, and G. Yoon, "Average bit-error rate of the Alamouti scheme in Gamma-Gamma fading channels," *IEEE Photonics Technology Letters*, vol. 23, no. 4, pp. 269–271, Feb. 2011.

[79] M. Safari and M. Uysal, "Do we really need OSTBCs for free-space optical communication with direct detection?," *IEEE Transactions on Wireless Communications*, vol. 7, no. 11, pp. 4445–4448, Nov. 2008.

[80] S. M. Haas, J. H. Shapiro, and V. Tarokh, "Space-time codes for wireless optical communications," *EURASIP Jounal on Applied Signal Processing*, vol. 2002, no. 3, pp. 211–220, Mar. 2002.

[81] E. Bayaki and R. Schober, "Performance and design of coherent and differential space-time coded FSO systems," *IEEE/OSA Journal of Lightwave Technology*, vol. 30, no. 11, pp. 1569–1577, June 2012.

[82] G. Ntogari, T. Kamalakis, and T. Sphicopoulos, "Analysis of indoor multiple-input multiple-output coherent optical wireless systems," *IEEE/OSA Journal of Lightwave Technology*, vol. 30, no. 3, pp. 317–324, Feb. 2012.

[83] M. Niu, J. Cheng, and J. F. Holzman, "A MIMO architecture for coherent optical wireless communication: System design and performance analysis," *IEEE/OSA Journal of Optical Communications and Networking*, submitted, 2012.

[84] N. Cvijetic and T. Wang, "A MIMO architecture for IEEE 802.16d (WiMAX) heterogeneous wireless access using optical wireless technology," in *Proceedings of the 6th International Conference on Next Generation Teletraffic and Wired/Wireless Advanced Networking*, 2006, pp. 441–451.

[85] M. Niu, J. Cheng, and J. F. Holzman, "Optical MIMO transmission using a heterodyne

receiver in K-distributed turbulence channels," in *Proceedings of IEEE Photonics Society Summer Topical Meetings*, July 2012.

[86] L. Kazovsky, S. Benedetto, and A. Willner, *Optical Fiber Communication Systems*. Artech House, 1996.

[87] G. P. Agrawal, *Fiber-Optic Communication Systems*, 3 ed. Wiley-Interscience, 2002.

[88] G. Parry, "Measurement of atmospheric turbulence induced intensity fluctuations in a laser beam," *Optica Acta: International Journal of Optics*, vol. 28, no. 5, pp. 715–728, May 1981.

[89] R. L. Phillips and L. C. Andrews, "Measured statistics of laser-light scattering in atmospheric turbulence," *Journal of the Optical Society of America*, vol. 71, no. 12, pp. 1440–1445, Dec. 1981.

[90] E. Jakeman and P. N. Pusey, "A model for non-Rayleigh sea echo," *IEEE Transactions on Antennas and Propagation*, vol. 24, no. 6, pp. 806–814, Nov. 1976.

[91] A. Consortini, F. Cochetti, J. H. Churnside, and R. J. Hill, "Inner-scale effect on irradiance variance measured for weak-to-strong atmospheric scintillation," *Journal of the Optical Society of America A*, vol. 10, no. 11, pp. 2354–2362, Nov. 1993.

[92] Z. Wang and G. B. Giannakis, "A simple and general parameterization quantifying performance in fading channels," *IEEE Transactions on Communications*, vol. 51, no. 8, pp. 1389–1398, Aug. 2003.

[93] I. S. Gradshteyn and I. M. Ryzhik, *Table of Integrals, Series, and Products*, 6 ed. Academic Press, 2000.

[94] X. Zhu and J. M. Kahn, "Free-space optical communication through atmospheric turbulence

channels," *IEEE Transactions on Communications*, vol. 50, no. 8, pp. 1293–1300, Aug. 2002.

[95] G. Karagiannidis, T. Tsiftsis, and R. Mallik, "Bounds for multihop relayed communications in Nakagami-*m* fading," *IEEE Transactions on Communications*, vol. 54, no. 1, pp. 18–22, Jan. 2006.

[96] J. Proakis, *Digital Communications*, 4 ed. McGraw-Hill, 2001.

[97] J. Gil-Pelaez, "Note on the inversion theorem," *Biometrika*, vol. 38, no. 3/4, pp. 481–482, 1951.

[98] C. Zhu, J. Mietzner, and R. Schober, "On the performance of non-coherent transmission schemes with equal-gain combining in generalized K-fading," *IEEE Transactions on Wireless Communications*, vol. 9, no. 4, pp. 1337–1349, Apr. 2010.

[99] M. Niu, J. Schlenker, J. Cheng, J. F. Holzman, and R. Schober, "Coherent wireless optical communications with predetection and postdetection EGC over Gamma–Gamma atmospheric turbulence channels," *IEEE/OSA Journal of Optical Communications and Networking*, vol. 3, no. 11, pp. 860–869, Nov. 2011.

[100] M. Simon, S. Hinedi, and W. Lindsey, *Digital Communication Techniques: Signal Design and Detection*. PTR Prentice Hall, 1995.

[101] I. Kim, B. McArthur, and E. Korevaar, "Comparison of laser beam propagation at 785 nm and 1550 nm in fog and haze for optical wireless communications," in *Proceedings of SPIE*, 2001, vol. 4214, pp. 26–37.

[102] A. A. Farid and S. Hranilovic, "Outage capacity optimization for free-space optical links with pointing errors," *IEEE/OSA Journal of Lightwave Technology*, vol. 25, no. 7, pp. 1702–1710, July 2007.

[103] M. Khalighi, F. Xu, Y. Jaafar, and S. Bourennane, "Doublelaser differential signaling for reducing the effect of background radiation in free-space optical systems," *IEEE/OSA Journal of Optical Communications and Networking*, vol. 3, no. 2, pp. 145–154, Feb. 2011.

[104] J. M. Hunt, F. Holmes, and F. Amzajerdian, "Optimum local oscillator levels for coherent detection using photoconductors," *Applied Optics*, vol. 27, no. 8, pp. 3135–3141, Aug. 1988.

[105] S. Yamazaki, "A 2Gb/s optical CPFSK heterodyne detection transmission experiment using newly developed MQW-DFB laser diodes," in *Proceedings of Fourteenth European Conference on Optical Communication*, 1988, pp. 467–470.

[106] R. Shechter, Y. Amitai, and A. A. Friesem, "Compact wavelength division multiplexers and demultiplexers," *Applied Optics*, vol. 41, no. 7, pp. 1256–1261, Mar. 2002.

[107] D.-S. Ly-Gagnon, S. Tsukamoto, K. Katoh, and K. Kikuchi, "Coherent detection of optical quadrature phase-shift keying signals with carrier phase estimation," *IEEE/OSA Journal of Lightwave Technology*, vol. 24, no. 1, pp. 12–21, Jan. 2006.

[108] E. Ip and J. Kahn, "Feedforward carrier recovery for coherent optical communications," *IEEE/OSA Journal of Lightwave Technology*, vol. 25, no. 9, pp. 2675–2692, Sept. 2007.

[109] M. Kuschnerov, F. Hauske, K. Piyawanno, B. Spinnler, M. Alfiad, A. Napoli, and B. Lankl, "DSP for coherent single-carrier receivers," *IEEE/OSA Journal of Lightwave Technology*, vol. 27, no. 16, pp. 3614–3622, Aug. 2009.

[110] M. Niu, X. Song, J. Cheng, and J. F. Holzman, "Performance analysis of coherent wireless optical communications with atmospheric turbulence," *Optics Express*, vol. 20, no. 6, pp. 6515–6520, Mar. 2012.

[111] W. Gappmair, S. Hranilovic, and E. Leitgeb, "Performance of PPM on terrestrial FSO links with turbulence and pointing errors," *IEEE Communications Letters*, vol. 14, no. 5, pp. 468–470, May 2010.

[112] E. Jakeman and R. J. A. Tough, "Generalized K distribution: a statistical model for weak scattering," *Journal of the Optical Society of America A*, vol. 4, no. 9, pp. 1764–1772, Sept. 1987.

Appendix A

SNR Derivation of EGC Reception

At the output of the lth photodetector, the AC photocurrent is given as

$$i_{ac,l}(t) = 2R\sqrt{P_{s,l}P_{LO}}\cos(\omega_{IF}t + \phi + \phi_{s,l}). \tag{A.1}$$

Let $c_l = 2R\sqrt{P_{LO}P_{s,l}}$, and this AC photocurrent can be expressed as

$$i_{ac,l}(t) = c_l\left[\cos\phi\cos(\omega_{IF}t + \phi_{s,l}) - \sin\phi\sin(\omega_{IF}t + \phi_{s,l})\right]. \tag{A.2}$$

Then, two filters are used to implement the complex filtering in the down-converter process. The real and imaginary parts of the baseband signal are, respectively, obtained as

$$y_{c,l}(t) = \sqrt{2}\left\{c_l[\cos\phi\cos(\omega_{IF}t + \phi_{s,l}) - \sin\phi\sin(\omega_{IF}t + \phi_{s,l})]\right\}\cos(\omega_{IF}t) \tag{A.3}$$

and

$$y_{s,l}(t) = -\sqrt{2}\left\{c_l[\cos\phi\cos(\omega_{IF}t + \phi_{s,l}) - \sin\phi\sin(\omega_{IF}t + \phi_{s,l})]\right\}\sin(\omega_{IF}t). \tag{A.4}$$

After a lowpass filter, the inphase and quadrature components become

$$\tilde{y}_{c,l}(t) = \frac{c_l}{\sqrt{2}}\left[\cos\phi\cos\phi_{s,l} - \sin\phi\sin\phi_{s,l}\right] \tag{A.5}$$

and

$$\tilde{y}_{s,l}(t) = \frac{c_l}{\sqrt{2}}\left[\cos\phi\cos\phi_{s,l} + \sin\phi\sin\phi_{s,l}\right]. \tag{A.6}$$

Now we combine (A.5) and (A.6) to obtain the equivalent baseband signal as

$$\tilde{y}_l(t) = \tilde{y}_{c,l}(t) + j\tilde{y}_{s,l}(t) = \frac{c_l}{\sqrt{2}}[\cos\phi + j\sin\phi]e^{j\phi_{s,l}}. \tag{A.7}$$

The last step is to compensate the phase noise, giving the branch signal before combining as

$$\tilde{y}_l(t)e^{-j\phi_{s,l}} = \sqrt{2}R\sqrt{P_{LO}P_{s,l}}e^{j\phi}. \tag{A.8}$$

Consequently, with the assumption of equal noise variance in each diversity branch, the instantaneous SNR at the output of the equal gain combiner becomes

$$\gamma_{EGC} = \frac{\left(\sum_{l=1}^{L}\sqrt{2}R\sqrt{P_{LO}P_{s,l}}\right)^2}{\sum_{l=1}^{L}\sigma_{n,l}^2} = \frac{\left(\sum_{l=1}^{L}\sqrt{2}R\sqrt{P_{LO}P_{s,l}}\right)^2}{L(2qRP_{LO}\Delta f)} = \frac{R\left(\sum_{l=1}^{L}\sqrt{P_{s,l}}\right)^2}{Lq\Delta f} \tag{A.9}$$

where $\sigma_{n,l}^2 = 2qRP_{LO}\Delta f, l = 1, \cdots, L$, is the noise variance [86] in the lth diversity branch at the receiver side, and it is assumed to be the same for all diversity branches.

Appendix B

CHF of the Squareroot of K-Distributed RV

We denote the square root of K-distributed irradiance by z, i.e., $z \triangleq \sqrt{I_s}$, and the PDF of z is

$$f(z) = \frac{4}{\Gamma(\alpha)\eta^{\alpha+1}} \alpha^{\frac{\alpha+1}{2}} z^{\alpha} K_{\alpha-1}\left(\frac{2\sqrt{\alpha}}{\eta} z\right), \quad z > 0 \tag{B.1}$$

which is used to model displacement in two-dimensional unbiased random walk problems [112].

To obtain the CHF of z, we now consider the property of $I_s = I_x I_y$ [42], where I_x and I_y are two independent RVs having the exponential and Gamma PDFs, respectively, as

$$f(I_x) = \frac{1}{\eta^2} e^{-\frac{I_x}{\eta^2}}, \;\; I_x > 0 \tag{B.2}$$

and

$$f(I_y) = \frac{\alpha(\alpha I_y)^{\alpha-1} e^{-\alpha I_y}}{\Gamma(\alpha)}, \;\; I_y > 0. \tag{B.3}$$

We let $z = xy$ with $x \triangleq \sqrt{I_x}$ and $y \triangleq \sqrt{I_y}$, and x and y can be shown to be two independent RVs with Rayleigh and Nakagami (only if $\alpha \geqslant 1/2$) distributions. The PDFs are

$$f(x) = \frac{2}{\eta^2} x e^{-\frac{x^2}{\eta^2}}, \;\; x > 0 \tag{B.4}$$

and

$$f(y) = \frac{2\alpha^{\alpha} y^{2\alpha-1} e^{-\alpha y^2}}{\Gamma(\alpha)}, \;\; y > 0 \tag{B.5}$$

respectively. The CHF of z is defined as $\Phi_z(\omega) = \int_{-\infty}^{\infty} e^{j\omega z} f(z) dz = E[e^{j\omega z}]$ where $\omega \in \mathbf{R}$. Then,

with [93, eq.3.462(1)], the CHF of z conditioned on x can be obtained as

$$\Phi_{z|x}(\omega) = E_{z|x}[e^{j\omega z}] = \frac{2^{1-\alpha}\Gamma(2\alpha)}{\Gamma(\alpha)} \exp\left[\frac{-\omega^2 x^2}{8\alpha}\right] D_{-2\alpha}\left(\frac{-j\omega x}{\sqrt{2\alpha}}\right) \tag{B.6}$$

where $D_\rho(\cdot)$ is the parabolic cylinder function of the ρth order. The parabolic cylinder function in (B.6) can be expanded as [93, eq.9.240]

$$\begin{aligned} D_{-2\alpha}\left(\frac{-j\omega x}{\sqrt{2\alpha}}\right) &= 2^{-\alpha}\exp\left(\frac{\omega^2 x^2}{8\alpha}\right)\frac{\sqrt{\pi}}{\Gamma\left(\alpha+\frac{1}{2}\right)}{}_1F_1\left(\alpha,\frac{1}{2};-\frac{\omega^2 x^2}{4\alpha}\right) \\ &\quad + 2^{-\alpha}\exp\left(\frac{\omega^2 x^2}{8\alpha}\right)\frac{\sqrt{2\pi}}{\Gamma(\alpha)}\frac{j\omega x}{\sqrt{2\alpha}}{}_1F_1\left(\alpha+\frac{1}{2},\frac{3}{2};-\frac{\omega^2 x^2}{\alpha}\right). \end{aligned} \tag{B.7}$$

Substituting (B.7) into (B.6), we can rewrite (B.6) as

$$E_{z|x}[e^{j\omega z}] = {}_1F_1\left(\alpha,\frac{1}{2};-\frac{\omega^2 x^2}{4\alpha}\right) + j\frac{\Gamma\left(\alpha+\frac{1}{2}\right)}{\Gamma(\alpha)}\left(\frac{\omega x}{\sqrt{\alpha}}\right){}_1F_1\left(\alpha+\frac{1}{2},\frac{3}{2};-\frac{\omega^2 x^2}{\alpha}\right). \tag{B.8}$$

Averaging (B.8) over x gives the desired CHF. In the averaging operation, the real and imaginary parts of (B.8) are treated separately. Employing a change of variables and applying [93, eq.7.522(9)] to the real part, we obtain

$$\Re\{\Phi_z(\omega)\} = {}_2F_1\left(\alpha,1,\frac{1}{2};-\frac{\omega^2\eta^2}{4\alpha}\right). \tag{B.9}$$

Similarly, applying [93, eq.7.522(5)] to the imaginary part, we obtain

$$\Im\{\Phi_z(\omega)\} = \frac{\omega\Gamma\left(\alpha+\frac{1}{2}\right)\Gamma(3/2)}{\Gamma(\alpha)}\left(\frac{\eta^2}{\alpha}\right)^{\frac{1}{2}}{}_2F_1\left(\alpha+\frac{1}{2},\frac{3}{2},\frac{3}{2};-\frac{\omega^2\eta^2}{4\alpha}\right). \tag{B.10}$$

Thus, the CHF of z is obtained as

$$\Phi_z(\omega) \quad = \quad \Re\{\Phi_z(\omega)\} + j\Im\{\Phi_z(\omega)\}. \tag{B.11}$$

Appendix C

MGF of the Square of Summed Squareroots of Gamma-Gamma RVs

Based on the coherent EGC combiner SNR expression in (6.12), we derive the MGF of this summed RV $U = (\sum_{l=1}^{L} \sqrt{I_{s,l}})^2$. With the power series expansion of the modified Bessel function of the second kind, we obtain the PDF[19] of $\sqrt{I_s}$ to be

$$f_{\sqrt{I_s}}(x) = 2\sum_{p=0}^{\infty}\left[a_p(\alpha,\beta)x^{2(p+\beta)-1} + a_p(\beta,\alpha)x^{2(p+\alpha)-1}\right]. \tag{C.1}$$

This alternative closed-form PDF expression for the squareroot of Gamma-Gamma irradiance will facilitate the derivation for the MGF of the composite RV U.

Thus, using (C.1) we can obtain the MGF of $\sqrt{I_s}$ in terms of a series expansion as

$$M_{\sqrt{I_s}}(s) = 2\sum_{p=0}^{\infty}\left[a_p(\alpha,\beta)\Gamma(2p+2\beta)(-s)^{-2(p+\beta)} + a_p(\beta,\alpha)\Gamma(2p+2\alpha)(-s)^{-2(p+\alpha)}\right]. \tag{C.2}$$

Letting $Z = \sum_{l=1}^{L} \sqrt{I_{s,l}}$ and using the Binomial expansion, we have

$$\begin{aligned} M_Z(s) = 2^L \sum_{q=0}^{L} \binom{L}{q} &\left(\sum_{p=0}^{\infty} a_p(\alpha,\beta)\Gamma(2p+2\beta)(-s)^{-2(p+\beta)}\right)^{L-q} \\ &\times \left(\sum_{p=0}^{\infty} a_p(\beta,\alpha)\Gamma(2p+2\alpha)(-s)^{-2(p+\alpha)}\right)^{q}. \end{aligned} \tag{C.3}$$

[19] A closed-form of this PDF in terms of the modified Bessel function was obtained in [99, Eq. (17)].

By taking the inverse Laplace transform of (C.3), we derive the PDF of Z as

$$f_Z(z) = 2^L \sum_{q=0}^{L} \binom{L}{q} \sum_{p=0}^{\infty} \frac{b_p^{[L-q]}(\alpha,\beta) * b_p^{[q]}(\beta,\alpha)}{\Gamma(2p+2(L-q)\beta+2q\alpha)} Z^{2p+2(L-q)\beta+2q\alpha} \tag{C.4}$$

where $b_p(\alpha,\beta) \triangleq a_p(\alpha,\beta)\Gamma(2p+2\beta)$. Again, with $U = Z^2$, the PDF of U is found to be

$$f_U(u) = 2^{L-1} \sum_{q=0}^{L} \binom{L}{q} \sum_{p=0}^{\infty} \frac{b_p^{[L-q]}(\alpha,\beta) * b_p^{[q]}(\beta,\alpha)}{\Gamma(2(p+(L-q)\beta+q\alpha))} u^{p+(L-q)\beta+q\alpha-1}. \tag{C.5}$$

The MGF of U is finally obtained as

$$M_U(s) = 2^{L-1} \sum_{q=0}^{L} \binom{L}{q} \sum_{p=0}^{\infty} \frac{b_p^{[L-q]}(\alpha,\beta) * b_p^{[q]}(\beta,\alpha)\Gamma((p+(L-q)\beta+q\alpha))}{\Gamma(2(p+(L-q)\beta+q\alpha))} (-s)^{-[p+(L-q)\beta+q\alpha]}. \tag{C.6}$$

Appendix D

PDF of the RV $I_m = \max\{I_{s,l}, l = 1, \cdots, L\}$

We present the closed-form PDF of I_m in the following. The series expression of the Gamma-Gamma CDF[20] $F_{I_s}(I_s)$ is given by

$$F_{I_s}(I_s) = \sum_{p=0}^{\infty} \left[\frac{a_p(\alpha,\beta)}{p+\beta} I_s^{p+\beta} + \frac{a_p(\beta,\alpha)}{p+\alpha} I_s^{p+\alpha} \right]. \tag{D.1}$$

The coefficient $a_p(x,y)$ is defined in (6.20). A series expression in the symmetric form of channel parameters α and β for the PDF of I_m is desired. In order to obtain such a PDF expression, replacing the argument I_s in $F_{I_s}(I_s)$ with I_m, we express $[F_{I_s}(I_m)]^{L-1}$ as

$$\begin{aligned}
[F_{I_s}(I_m)]^{L-1} &= \sum_{k=0}^{L-1} \binom{L-1}{k} \left(\sum_{p=0}^{\infty} \frac{a_p(\alpha,\beta)}{p+\beta} I_m^{p+\beta} \right)^{L-1-k} \left(\sum_{p=0}^{\infty} \frac{a_p(\beta,\alpha)}{p+\alpha} I_m^{p+\alpha} \right)^{k} \\
&= \sum_{k=0}^{L-1} \binom{L-1}{k} \sum_{p=0}^{\infty} \left(\frac{a_p(\alpha,\beta)}{p+\beta} \right)^{[L-1-k]} * \left(\frac{a_p(\beta,\alpha)}{p+\alpha} \right)^{[k]} I_m^{p+(L-k-1)\beta+k\alpha}
\end{aligned} \tag{D.2}$$

and

$$\begin{aligned}
[F_{I_s}(I_m)]^{L-1} &= \sum_{k=0}^{L-1} \binom{L-1}{k} \left(\sum_{p=0}^{\infty} \frac{a_p(\beta,\alpha)}{p+\alpha} I_m^{p+\alpha} \right)^{L-1-k} \left(\sum_{p=0}^{\infty} \frac{a_p(\alpha,\beta)}{p+\beta} I_m^{p+\beta} \right)^{k} \\
&= \sum_{k=0}^{L-1} \binom{L-1}{k} \sum_{p=0}^{\infty} \left(\frac{a_p(\beta,\alpha)}{p+\alpha} \right)^{[L-1-k]} * \left(\frac{a_p(\alpha,\beta)}{p+\beta} \right)^{[k]} I_m^{p+(L-k-1)\alpha+k\beta}.
\end{aligned} \tag{D.3}$$

[20] The CDF of the Gamma-Gamma RV was also obtained in [36, Eq. (28)] in terms of a generalized hypergeometric function and in [64, Eq. (7)] in terms of the Meijer's G-function. After a correction of some typographical errors in [36, Eq. (28)], the correct CDF of the Gamma-Gamma RV is $\frac{\pi}{\sin[\pi(\alpha-\beta)]} \left[\frac{(\alpha\beta I/2)^{\beta}}{\beta\Gamma(\beta-\alpha+1)} \, {}_1F_2(\beta,\beta+1,\beta-\alpha+1;\alpha\beta I/2) - \frac{(\alpha\beta I/2)^{\alpha}}{\alpha\Gamma(\alpha-\beta+1)} \, {}_1F_2(\alpha,\alpha+1,\alpha-\beta+1;\alpha\beta I/2) \right]$ where ${}_1F_2(\cdot,\cdot,\cdot;\cdot)$ denotes a generalized hypergeometric function.

Thus, by making use of both (D.2) and (D.3), we obtain the series expression of $[F_{I_s}(I_m)]^L f_{I_s}(I_m)$ as

$$\begin{aligned}[F_{I_s}(I_m)]^{L-1} f_{I_s}(I_m) = &\sum_{k_1=0}^{L-1} \binom{L-1}{k_1} \left[\sum_{p=0}^{\infty} e_p(L-k_1-1, k_1, \alpha, \beta) I_m^{p+(L-k_1)\beta+k_1\alpha-1} \right] \\ &+ \sum_{k_2=0}^{L-1} \binom{L-1}{k_2} \left[\sum_{p=0}^{\infty} e_p(L-k_2-1, k_2, \beta, \alpha) I_m^{p+(L-k_2)\alpha+k_2\beta-1} \right]\end{aligned} \tag{D.4}$$

where

$$e_p(m,n,x,y) = \left(\frac{a_p(x,y)}{p+y} \right)^{[m]} * \left(\frac{a_p(y,x)}{p+x} \right)^{[n]} * a_p(x,y). \tag{D.5}$$

We drop subscripts for k_1 and k_2 and simplify the closed-form solution for $[F_{I_s}(I_m)]^{L-1} f_{I_s}(I_m)$ as

$$\begin{aligned}[F_{I_s}(I_m)]^{L-1} f_{I_s}(I_m) = &\sum_{k=0}^{L-1} \binom{L-1}{k} \left[\sum_{p=0}^{\infty} e_p(L-k-1, k, \alpha, \beta) I_m^{p+(L-k)\beta+k\alpha-1} \right. \\ &\left. + \sum_{p=0}^{\infty} e_p(L-k-1, k, \beta, \alpha) I_m^{p+(L-k)\alpha+k\beta-1} \right].\end{aligned} \tag{D.6}$$